MICROTUBULE POST-TRANSLATIONAL DETYROSINATION COORDINATES NETWORK STABILITY AND MECHANICS IN THE CARDIOMYOCYTE

Alexander K. Salomon

A DISSERTATION

in

Cell and Molecular Biology

Presented to the Faculties of the University of Pennsylvania

in

Partial Fulfillment of the Requirements for the

Degree of Doctor of Philosophy

2021

Supervisor of Dissertation

_____

Benjamin L. Prosser, PhD

Associate Professor of Physiology

Graduate Group Chairperson

_____

Daniel S. Kessler, PhD

Associate Professor of Cell and Developmental Biology

Dissertation Committee

Melike Lakadamyali, PhD; Associate Professor of Physiology

Tejvir Khurana, MD, PhD; Professor of Physiology

Matthew C. Good, PhD; Assistant Professor of Cell and Developmental Biology

Rajan Jain, MD; Assistant Professor of Medicine

Dedication page

To those that have listened to me talk about the heart in line for the bathroom at a party.

ACKNOWLEDGMENTS

This dissertation represents the cumulative investment made by mentors, family, and friends. I can't thank you enough. Ben: thank you for seeing something in me that I was blind to. Over the past four years, you've nurtured a more thoughtful, confident, and ambitious version of myself and I'm so incredibly excited to continue on this trajectory. Kelly: thank you for teaching me that I'm worthy. Worthy to take up space, worth to be mentored, worthy of opportunity. I hope to leave the same impact on the world as you have. Emily and Keita: thank you for being friends and mentors in and out of the lab. You both are a constant source of light and I'm excited to be friends for life. Julie, Matt, Pat, Christina, Sai, Alexey, Jennine: thank you for being a constant source of scientific inspiration and support, I'm in perpetual awe of all of you.

Mom: thank you for unconditionally loving and supporting me in every decision I make. Even though I may feel distant at times, you are the ember that keeps me going, I love you. Oma and Opa: thank you for providing a safe perch to explore the world and impressing a lifelong love of learning and curiosity. I love you both so much. Dee and Rob: thank you for expanding my worldview with every visit.

To my friends in Philly: thank you for taking me in and providing the salve to long nights spent in the lab. To my friends in nyc: thank you for dancing, laughing, and loving me.

ABSTRACT

MICROTUBULE POST-TRANSLATIONAL DETYROSINATION COORDINATES NETWORK STABILITY AND MECHANICS IN THE CARDIOMYOCYTE

Alexander K. Salomon

Benjamin L. Prosser

The microtubule network of the cardiomyocyte exhibits specialized architecture, stability, and mechanical behavior that accommodates the demands of a working muscle cell. Post-translationally detyrosinated microtubules are physically coupled to the sarcomere, the contractile unit of the muscle, and resist both the contraction and relaxation of the muscle. The cumulative impact of the microtubule network on myocyte mechanics and the enzyme responsible for detyrosinating tubulin are unknown. Further, control of microtubule growth and shrinkage dynamics represents a potential intermediate in the formation of the stable, physically coupled microtubule network, yet the molecular determinates that govern dynamics have not been studied in the cardiomyocyte. I hypothesize that depolymerization of the microtubule network or knockdown of the vasohibin/small vasohibin binding protein complex, a putative tubulin carboxypeptidase in cardiomyocytes, will improve the contractile kinetics of cardiomyocytes isolated healthy or failing human hearts. Additionally, I hypothesize that desmin intermediate filaments may stabilize growing microtubules at the sarcomere Z-disk in a detyrosination-dependent manner. Using a combination of biochemical assays in tandem with direct observation of myocyte mechanics and microtubule dynamics in primary adult

cardiomyocytes I find the following: 1) depolymerization of the microtubule network improves contraction and relaxation kinetics in cardiomyocytes isolated from failing human hearts; 2) knockdown of either vasohibin 1 or small vasohibin binding protein reduced levels of microtubule detyrosination resulting in improvements in contractile kinetics and a reduction in cellular stiffness; and 3) tyrosination increases renders the microtubule more dynamic while desmin intermediate filaments stabilize the growing microtubule.

In summation, this dissertation establishes a mechanism for the formation of the post-translationally detyrosinated microtubule network, and further underscores the potential of detyrosination as a therapeutic target for the treatment of heart disease.

TABLE OF CONTENTS

LIST OF FIGURES

CHAPTER 1: INTRODUCTION

Cardiomyocytes functionalize the heart

The capacity of the heart to pump blood at a rate sufficient to meet the demands of the body is governed by the cardiomyocytes that make up the myocardium, or muscular layer of the heart. The functional unit of the cardiomyocyte is the sarcomere, which contains the actin and myosin that power cardiomyocyte contraction. Upon calcium release from the sarcoplasmic reticulum during systole, myosin interacts with actin to produce force leading to myocyte shortening.[1] The subsequent reuptake of calcium during diastole dissociates actin and myosin leading to myocyte relaxation. The magnitude and duration of calcium release thus controls the strength and speed of myocyte contraction and relaxation.[2]

The left ventricle of the heart is the chamber responsible for circulating oxygenated blood through the body. Inadequate relaxation of the ventricle due to stiffening of the myocardium or diastolic dysfunction, alters the contractile kinetics of the heart, potentiating a mismatch between the needs of the body and cardiac output.[3] Diastolic dysfunction is a hallmark of hypertrophic cardiomyopathy and heart failure with preserved ejection fraction, complex diseases characterized in part by stiffening of the ventricle leading to impaired ventricular relaxation and slow ventricular filling.[4] Impaired ventricular relaxation

is driven by both factors extrinsic to the cardiomyocyte, such as the composition of the extracellular matrix, and intrinsic factors such as slowed or incomplete reuptake of calcium which prevents complete deactivation of the sarcomere.[5]

Besides the contractile machinery, cardiomyocyte relaxation is influenced by the presence of the non-sarcomeric cytoskeleton which includes microtubules, intermediate filaments, and actin.

Cardiac microtubules resist myocyte motion

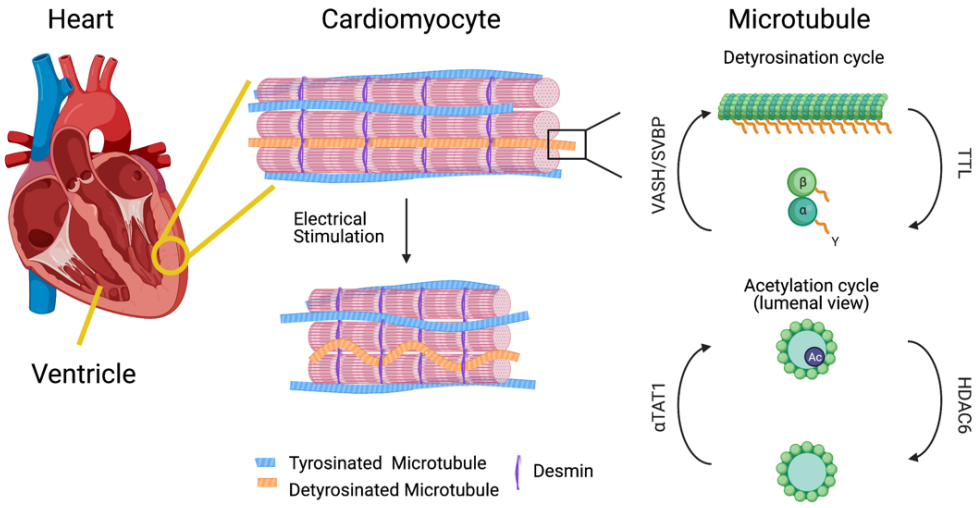

Figure 1. Schematic depicting microtubule organization in the cardiomyocyte

Microtubules are polymers of α and β tubulin that are critical in maintaining cellular architecture[6], signaling[7,8], and proper RNA localization[9] in the cardiomyocyte. Individual α/β tubulin heterodimers self-assemble in a head-to-tail fashion to form polarized protofilaments, of which 13 come together to form a hollow tube with an outer diameter of ~25nm.[10] Microtubules are characterized

by cyclical transitions between polymerization and depolymerization at their plus-end, a behavior called dynamic instability.[11–13] Both α and β tubulin isoforms bind one guanosine triphosphate (GTP) molecule. While the GTP molecule bound to α tubulin is not hydrolyzed nor exchanged, β tubulin hydrolyzes its GTP molecule upon incorporation into the microtubule polymer. GTP hydrolysis to GDP by β tubulin changes the conformation of the inter-dimer interface, which favors depolymerization of the tubulin dimer.[14,15] Thus, the presence of a GTP-cap on the plus end of the microtubule stabilizes the growing tip[16]. Spatiotemporal control of microtubule dynamics is cell type- and context-specific and can occur either by controlling polymer addition or subtraction at the ends, or through lateral interaction with the microtubule polymer.[17]

Control of microtubule dynamics and the resulting function of microtubule sub-populations is maintained in part by post-translational modification of tubulin or interaction with microtubule associated proteins. [17,18] Microtubules can be post-translationally modified via the tubulin C-terminal tails that emanate from the microtubule surface, as is the case of detyrosination[19], glutamylation[20], and glycylation[21]. Post-translational acetylation[22] and phosphorylation[23] can also occur within the globular region tubulin. By accruing post-translational modifications, a microtubule code is thought to be ‘written’ that can be ‘read’ by microtubule associated proteins.[18] Microtubule associated proteins can either provide structure to the microtubule, or utilize the microtubule as a substrate for transport or depolymerization.[24]

Although microtubules are highly dynamic, they possess a relatively high resistance to bending, or flexural rigidity, in relation to other cytoskeletal elements.[10,25] Upon compression, microtubules will bear compressive loads until they reach a critical force that causes them to buckle. The critical buckling force dictates how much resistance a microtubule provides to a compressive load.[26–28] At relatively small compressive forces (1pN), a single *in vitro* microtubule will form a single wavelength buckle. Through physical crosslinking with other cytoskeletal elements in the cell and support from the crowded cytoplasm, the compressive force microtubules can withstand can increase 1000x.[29,30]

The physical properties of the microtubule network are relevant to myocyte contraction due to the organization of the network. In the cardiomyocyte cytoplasm, hundreds of microtubules form a predominantly longitudinal network that runs perpendicular to the transverse Z-discs that define the sarcomere. Detyrosinated microtubules are physically coupled to the Z-disc via the intermediate filament desmin that forms a honeycomb-like lattice around the sarcomere.[31] Upon contraction of the cardiomyocyte, these physically coupled microtubules form short-wavelength buckles that provide resistance to cardiomyocyte contraction.[32] The interaction between the sarcomere and the microtubule is dynamic and thought to function like a catch-bond, where the strength of the bond increases with mechanical force.[33] For example, at slow rates of strain the microtubule will not engage with the sarcomere and produce very little resistance to myocyte stretch, whereas at rapid length changes the

microtubule-sarcomere interaction will be engaged, producing what is known as viscoelastic resistance.

The viscoelastic resistance provided by the microtubule network is amplified during the progression of heart disease, where the microtubule network proliferates and becomes largely detyrosinated. Experiments by George Cooper's group in animal models of heart disease established that the cardiomyocyte microtubule network increases in density with cardiac hypertrophy [34]. Specifically, they found that pressure overload of the right ventricle in a feline model of heart failure resulted in increased tubulin translation as well as increased tubulin associated with the polymerized microtubule network. Depolymerization of microtubules via the small molecule, colchicine, improved the contractility of cardiomyocytes isolated from failing feline hearts. The resistive effect of microtubules on the contractility of isolated wildtype cardiomyocytes could be recapitulated by taxol treatment, a pharmacologic that promotes microtubule stability. The role of microtubules in mediating pathologic changes to contractility was further explored *in vivo* using a canine model of right ventricular pressure overload [35]. Colchicine treatment of dogs with heart failure resulted in depolymerization of the microtubule network and restored ventricular contractility, suggesting that microtubules resist cardiomyocyte contractility.

While Cooper's data suggest that microtubules resist cardiomyocyte contraction, other groups found that microtubule depolymerization has a negligible impact on improving ventricular contractility in a guinea pig model of heart failure[36] and in a feline model of cardiac hypertrophy[37]. In chapter 2, I

interrogate the role of microtubules in cardiomyocyte contractile dynamics in wildtype rat cardiomyocytes and in cardiomyocytes isolated from non-failing and failing human hearts. In collaboration with Matthew Caporizzo and Christina Chen, the lead authors of the articles in which my work was published, we hypothesize that the microtubule network resists myocyte contractility. I find that depolymerization of the microtubule network with colchicine, a small molecule that depolymerizes microtubules, improves the contractility of isolated rat cardiomyocytes and cardiomyocytes from failing human hearts independent of changes to the calcium transient.

Identification of the tubulin carboxypeptidase in cardiomyocytes

Detyrosination was one of the first identified post-translational modifications of tubulin[19] and is commonly associated with a stable microtubule population that has a comparatively longer half-life than tyrosinated microtubules[38]. Detyrosination on its own is not sufficient to change the inherent stability of the microtubule.[39,40] The observed increase in relative stability of detyrosinated microtubules is due to altered interaction with microtubule associated proteins[41]. For example, tyrosination selectively increases the localization of CLIP-170, a protein found at the plus-end tip of the microtubule that increases microtubule catastrophe rate. [41]

Initially, the contribution of detyrosinated microtubules to myocyte mechanics was interrogated by treatment with parthenolide, a sesquiterpene lactone thought to inactivate the tubulin carboxypeptidase. While treatment of

isolated cardiomyocytes with parthenolide reduces detyrosination and subsequently increases contractility, parthenolide treatment also alters the calcium transient.[42] Further, parthenolide has been shown to covalently bind to tubulin which prevents tubulin incorporation into microtubules.[43] Detyrosination can more specifically be decreased by overexpression of tubulin tyrosine ligase (TTL), the enzyme responsible for ligating the terminal tyrosine residue back to detyrosinated tubulin.[44,45] Overexpression of TTL in cardiomyocytes from patients with heart failure reduces cardiomyocyte stiffness and improves contractility.[32,46] However, the precise mechanism by which TTL modulates myocyte mechanics is unclear, as in addition to its tyrosination activity, TTL can depolymerize microtubules by binding free tubulin dimers, preventing their incorporation into polymerized microtubules.[44] Because it is mechanistically unclear if TTL exerts its effects via changes in microtubule detyrosination, depolymerization, or both, methods to more specifically alter detyrosination are necessary to fully understand the mechanism of TTL action and to better define therapeutic targets for heart failure.

The identity of the carboxypeptidase responsible for tubulin detyrosination was unknown until recently, when two groups independently identified the complex of vasohibin-1/2 (VASH-1/2) and small vasohibin binding protein (SVBP) as the primary detyrosinating enzyme in neurons[47,48]. It is currently unknown if the VASH-SVBP complex functions as a detyrosinating enzyme in

cardiomyocytes and may represent an important therapeutic target in the treatment of heart disease.

In chapter 3 I provide evidence that the VASH-SVBP complex functions as a primary detyrosinating enzyme in cardiomyocytes. I find that knockdown of either VASH or SVBP results in a reduction of detyrosination. VASH1 or SVBP knockdown improved contractility and reduced cellular stiffness in cardiomyocytes isolated from rats or failing human hearts. I also identify that the microtubule binding activity of TTL is sufficient to depolymerize the cardiomyocyte microtubule network; however, only the tyrosination specific effects of TTL improve myocyte relaxation. This research was published in Circulation Research with my co-author Christina Chen.

Myocyte microtubule dynamics are influenced by tubulin tyrosination status and desmin intermediate filaments

The regulation of microtubule dynamics potentially represents an important intermediate in the formation of the dense microtubule network observed in disease. However, little is known about the regulation of microtubule dynamics in the healthy cardiomyocyte. In skeletal myocytes microtubules are nucleated from golgi elements which contain γ-tubulin, a tubulin isoform critical for microtubule nucleation, and the scaffolding protein, pericentrin.[49] Microtubules grow along the structural protein dystrophin and other microtubules, producing a well-organized orthogonal network[49] In the cardiomyocyte, microtubules are

stabilized at the Z-disc and predominantly grow longitudinally from adjacent Z-discs.[50] The mechanism underlying the stabilizing effect of the Z-disc and how the progressive growth is regulated is unknown.

One potential mechanism underlying the regulation of microtubule dynamics are tubulin post-translational modifications. Post-translational modification of tubulin are known to impact microtubule dynamics either through changes to the biophysical properties of the microtubule or through altered interaction with microtubule associated proteins[51,52]. For example, acetylation of K70 of α tubulin occurs on the luminal surface of the polymerized microtubule.[53] Structural studies indicate that acetylation weakens the lateral interactions between protofilaments[53] lowering the microtubule's flexural rigidity and subsequently increasing its resistance to breakage[54]. In contrast, microtubule detyrosination does not alter the inherent stability of the microtubule; however, detyrosination reduces the affinity of depolymerizing kinesins for the microtubule which contributes to the observed relative stability of detyrosinated microtubules.[55]

The desmin intermediate filament network is also likely to influence microtubule dynamics and may stabilize the growing microtubule at the Z-disc. A recent pre-print indicates that intermediate filaments can directly stabilize growing microtubules via increased hydrophobic and electrostatic interactions.[56] Desmin may also reinforce microtubule stability through interactions along the length of the microtubule. For example, detyrosinated microtubules are known to

preferentially interact with intermediate filaments via the plakin family of scaffolding proteins[57] (and through kinesin-1)[58].

In chapter 4 I investigate the impact of tubulin post-translational modifications and the structural components on the Z-disc of the dynamics of cardiac microtubules. I find that tyrosinated microtubules are more dynamic, precluding their ability to grow to subsequent Z-discs. I also find that desmin intermediate filaments structure and stabilize the growing microtubule network and directly mediate the formation of microtubule buckles.

CHAPTER 2: MICROTUBULES RESIST MYOCYTE CONTRACTION

Depolymerization of the microtubule network in rat cardiomyocytes improves contractility independent of the calcium transient

Published in: Caporizzo, M. A., Chen, C. Y., **Salomon, A. K**., Margulies, K. B., & Prosser, B. L. (2018). Microtubules provide a viscoelastic resistance to myocyte motion. *Biophysical journal*, *115*(9), 1796-1807.

Cardiomyocyte microtubules form a longitudinal network that runs perpendicular to the transverse Z-discs that define the sarcomere. Upon myocyte contraction, microtubules that are physically coupled to the sarcomere buckle to accommodate the change in cell shape.[32] The resulting buckles visually suggest that cardiac microtubules may provide elastic resistance to myocyte contraction, in that microtubules may resist compression while providing a restoring force to aid in myocyte relaxation. Alternatively, microtubules may provide viscoelastic resistance where energy is dissipated through physical crosslinks made between the microtubule and sarcomere. Previous attempts at prescribing a mechanical role for cardiac microtubules have been inconclusive as measurements of singe cell stiffness have shown microtubules provide viscous[59], elastic[60], or no resistance.[61]

We sought to definitively provide a mechanical role for microtubules in the contracting cardiomyocyte. To this end I collected paired calcium and contractility measurements of freshly isolated adult rat cardiomyocytes with or without an intact microtubule network. To depolymerize the microtubule network, I treated

freshly isolated cardiomyocytes with 10 μM colchicine for 1.5 hours. Myocytes were then loaded with Flou-4 to allow for quantification of the calcium transient and electrically stimulated at 1Hz. Colchicine treatment did not affect the calcium transient as peak calcium levels as well as calcium rise, and decay times were no different than DMSO controls (**Figure 1A**). In contrast, colchicine treatment increased myocyte fractional shortening over a similar timescale as control myocytes (**Figure 1B),** resulting in increased peak shortening and relaxation velocities (**Figure 1C).** This result suggests that microtubules resist cardiomyocyte contractility independent of changes to calcium handling.

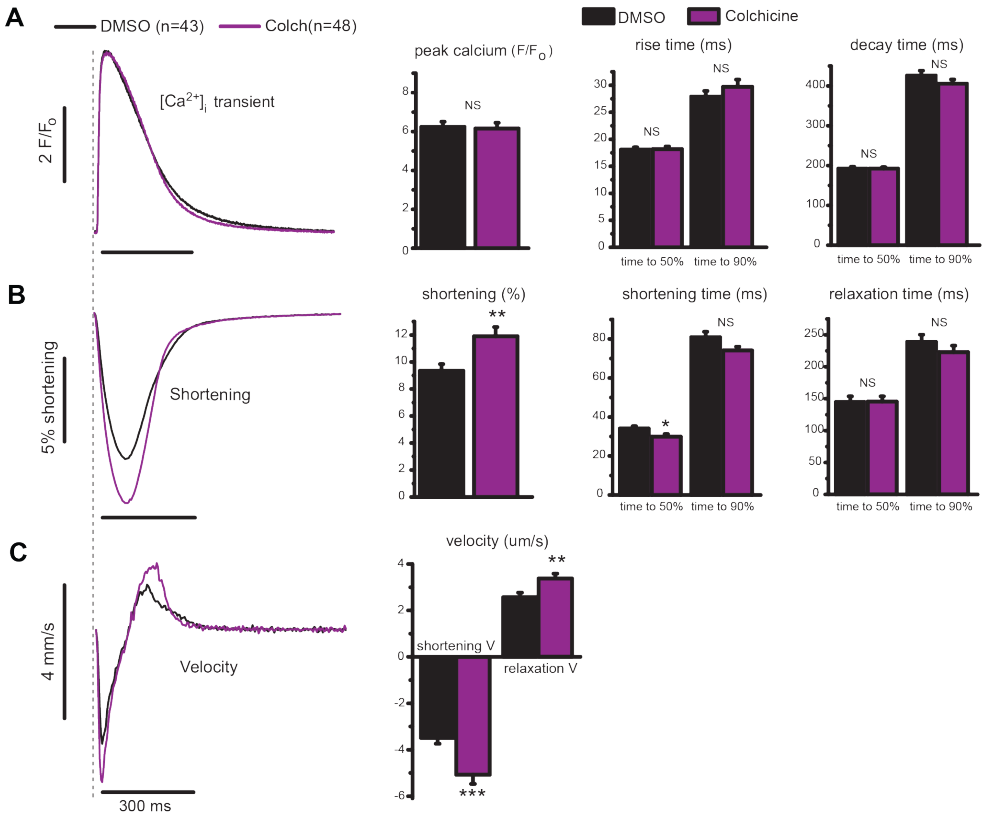

Figure 2. Microtubule depolymerization enhances myocyte contractility. (**A Left**) Normalized calcium transient (F/Fo) for DMSO control (black) and colchicine-treated (purple) cells and (**Right)** peak calcium, time to peak, and decay time determined from individual traces (N = 6 hearts, n = 43 DMSO cells, n = 48 colchicine-treated cells). (**B Left**) Relative shortening (change in SL divided by resting SL) with time and (**Right**) peak shortening, shortening, and relaxation times from individual traces. **(C Left**) The average shortening velocity for DMSO- and colchicine-treated RCMs and (**Right**) Peak shortening and relaxation velocity determined for individual data points. Statistical significance was determined as *p<0.05, **p < 0.01 or ***p <0.001 compared to DMSO, Student's t-test.

Depolymerization of the microtubule network improves contractility of failing human cardiomyocytes

Published in: Chen, C.Y., Caporizzo, M.A., Bedi, K., Vite, A., Bogush, A.I., Robsion, P … **Salomon, A. K.,** …& Prosser, B. L. (2018). Suppression of detyrosinated microtubules improves cardiomyocyte function in human heart failure. *Nature medicine*, 24(8), 1225-1233.

To assess the role that microtubules play in failing human cardiomyocytes, I worked with Christina Chen to isolate cardiomyocytes from non-failing and failing human hearts. Failing human hearts included heart failure with preserved ejection fraction (HFpEF), heart failure with reserved ejection fraction (HFrEF), dilated cardiomyopathy (DCM), and ischemic cardiomyopathy (ICM). Prior to treatment, cardiomyocytes isolated from failing hearts exhibited less fractional shortening with slower contractility (**Figure 2A, D**). Depolymerization of the microtubule network by colchicine in cardiomyocytes from non-failing hearts had a marginal, but significant effect in improving fractional shortening as well as contraction and relaxation velocities (**Figure 2B, E).** Colchicine treatment significantly improved contractility of failing cardiomyocytes as demonstrated by representative traces from myocytes isolated from DCM and ICM hearts (**Figure**

2C). Specifically, colchicine treatment of failing cardiomyocytes significantly improved fractional shortening in addition to contraction and relaxation velocities (**Figure 2 D,E).**

Taken together, I identified that depolymerization of the microtubule network with colchicine improves myocyte contractility independent of changes to the calcium transient. Additional studies led by Matthew Caporizzo and Christina Chen identified that microtubule depolymerization reduces transverse myocyte stiffness specifically at fast indentation rates. The rate dependent contribution of microtubules to myocyte stiffness suggests that the microtubule network is viscoelastic, because the resistive microtubule-sarcomere interactions become engaged only a rapid length changes.

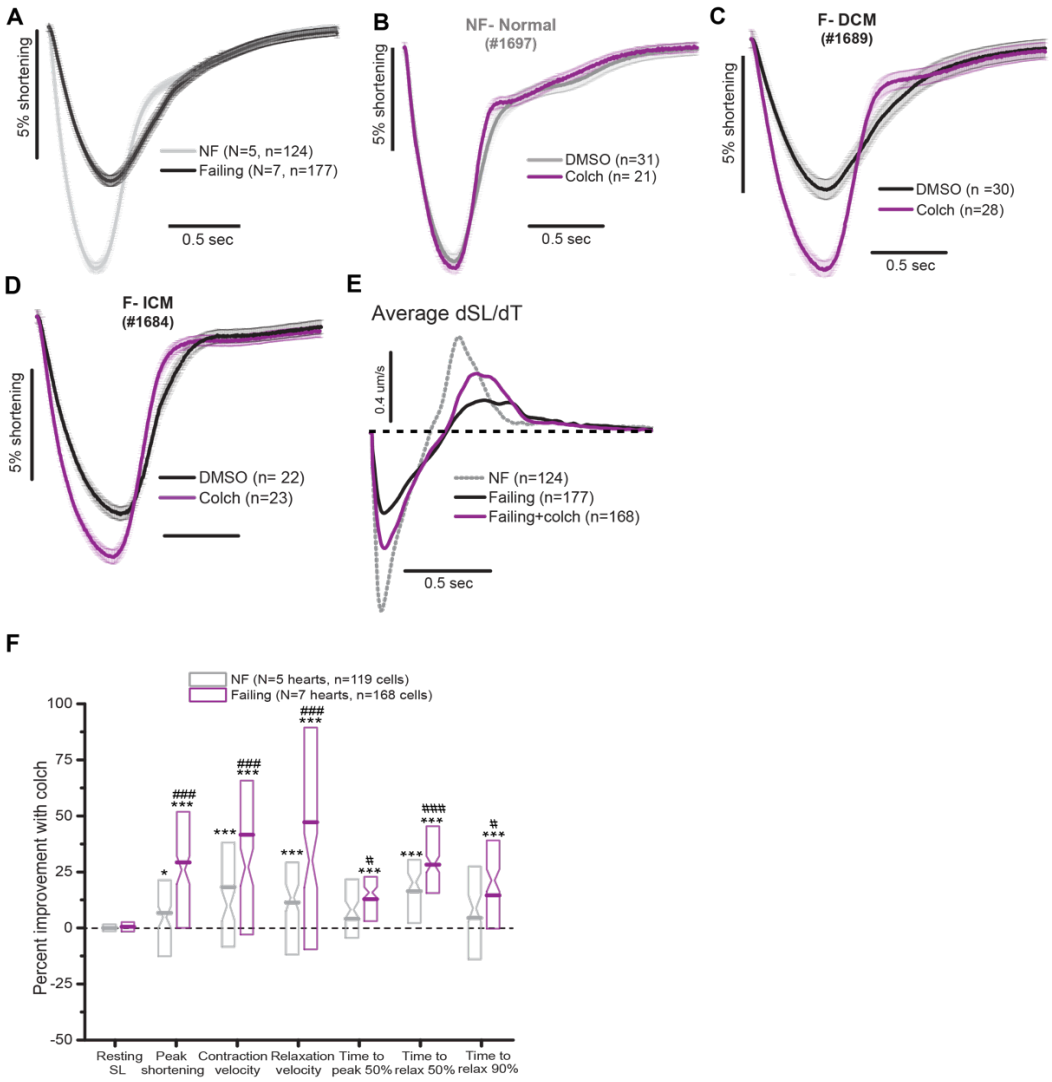

Figure 3. Depolymerization of the microtubule networking improves contractility of failing human cardiomyocytes. (A) Average sarcomere shortening from DMSO treated myocytes from failing (black) and non-failing (gray) hearts. Shortening is shown to normalized resting length. Effect of colchcine (colch) on cardiomyocytes from **(B)** non-failing, dilated cardiomyopathy (DCM), and **(C)** ischemic cardiomyopathy (ICM). **(D)** Average velocity traces from non-failing, failing, and colchicine treated myocytes. **(F)** Pooled data showing percentage improvement in the indicated contractile parameters following treatment of non-failing or failing hearts with colch or DMSO-treated cells. Statistical significance was determined via two-sided t-tests as *p<0.05, **p < 0.01 or ***p <0.001 compared to DMSO; #p < 0.05, #p < 0.001, ###p < 0.001 versus non failing.

CHAPTER 3: DEPLETION OF VASOHIBIN 1 SPEED CONTRACTION AND RELAXATION IN FAILING HUMAN CARDIOMYOCYTES

Adapted from article published as: Chen, C. Y*., **Salomon, A. K*.,** Caporizzo, M. A., Curry, S., Kelly, N. A., Bedi, K., … & Prosser, B. L. (2020). Depletion of vasohibin 1 speeds contraction and relaxation in failing human cardiomyocytes. *Circulation research*, 127(2), e14-e27.

*Co-authors

Introduction

Heart failure is often characterized by diastolic dysfunction, or inadequate ventricular filling due to the inability of the myocardium to fully relax. Diastolic dysfunction is a hallmark of hypertrophic cardiomyopathy (HCM)[62] and heart failure with preserved ejection fraction (HFpEF), diseases often characterized by prolonged and impaired left ventricular (LV) relaxation, slow LV filling, and increased diastolic LV stiffness.[4] Diastolic dysfunction can be initiated by factors extrinsic to the cardiomyocyte such as hypertension and fibrosis, or intrinsic impairments to cardiomyocyte calcium cycling and myofilament calcium sensitivity.

In addition to mechanisms that directly control sarcomere contraction and relaxation, myocyte motion can be modulated by the mechanical properties of the non-sarcomeric cytoskeleton.

Cardiac microtubules provide viscoelastic resistance to myofilament shortening and re-lengthening through physical coupling of microtubules to the myofilaments.[32,63] This physical interaction is tuned by detyrosination, a post-translational modification of the C-terminal tail of α-tubulin (**Figure 4A**). In human heart failure (HF), the cardiac microtubule network proliferates and becomes more detyrosinated, increasing viscous drag on the myofilaments.[46] Multiple recent proteomic and biochemical assessments of patient myocardium suggest that detyrosinated microtubules are upregulated across the spectrum of end-stage HF,[46] as well as in patients with aortic stenosis[64] or inherited HCM.[65] Together, this data implicates microtubule detyrosination as a therapeutic target to lower stiffness and improve myocyte motion in HF.

Detyrosination can be genetically decreased by overexpression of tubulin tyrosine ligase (TTL), an enzyme highly specific for tubulin and responsible for ligating the terminal tyrosine residue back to detyrosinated tubulin.[44] Promisingly, overexpression of TTL in cardiomyocytes from patients with HF reduces cardiomyocyte stiffness, improves contractility,[32,46] and reduces cell stiffness during diastolic stretch.[66] However, the precise mechanism by which TTL modulates myocyte mechanics is unclear, as beyond its tyrosinating activity, TTL can also depolymerize microtubules by binding free tubulin dimers, preventing their incorporation into polymerized microtubules.[44,67] Because it is mechanistically unclear if TTL exerts its effect via changes in microtubule detyrosination, depolymerization, or both, methods to more specifically alter

detyrosination are necessary to fully understand the mechanism of TTL action and to better define therapeutic targets for HF. Prior to the identification of tubulin carboxypeptidases responsible for detyrosination, tools to inhibit a detyrosinase have been limited to sesquiterpene lactones such as parthenolide, which must be used at high concentrations that elicit off target consequences.[46,68]

The recent identification of a detyrosinating enzyme complex of vasohibin-1 or -2 (VASH1/2) and their obligate partner small vasohibin binding protein (SVBP) potentially enables the development of more specific approaches to reduce detyrosination.[47,48] However, alternative tubulin carboxypeptidases beyond VASH exist in other cell types,[47] and it remains to be determined if either VASH1 or VASH2 are active detyrosinases in cardiomyocytes, and whether their selective inhibition is sufficient to improve contractility. In this study, we identify the VASH1-SVBP complex as a predominant tubulin carboxypeptidase in cardiomyocytes, and confirm that genetic depletion of VASH1 is sufficient to lower stiffness and improve contractility in cardiomyocytes from patients with HF. Further, we identify tyrosination-dependent and independent effects of TTL overexpression and find that tyrosination preferentially improves the relaxation kinetics of cardiomyocytes, and exerts its most profound effects on cardiomyocytes from patients with HF and diastolic dysfunction.

Results

A note on human samples

Twenty-two human hearts were used in this study for functional tests. All patient studies were conducted on explanted human hearts from patients with non-ischemic heart failure (hypertrophic or dilated cardiomyopathy, HCM or DCM, respectively). When sufficient samples were available, hearts were further sub-classified as either heart failure with reduced ejection fraction (HFrEF) for patients with left-ventricular ejection fraction (LVEF) below 30%, or HFpEF for those with LVEF above 50% at time of transplant. Non-failing (NF) donor hearts were used as controls. For relevant clinical characteristics please see **Table 1**, and for descriptions of experiments performed on each heart, please see **Appendix Table 2**.

Table 1. Summary descriptive statistics of human hearts used in chapter 3

Etiology	No. of hearts	Age (year)	LVMI (g/m^2)	LVEF (%)
NF	2M, 4F	54.83 ± 6.09	101.03 ± 8.96	58.33 ± 5.27
HFpEF	3M, 3F	52.17 ± 5.06	150.26 ± 10.96	67.5 ± 2.81
HFrEF	6M, 4F	48.1 ± 3.75	116.18 ± 6.49	18 ± 1.53

Each value is presented as mean ± s.e.m. Abbreviations: F, female; LVMI, left ventricular mass index; M, male.

TTL overexpression improves contractility in isolated cardiomyocytes from failing human hearts independent of changes to the calcium transient

We previously showed that TTL overexpression reduces viscoelasticity and improves contractility in NF human cardiomyocytes.[46] Because the microtubule network increases in density and becomes highly detyrosinated during heart disease, we wanted to extend these studies to cardiomyocytes from failing hearts, and examine any effect of TTL overexpression on calcium handling. We transduced cardiomyocytes from patients with HF with adenovirus overexpressing TTL or a control virus (null), and assessed electrically stimulated $[Ca^{2+}]_i$ transients and sarcomere shortening. TTL overexpression robustly improved myocyte contraction and relaxation kinetics, with no detectable change to the kinetics or amplitude of the calcium transient (**Figure 4B**, **Appendix Table 2**). These results are consistent with the hypothesis that reducing detyrosination improves the contractility of failing cardiomyocytes through mechanisms predominantly independent of a change in calcium cycling.

Generation of constructs to isolate TTL tubulin sequestration from tyrosination

Although TTL overexpression reduces the proportion of detyrosinated microtubules, the precise mechanism by which TTL improves contractility is not clear, as TTL can depolymerize the microtubule network via sequestration of free tubulin,[44] which is sufficient to improve contractility.[69] To isolate effects of TTL attributable to tubulin sequestration vs. tyrosination, we generated adenovirus

encoding an established TTL catalytic-dead construct (TTL-E331Q) that binds tubulin with wildtype kinetics, but cannot enzymatically tyrosinate tubulin.[44] We validated this tool in healthy rat cardiomyocytes, where adenoviral overexpression of TTL-E331Q to the same level of TTL did not significantly reduce detyrosinated tubulin (**Figure 4C**)**.**

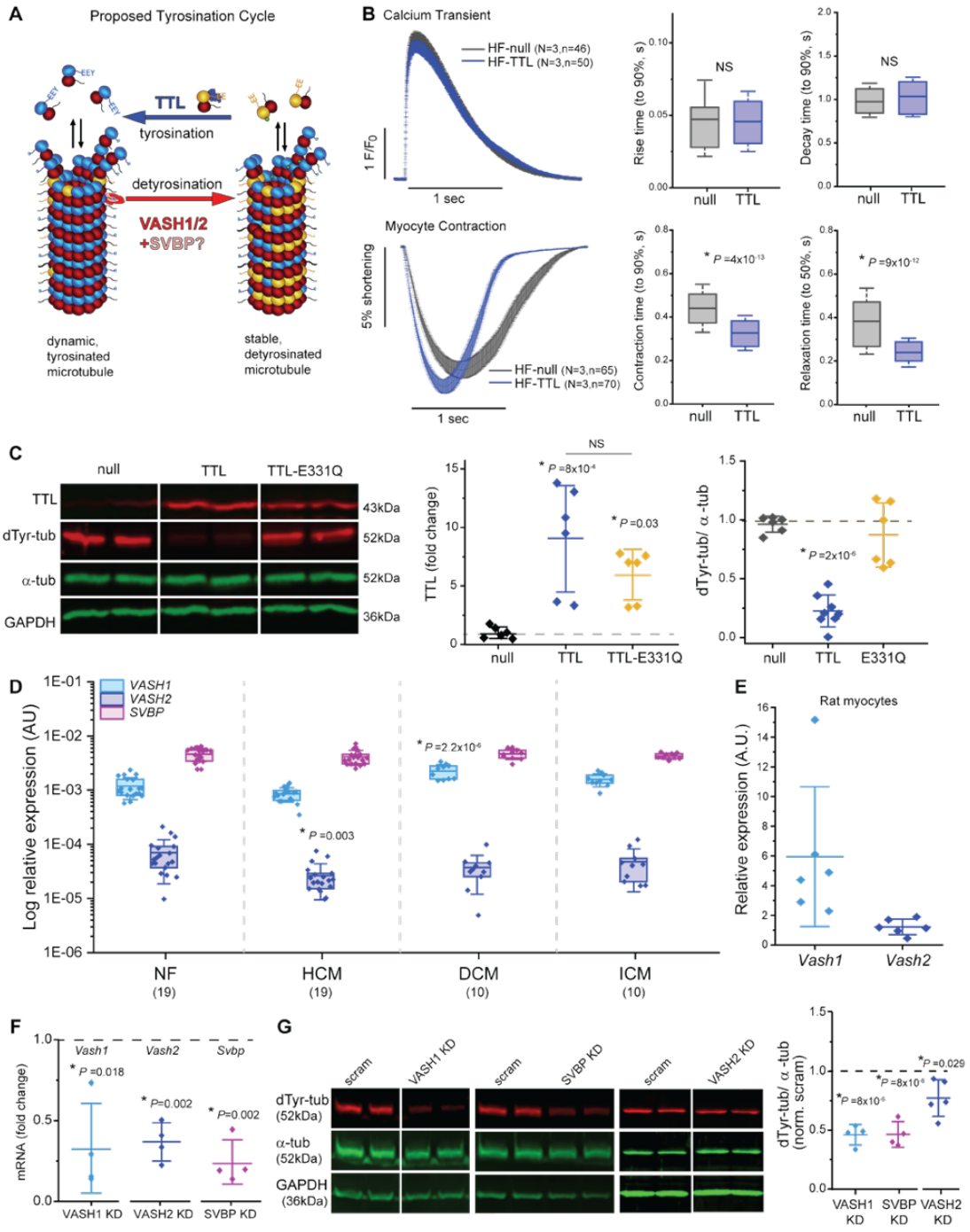

Figure 4. Identification of the primary cardiac detyrosinase and development of tools to probe the tyrosination cycle. A, Schematic of proposed microtubule tyrosination cycle in cardiomyocytes. **B,** Average traces of electrically stimulated $[Ca^{2+}]_i$ transients (top) and sarcomere shortening (bottom) from failing human cardiomyocytes infected with a null (grey) or

TTL-encoding (blue) adenovirus. Traces depict change in signal normalized to resting fluorescence (F_0) or resting length. Kinetic parameters of calcium transients and sarcomere shortening are quantified to the right. Statistical significance determined via two-sided t-tests with Bonferroni correction for two comparisons, unadjusted P value are shown * vs. null. **C,** Validation of TTL-E331Q construct. Representative western blot and quantification of TTL, detyrosinated tubulin (dTyr-tub), α-tubulin (α-tub), and GAPDH levels in whole cell extracts from isolated rat cardiomyocytes expressing null, TTL, or TTL-E331Q constructs. Statistical significance determined via one-way analysis of variance (ANOVA) with post-hoc Bonferroni test from duplicates of N=3 rat hearts, * vs. null. **D,** Expression profiling of *VASH1*, *VASH2* and *SVBP* genes via RT-qPCR of patient myocardial samples. Statistical significance determined via one-way ANOVA with post-hoc Bonferroni test, * vs. NF. **E**, Expression levels of *Vash1* and *Vash2* in isolated rat cardiomyocytes. **F,** Validation of knockdown (KD) via RT-qPCR quantification of *Vash1*, *Vash2*, and *Svbp* in rat cardiomyocytes. **G,** Representative western blot and quantification of detyrosinated tubulin, α-tubulin, and GAPDH levels from isolated rat cardiomyocytes treated with different concentrations of adenovirus encoding SVBP or VASH1 KD constructs. Data presented as fold change from scramble (scram) control. Statistical significance determined via two-sided Student's t-tests for RT-qPCR (**F**) and VASH2 KD western blot (**G**), and via one-way ANOVA for VASH1 and SVBP KD western blot, * vs. scram. Data are presented as mean ± s.d. if not otherwise specified.

VASH1/SVBP is a predominant cardiac tubulin carboxypeptidase

To interrogate detyrosination, independent of any potential microtubule depolymerization via TTL, we sought to directly manipulate a cardiac detyrosinase. We conducted experiments to verify if the recently identified VASH-SVBP complex is a primary detyrosinase in myocardium, to determine if any isoform of VASH is dominant, and whether VASH/SVBP expression changes in disease. Transcriptional profiling of healthy and diseased human myocardium identified that *VASH1* has approximately 15-fold (±5) higher expression level than *VASH2* in NF tissue (**Figure 4D**). In isolated rat cardiomyocytes, we found *Vash1* to be expressed ~5 fold (±2.2) more than *Vash2* (**Figure 4E**). In diseased myocardium, *VASH1* gene expression was higher in dilated cardiomyopathy (DCM) and did not significantly change in ischemic cardiomyopathy or HCM, while *VASH2* gene expression was modestly decreased in HF (**Figure 4D**).

When comparing the expression of *VASH1* to *VASH2* across all etiologies of HF, *VASH1* was expressed ~28-50 fold higher than *VASH2*. *SVBP* was consistently expressed at a high level and did not show differential expression with disease.

We also sought to evaluate protein abundance of VASH1/2 and SVBP, but were aware of the lack of well-validated antibodies for these targets (note the lack of any such antibodies used in recent publications identifying the role and structure of these enzymes). To address this, we generated new antibodies that were validated in parallel with commercial antibodies in vitro (please see **Appendix Figure 1** for details). While the custom VASH1 antibody was indeed more sensitive and specific than commercially available options, we still were unable to detect a reliable band in cardiac cell or tissue lysate. Thus, further work is needed to detect these enzymes, which are likely of relatively low abundance in the cardiac proteome.

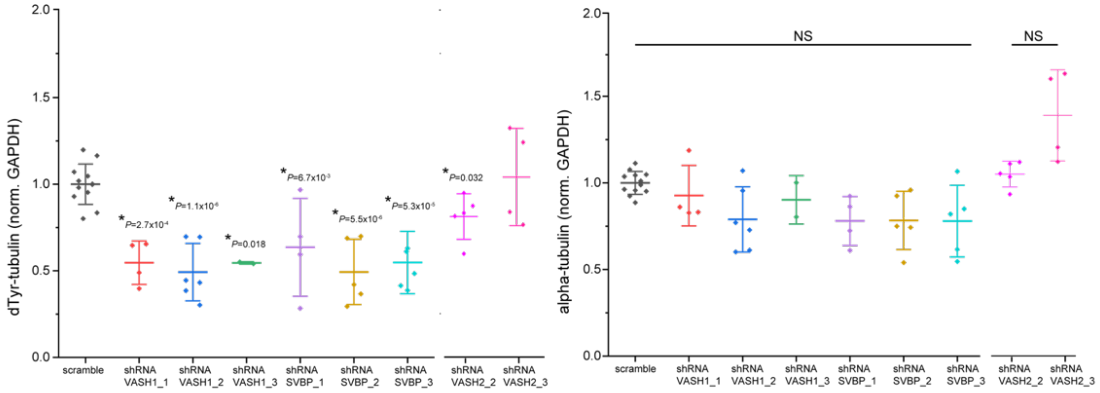

Figure 5: Validation of shRNAs specific for VASH1, VASH2 and SBVP transcripts. Quantification of western blots from isolated rat cardiomyocytes transduced with shRNAs specific for VASH1, VASH2 or SVBP probed for (**A**) detyrosinated tubulin or (**B**) α-tubulin. Statistical significance determined via ANOVA with post-hoc Bonferroni test for data from VASH1/SVBP KD or two-sided t-test for separate data from VASH2 KD experiments, *vs. scram.

We next depleted VASH1, VASH2, and SVBP in healthy rat cardiomyocytes to determine if they function as tubulin carboxypeptidases. For each of these genes, we generated three adenoviruses encoding short hairpin RNAs (shRNAs) specific for three target sites conserved between rats and humans. Delivery of each of these shRNAs by adenovirus to isolated rat cardiomyocytes resulted in a reduction of detyrosinated tubulin, without changing total tubulin levels (**Figure 4G**; **Figure 5**)**.** We selected the shRNAs that resulted in the most robust and consistent decrease in detyrosinated tubulin levels and confirmed that they depleted *Vash1, Vash2* and *Svbp* transcripts via RT-qPCR (**Figure 4F**). With similar decreases in transcript levels (**Figure 4F**), VASH1 and SVBP KD induced an ~55% (± 5) reduction in detyrosinated tubulin while VASH2 KD caused a ~25% (± 6.5%) reduction (**Figure 4G**). As SVBP depletion inhibits the functionality of both VASH1 and VASH2,[70–72] SVBP depletion would be predicted to lead to a greater reduction in detyrosinated tubulin than depletion of VASH1 or VASH2 alone. We did not observe this, which could be due to incomplete SVBP KD or SVBP-autonomous activity of VASH2, as indicated in a recent report.[73] Regardless, our results support a more prominent role of VASH1 in cardiomyocyte detyrosination, which is consistent with a recent patent[74] demonstrating that VASH1 KO robustly reduces detyrosinated tubulin in the heart, while VASH2 KO has a more modest effect. The fact that TTL overexpression reduces detyrosinated-tubulin by ~80% (± 5) while VASH1/SVBP depletion lowers levels by ~55% is consistent with the abundant expression of TUBA4A in cardiomyocytes,[46,48] an α-tubulin isotype translated in its

detyrosinated form, and thus insensitive to manipulation of a detyrosinase, but readily tyrosinated by TTL.

Tubulin sequestration by TTL, and not VASH1/SVBP knockdown, decreases microtubule stability in healthy cardiomyocytes

With these new tools generated, we next sought to determine the effect that TTL/TTL-E331Q overexpression or VASH1/SVBP knockdown has on the stability of the microtubule network. Using a fractionation assay that allows for separation of soluble, free tubulin from polymerized microtubules, we found that overexpression of TTL (~9 ± 2 fold) in healthy rat cardiomyocytes led to a robust (~80% ± 5) reduction in detyrosinated tubulin that did not occur with TTL-E331Q (**Figure 6A and 6B**). Both TTL and TTL-E331Q overexpression increased the amount of free tubulin relative to polymerized microtubules (**Figure 6A and 6C**), indicating modest depolymerization of the microtubule network. In contrast, knockdown of either VASH1 or SVBP reduced the level of detyrosinated tubulin in polymerized microtubules (~40% ± 2), yet the free:polymerized tubulin ratio remained unchanged (**Figure 6A** through **6C**). These results suggest that tubulin binding via TTL is sufficient to depolymerize the microtubule network in isolated rat cardiomyocytes, and that modest reductions in detyrosination alone are not sufficient to depolymerize microtubules.

We noted that TTL overexpression or knockdown resulted in variable changes in the ratio of free:polymerized tubulin that seemed to mirror changes in

detyrosination. Indeed, plotting the change in detyrosinated tubulin from each experiment against the change in free:polymerized tubulin revealed an inverse correlation with levels of detyrosination (**Figure 6D**), suggesting that decreasing detyrosination may decrease microtubule network stability in cardiomyocytes, but requires a threshold reduction in detyrosination. This would imply that any destabilizing effect of VASH1/SVBP depletion would be contingent on a sufficient initial proportion of detyrosinated microtubules in the network, such as occurs in HF.

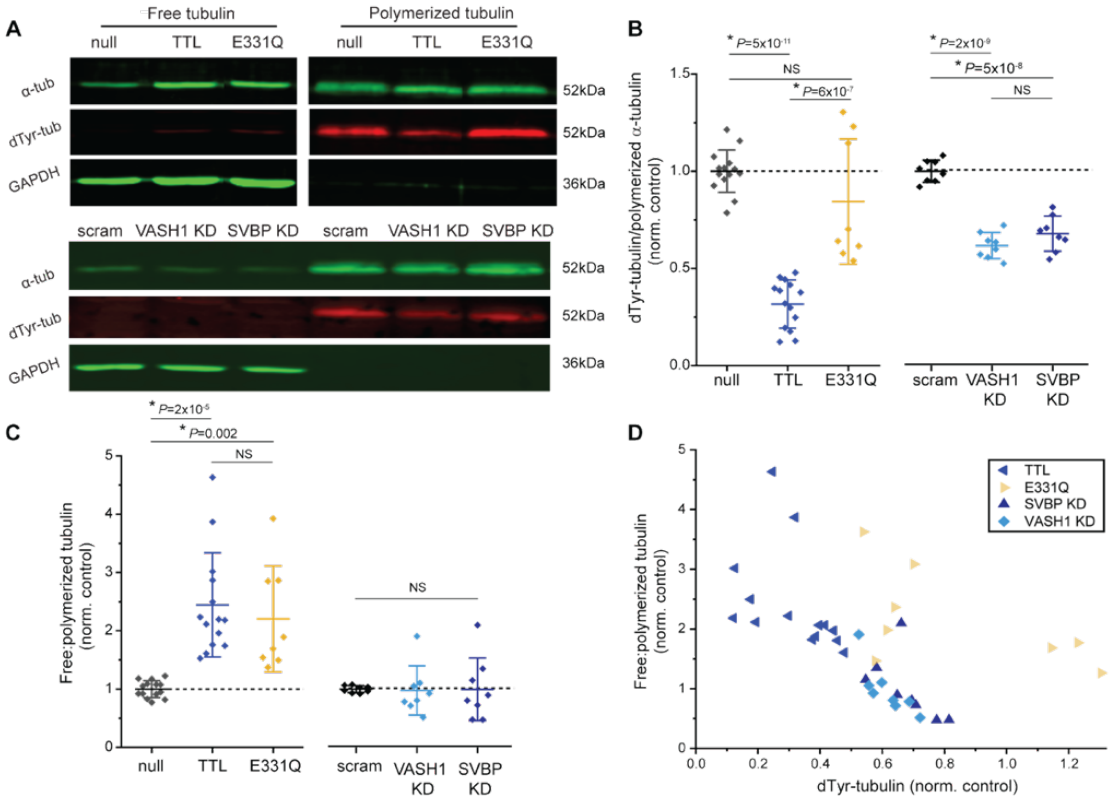

Figure 6. TTL tubulin sequestration, but not detyrosination, depolymerizes microtubules in healthy cardiomyocytes. A, Representative western blot of free and polymerized tubulin from isolated rat cardiomyocytes transduced with adenoviruses encoding null, TTL, TTL-E331Q, scram, VASH1 KD and SVBP KD. Quantification of (**B**) detyrosinated tubulin level found in the polymerized fraction and (**C**) free to polymerized tubulin ratio. Statistical significance determined via one-way ANOVA with post-hoc Bonferroni test, * vs. null or scram, with duplicates of N=7 rat

hearts for null and TTL and duplicates of N=4 for TTL-E331Q, scram, VASH1 KD, and SVBP KD. **D,** Correlation between detyrosinated tubulin levels found in the polymerized fraction and the ratio of free:polymerized tubulin.

Effects of VASH1 knockdown and TTL-E331Q overexpression on myocyte contractility

We next sought to determine how TTL/TTL-E331Q overexpression or VASH1 knockdown would affect the contractility of isolated cardiomyocytes from failing and NF hearts. In cardiomyocytes from NF donor hearts, VASH1 knockdown produced modest but consistent speeding of contraction and relaxation kinetics, and subtle effects on contractile amplitudes (**Figure 7A** through **3D**; **Appendix Table 2**). We also interrogated the effect of VASH1 depletion in cardiomyocytes from 6 patients with HF, 3 with HFrEF (systolic dysfunction), and 3 with HFpEF (diastolic dysfunction). As shown in the average traces of cardiomyocytes from these hearts transduced with control adenovirus (**Figure 7B**), failing heart cells exhibited lower contractile amplitudes and slower kinetics than NF controls. There was markedly slower relaxation in failing cardiomyocytes that was particularly evident in HFpEF cardiomyocytes (**Figure 7C**), consistent with the impaired relaxation implicated in this disease etiology. On average, relaxation velocity was 2.1-fold and 3.6-fold lower in HFrEF and HFpEF than in NF controls, respectively (scram groups: NF 1.51 ± 0.056, HFrEF 0.71 ± 0.083, and HFpEF 0.41 ± 0.041 μm/s). VASH1 depletion markedly improved contractile amplitudes and contraction and relaxation kinetics in failing

cardiomyocytes, eliciting a 1.6 and 2-fold improvement in relaxation velocity in HFrEF and HFpEF cardiomyocytes, respectively (VASH1 KD groups: NF 1.79 ± 0.062, HFrEF 1.12 ± 0.099, and HFpEF 0.81 ± 0.065 μm/s**; Figure 7A** through **7D**; **Appendix Table 2**).

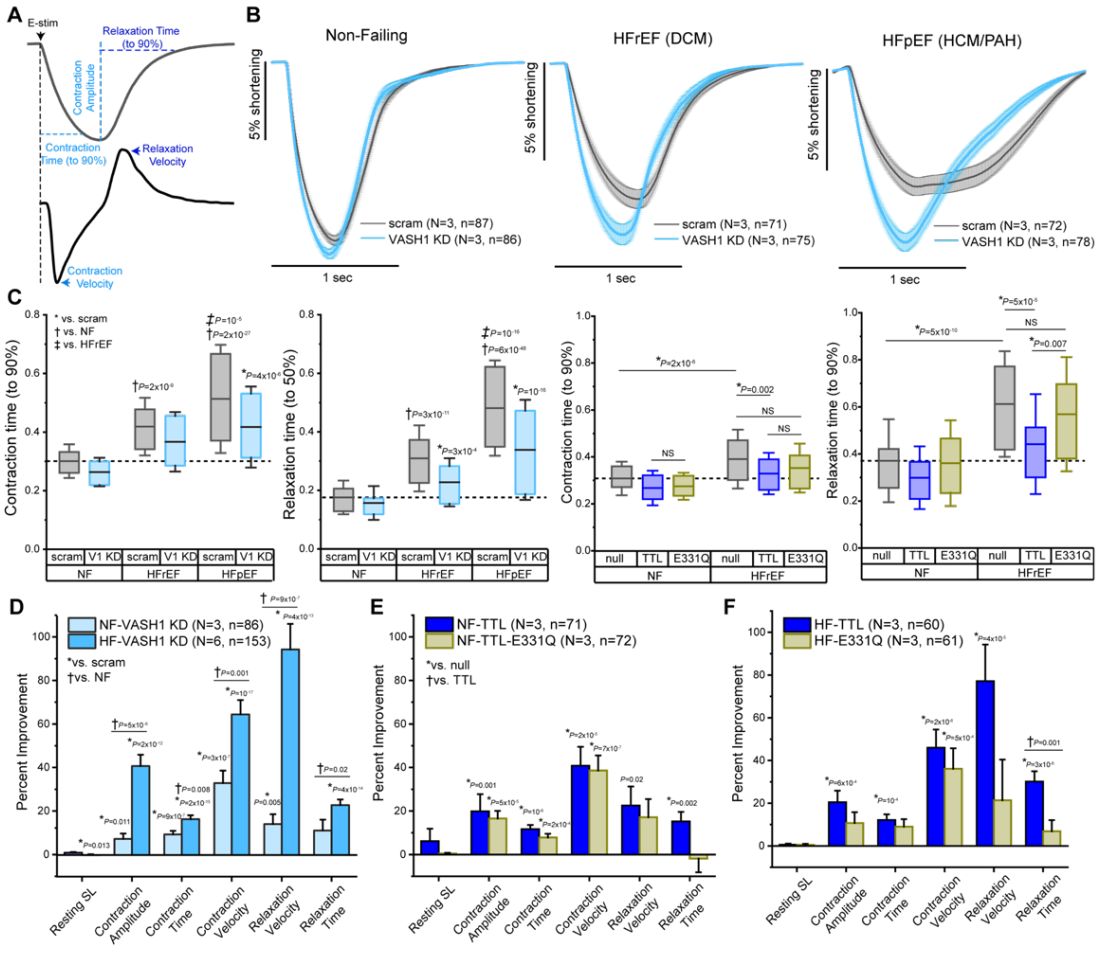

Figure 7. Reducing detyrosination speeds contraction and relaxation of failing human cardiomyocytes. A, Example of sarcomere shortening trace from myocyte responding to electrical stimulation and corresponding first derivative identifying key contractile parameters collected. **B,** Average traces of sarcomere shortening from cardiomyocytes isolated from NF donor hearts and from hearts from patients with HFrEF and HFpEF, with or without VASH1 KD. **C,** Contraction and relaxation times are quantified and grouped by etiology and experimental conditions. Statistical significance determined via two-way ANOVA between the effects of etiology and treatment. *P* values for significant interactions are shown. For detailed two-way ANOVA report, see Online Table 3. **D** through **F,** Percent improvement in contractile parameters by each genetic manipulation over null or scram is quantified and grouped by etiology and experimental conditions. **D**, statistical significance determined via two-sided Student's t-tests with Bonferroni

correction for six comparisons (adjusted α=0.05/6=0.0083), unadjusted P values are shown * vs. scram and † vs. NF. **E** and **F**, Statistical significance determined via two-sided Student's t-tests with Bonferroni correction for six comparisons

The effect of SVBP depletion was examined in cardiomyocytes from a separate subset of 3 failing hearts (2 HFrEF, 1HFpEF), where it elicited similar improvements in contraction and relaxation kinetics as VASH1 knockdown (**Figure 8C** and **8D**; **Appendix Table 2**).

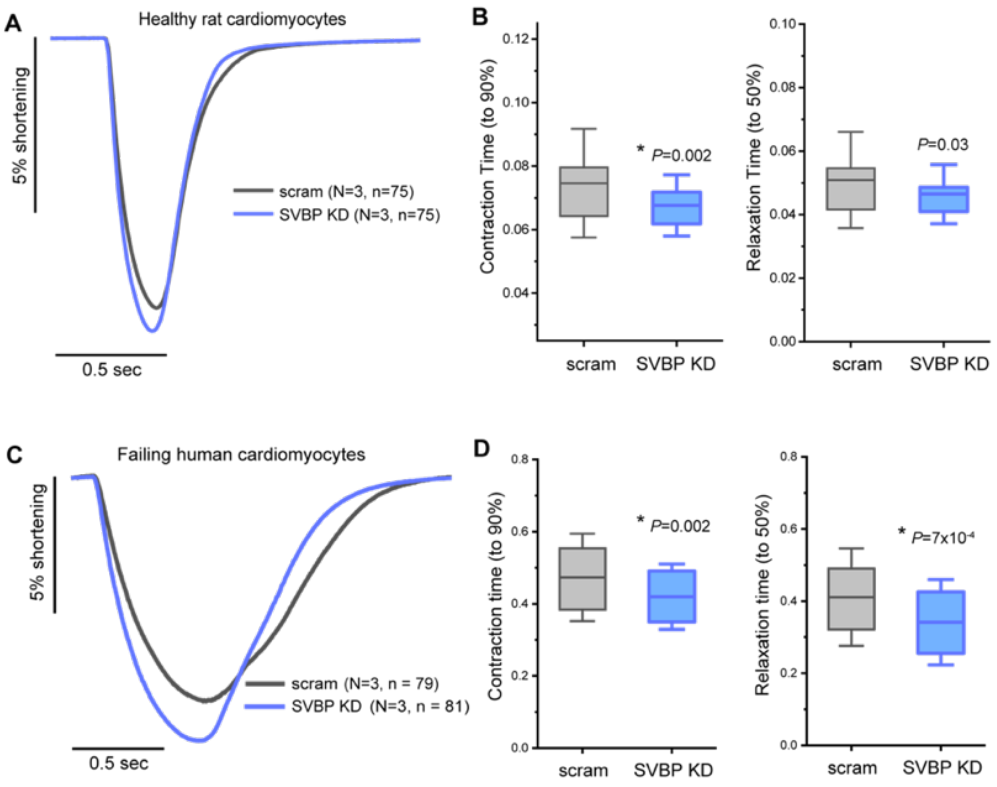

Figure 8. SVBP knockdown improves contractility in both healthy and failing isolated cardiomyocytes. Average sarcomere shortening traces from electrically stimulated (**A**) healthy isolated rat cardiomyocytes and (**C**) failing cardiomyocytes from patients with heart failure transfected with adenovirus containing either SVBP KD (blue) or scram (grey) constructs. **B** and **D,** Quantification of kinetic parameters. Statistical significance determined via two-sided t-tests with Bonferroni correction for two comparisons (adjusted α=0.025), * vs. scram.

In NF cardiomyocytes, both TTL and TTL-E331Q overexpression improved most metrics of systolic function compared to cells transduced with control adenovirus, although improvements in relaxation time appeared to only be sensitive to TTL, and not to TTL-E331Q (**Figure 7C** and **7E**). This became more apparent in cardiomyocytes from failing hearts (HFrEF), where both constructs improved systolic parameters, yet TTL had a significantly greater effect than its catalytically dead counterpart on relaxation time, and robustly improved relaxation velocity (**Figure 7C** and **7F**).

Together, this data indicates that 1) relaxation kinetics are particularly slowed in failing cardiomyocytes; 2) selectively targeting microtubule detyrosination via either the tyrosinase or detyrosinase is sufficient to robustly improve relaxation kinetics; 3) the effect of reducing microtubule detyrosination is most remarkable in failing cardiomyocytes; and 4) the microtubule depolymerizing activity of TTL is sufficient to augment systolic, but not necessarily diastolic parameters.

VASH-1 knockdown reduces myocyte stiffness and has negligible effects on $[Ca^{2+}]_i$ transients

Typically, we conduct myocyte contractility assays in the absence of Ca^{2+} indicator dye, as they can slow contractile kinetics due to Ca^{2+} buffering and obscure kinetic phenotypes. For this reason, the $[Ca^{2+}]_i$ transient data in Figure

4B was collected on a separate subset of cardiomyocytes from those evaluated for contractility. Recognizing that inhibition of tubulin detyrosination with parthenolide has off target consequences on calcium handling in human cardiomyocytes,[46] we sought to more directly examine the relationship between calcium handling and contractility after VASH1 knockdown in myocytes. Thus, cardiomyocytes from a separate subset of 5 hearts were loaded with a low concentration of the Ca^{2+} indicator dye fluo-3 and simultaneously assessed for $[Ca^{2+}]_i$ transients and contractility. As shown in the average trace of myocytes from a HFpEF heart (**Figure 8A**), VASH1 knockdown robustly improved fractional shortening, contraction and relaxation speed independent of any observable change in Ca^{2+} handling in those same cells. This Ca^{2+}-independent improvement in contractility was observed in both NF and failing cardiomyocytes (**Figure 9B** and **9C**).

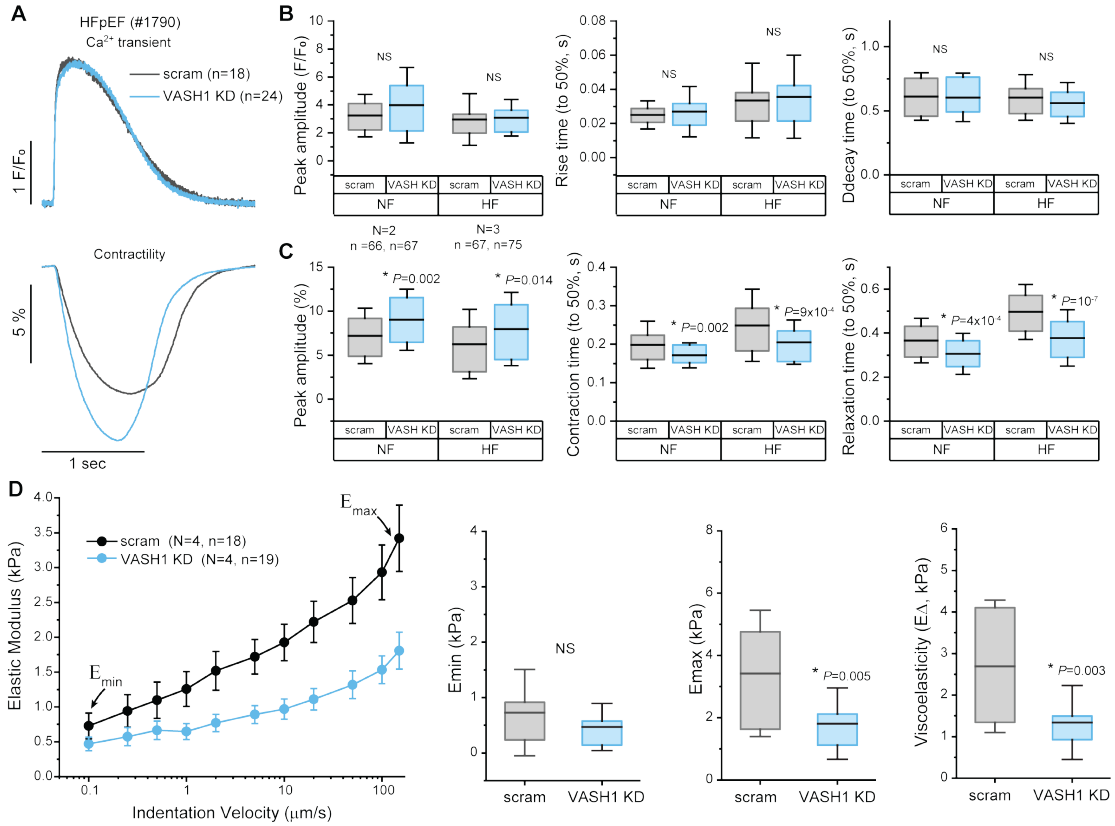

Figure 9. VASH1 knockdown reduces myocyte viscoelasticity and improves contractility independent of changes to the calcium transient. A, Average traces of simultaneously acquired $[Ca^{2+}]_i$ transients and sarcomere shortening from fluo-3 loaded cardiomyocytes isolated from the heart of patient #1790 with heart failure with preserved ejection fraction (HFpEF). Traces are normalized to baseline fluorescence (F_0) and sarcomere length, respectively. Amplitude and kinetic parameters from $[Ca^{2+}]_i$ transients (**B**) and sarcomere shortening (**C**) were quantified simultaneously in cardiomyocytes isolated from NF or failing hearts with or without VASH1 KD. Statistical significance determined via two-sided t-tests with Bonferroni correction for three comparisons (adjusted $\alpha=0.05/3=0.017$), unadjusted P values are shown * vs. scram of that etiology. **D,** Nanoindentation measurements of viscoelasticity. Stiffness (elastic modulus) of failing cardiomyocytes as a function of probe indentation velocity with or without VASH1 KD. Quantification of E_{min}, E_{max} and viscoelasticity ($E\Delta$) in right panels. Statistical significance determined via two-sided t-tests for three comparisons (adjusted $\alpha=0.017$), unadjusted P values are shown *vs. scram. Data are presented as mean ± s.e.m. in (**D**) left panel.

In the absence of any demonstrable effect on Ca^{2+} cycling, the observed improvement of systolic and diastolic kinetics with VASH1 knockdown are consistent with a reduction of viscoelastic resistance to sarcomere motion

contributed by detyrosinated microtubules.[63] To test this hypothesis, we directly probed viscoelasticity via transverse nanoindentation of failing human cardiomyocytes with or without VASH1 knockdown. In response to very slow deformation, the Young's modulus of VASH1-depleted cells was unchanged, suggesting a minimal effect on transverse elasticity (E_{min}, **Figure 9D**). Yet at rates of deformation relevant to the cardiac cycle, VASH1 knockdown reduced transverse stiffness, with a prominent reduction in peak stiffness at high speeds of deformation (E_{max}) and viscoelasticity ($E\Delta$, rate-dependent stiffness) in cardiomyocytes from failing human hearts. Together, these data are consistent with improved kinetics of failing ventricular cardiomyocytes conferred at least in part by reductions in viscoelasticity, due to depletion of VASH1 and reduction in detyrosinated microtubules.

Discussion

From the above data we come to the following conclusions: 1) the VASH1-SVBP complex acts as a tubulin carboxypeptidase in cardiomyocytes; 2) knockdown of VASH1 reduces cardiomyocyte stiffness and improves contractility, particularly in cardiomyocytes from patients with HF; and 3) targeting microtubule detyrosination specifically speeds cardiomyocyte relaxation, which does not require microtubule depolymerization or changes to the Ca^{2+} transient. This work identifies new therapeutic targets for the modulation of cardiomyocyte relaxation and diastolic function.

This study represents the first examination of direct suppression of a tubulin carboxypeptidase in cardiomyocytes. Prior to the discovery of VASH-SVBP as a detyrosinating enzyme complex, the putative carboxypeptidase was commonly inhibited pharmacologically with parthenolide. While effective at high concentrations, parthenolide enacts multiple off target effects including alterations in calcium handling[46] and cellular signaling cascades.[68,75]

Detyrosination can be genetically reduced by overexpression of the tyrosinating enzyme TTL, and like parthenolide, TTL overexpression reduces stiffness and improves contractility in human cardiomyocytes. Yet the mechanism of TTL action is confounded by the ability of TTL to depolymerize the microtubule network through its 1:1 interaction with free tubulin.[44,67] While mild depolymerization of the microtubule network might be acutely beneficial in improving cardiomyocyte contractility, chronic or gross depolymerization could lead to trafficking and signaling defects.[7,76] A TTL-based therapeutic approach is further complicated by a reliance on gene therapy to deliver TTL or the unlikely identification of a TTL agonist. In contrast, small molecule inhibitors of VASH1 or the VASH-SVBP interaction can be more readily designed based on recent structural studies of the complex[70–72] or identified using high-throughput screens, potentially facilitating translational studies. The role of VASH1 as a negative regulator of angiogenesis must be considered, but the vascular architecture of *Vash1* KO mice appears largely unchanged. [77]

A limitation of the current work is the difficulty in quantifying protein levels of VASH/SVBP, which may be aided by further antibody refinement or targeted mass-spectrometry approaches. Additionally, protein expression does not speak to enzymatic activity directly, and little is known about post-translational regulation of these enzymes and the effect it has on detyrosinase activity.

These results provide the first demonstration of the effects of VASH1/SVBP inhibition on the intrinsic relaxation and viscoelasticity of isolated cardiomyocytes. This is a simplified system, and the diastolic pressure-volume relationship *in vivo* is influenced by numerous additional factors, including filling pressures that load and stretch cardiomyocytes. Of note, similar reductions in viscoelasticity with parthenolide or TTL overexpression equate to increased compliance of cardiomyocytes upon loaded cell stretch,[69] so we surmise the same will hold true for inhibition of VASH1. The current study prompts future investigations of the role of VASH1 in animal models of diastolic dysfunction, yet care must be taken in experimental design.

It is difficult to predict how chronic manipulations of TTL may affect cardiac function (or how effects will be interpreted), given the numerous potential consequences of altering microtubule detyrosination,[66] for example on autophagy,[78] oxidative stress,[7,8] and intracellular trafficking.[79–81] Further, it is unclear whether common murine models of heart failure recapitulate the cytoskeletal remodeling that occurs in patients with HCM and heart failure. Studies utilizing small molecule inhibition or rapid, inducible depletion of VASH1

in models of diastolic dysfunction that recapitulate the patient cytoskeletal landscape will be most informative.[46,64,65]

Methods

Human myocardial tissue

Procurement of human myocardial tissue was performed under protocols and ethical regulations approved by Institutional Review Boards at the University of Pennsylvania and the Gift-of-Life Donor Program (Pennsylvania, USA) and as described.[46] Briefly, failing human hearts of non-ischemic origin were procured at the time of orthotropic heart transplantation at the Hospital of the University of Pennsylvania following informed consent from all participants. Non-failing (NF) hearts were obtained at the time of organ donation from cadaveric donors. In all cases, hearts were arrested in situ using ice-cold cardioplegia solution and transported on wet ice. Whole hearts and dissected left ventricle were weighed to determine levels of hypertrophy. Failing hearts are etiologically defined by clinical diagnosis of HF, which is subdivided into HFpEF (ejection fraction > 50%) and HFrEF (ejection fraction < 30%). Hearts were utilized for a particular experiment as they arrived until the required sample size was reached for each etiology of interest (e.g. triplicate quality isolations and experiments for NF, HFpEF and HFrEF).

For this study myocytes were isolated from 22 hearts (see method details below) for functional studies. For further details on classification, descriptive statistics, and experiments performed on each heart, see **Appendix Table 1.**

Human left ventricular myocyte isolation and cell culture

Human left ventricular myocytes were isolated as described previously.[46] Culture medium consisted of F-10 (1X) Nutrient Mixture (Ham) [+] L-Glutamine (Life Technologies, 11550-043) supplemented with insulin-transferrin selenium-X (Gibco, 51500-056), 20 mmol/L HEPES, 1 μg μl^{-1} primocin (Invivogen, ant-pm-1), 0.4 mmol/L extra $CaCl_2$, 5% FBS, and 25 μmol/L cytochalasin D (Cayman, 11330). Viable myocytes were concentrated by gravity and the proper amount of medium was added in culture so that neighboring cells were not in direct contact. Viral constructs were permitted to express for 48 hours with a multiplicity of infection = 100-200.

Animals

Animal care and procedures were approved and performed in accordance with the standards set forth by the University of Pennsylvania Institutional Animal Care and Use Committee and the Guide for the Care and Use of Laboratory Animals published by the US National Institutes of Health.

Rat cardiomyocyte isolation and culture

Primary adult ventricular cardiac myocytes were isolated from 6- to 8-week-old Sprague Dawley rats as previously described.[7] Briefly, the heart was removed from a rat anesthetized under isoflurane and retrograde-perfused on a Langendorff apparatus with a collagenase solution. The digested heart was then minced and triturated using a glass pipette. The resulting supernatant was separated and centrifuged at 300 revolution per minute (rpm) to isolate cardiomyocytes which were then resuspended in rat cardiomyocyte media at low density. Cardiomyocytes were cultured at 37°C and 5% CO_2 with 25 μmol/L of cytochalasin D. The viability of rat cardiomyocytes upon isolation is typically on the order of 50-75% rod-shaped, electrically excitable cells, and the survivability for 48hrs of culture is >80% (See Heffler et al.[6] for our quantification of cardiomyocyte morphology in culture). While the viability of human cardiomyocyte isolations is lower (with more variation between preparations), the 48hr survivability is similar to rat cardiomyocytes, and did not differ between experimental groups.

Rat cardiomyocyte media: medium 199 (Thermo Fisher 115090) supplemented with 1x Insulin-transferrin-selenium-X (Gibco 51500056), 1 μg μl^{-1} primocin (Invivogen ant-pm-1), 20 mmol/L HEPES at pH 7.4 and 25 μmol/L cytochalasin D.

Contractility and Calcium transient measurement

Experiments were performed as previously described.[46] Briefly, prior to contractility measurement, cultured human myocytes were transferred to fresh warm medium without cytochalasin D. Contractility was measured in a custom-fabricated cell chamber (IonOptix) mounted on an LSM Zeiss 880 inverted confocal microscope using either a 40 or 63 X oil 1.4 numerical aperture objective and transmitted light camera (IonOptix MyoCam-S). Experiments were conducted at room temperature and field stimulation was provided at 0.5 Hz with a cell stimulator (MyoPacer, IonOptix). After 10-30 seconds of pacing to achieve steady state, five traces were recorded and analyzed. Sarcomere length was measured optically by Fourier transform analysis (IonWizard, IonOptix).

For simultaneous calcium and contractility measurement, myocytes were incubated with 2 μmol/L fluo-3-acetoxymethyl ester (Invitrogen) on rocker for 10 minutes at room temperature, then enriched by gravity for 5 minutes and replenished with fresh warm medium without cytochalasin D. Sarcomere length and fluo3 fluorescence were measured in a custom-fabricated cell chamber (IonOptix) mounted on a Zeiss inverted microscope using a 40 X water 1.2 numerical aperture objective and CCD video camera (MyoCam-S3) coupling to a cell framing adaptor that connects to a photomultiplier tube (PMT400 Sub-System, IonOptix). Cell framing box for fluorescence detection was set at a fixed size. Fluorescence level of a blank area in the dish was recorded to account for background noise. Myocytes were electrically paced at 0.5 Hz at room

temperature and both sarcomere length and fluorescence counts were recorded simultaneously for five steady-state transients.

Generation of short hairpin RNAs

Adenoviruses encoding shVASH and shSVBP constructs were generated and produced in a similar manner as previously described[3], but directed towards single target sites under the U6 promotor in three separate viruses. Target sites for VASH1: sh1: gctgcagtacaatcacacagg, sh2: gggacacagttctttgaaatt, sh3: gggaatttacctcaccaacag; for SVBP: sh1: gacaaagagcagagatctatg, sh2: gcagcagcagtttgatgagtt, sh3: gcagcagtttgatgagttctg; for VASH2: sh1: gtcaagaaggtcaagattggg, sh2: ggtcaagattgggctgtacgt, sh3: gtcaagattgggctgtacgt. eBFP2 was used as a marker of transduction. For data in the primary figures, *VASH1* sh1, *SVBP* sh3, and *VASH2* sh2 were utilized.

RNA isolation, cDNA synthesis, and RT-qPCR

RNA was isolated from cardiomyocytes using RNAzol RT (Molecular Research Center RN190) following the manufacturer's instructions. Briefly, cardiomyocytes were lysed in RNAzol RT reagent. One ml of the lysate was combined with 0.4 ml of water and shaken vigorously for 15 seconds and stored for 15 minutes at room temperature. Samples were then centrifuged at 12,000 g for 15 minutes. The supernatant was removed to a new tube and mixed with one volume of isopropanol, stored at room temperature for 10 minutes, then centrifuged at 12,000 g for 10 minutes. The RNA pellet was then washed with

75% ethanol two times and solubilized in RNase-free water. RNA concentration was determined using a Nanodrop (ThermoFisher) and 2µg RNA was reverse transcribed using cDNA synthesis kit (TaKaRa #6110A or SuperScript IV Thermo Fisher #18091150) following manufacturer's instructions. Twenty ng of cDNA template was then used to conduct RT-qPCR in three technical replicates. For *Vash1* and *Svbp* knockdown data sets, Powerup SYBR green master mix (#A25742, Thermo Fisher) was used with the following primers and thermocycle conditions: *Gapdh* (F-5'-CGTGCCGCCTGGAGAAAC-3' and R-5'-TGGGAGTTGCTGTTGAAGTCG-3'), *Vash1* (F-5'-TCGTCGGCTGGAAAGTAGGCAC-3' and R-5'-TCGTCGGCTGGAAAGTAGGCAC-3'), *Svbp* (F-5'-AACCAGCCTTCAGAGTGGAGAAGG-3' and R-5'-GCTCCGTCATGACTCTGTTGAGAGC-3'); Polymerase activation at 95 ˚C for 10 minutes and 40 cycles of denaturation at 95˚C for 15 seconds and annealing/extension at 60˚C for 1 minutes. For *Vash2* knockdown and relative transcript levels of *Vash1* and *Vash2* in rat myocytes, PrimeTime gene expression master mix (#1055772) with the following primers/probes and thermocycle conditions: *Vash2* (probe 5'-/56-FAM/TCAAGATCT/ZEN/TCATCCGCATGTCCCTG/3IABkFQ/-3', F-5'-GAAGCAACTTGTCCTCAATGTC-3' and R-5'-GGATTCTCACTTGGGTTGGAG-3') (assay name Rn.PT.58.45226291); *Vash1* (probe 5'-56-FAM/TGCCTACTT/ZEN/TCCAGCCGACAACG/3IABkFQ/-3', F-5'-GCCCAAGATTCCCATACCAA-3' and R-5'-ACTGTGTCCCTGTGTGATTG-3')

(assay name Rn.PT.58.37363926); *Gapdh* (probe 5'-/56-FAM/CAGCACCAG/ZEN/CATCACCCCATTTG/3IABkFQ/-3', F-5'-AACCCATCACCATCTTCCAG-3' and R-5'-CCAGTAGACTCCACGACATAC-3') (assay name Rn.PT.39a.11180736.g) (Integrated DNA Technologies); Polymerase activation at 95 ˚C for 3 minutes and 40 cycles of denaturation at 95˚C for 15 seconds and annealing/extension at 60˚C for 1 minutes. Cycle threshold (Ct) values were quantified on a QuantStudio 3 Real Time PCR system (ThermoFisher). Gene expression fold change was quantified using the delta-delta Ct method normalized to *Gapdh* and the scram group.

For RT-qPCR experiments in human samples, total RNA was extracted from septal myectomies of HCM patients (N=19), from explanted hearts of DCM patients (N=10) and from ischemic cardiomyopathy (ICM, N=10) patients as well as from NF human heart tissue not suitable for transplantation or from donors that did not die from cardiac disease but of another cause (NF, N=10-11) using the SV Total RNA Isolation Kit (Promega) according to the manufacturer's instructions and as described previously.[82] RNA concentration and purity was determined photometrically using the Nanodrop ND-1000. RNA was reverse-transcribed to cDNA using the Superscript III (Invitrogen) kit. Subsequently, RT-qPCR was performed using the Maxima SYBR Green/ROX qPCR Master Mix (Thermo Scientific) and the specific following primers and thermocycle conditions: *GAPDH* (F-5'- ATGTTCGTCATGGGTGTGAA -3' and R-5'-TGAGTCCTTCCACGATACCA -3'), *VASH1* (F-5'-

AGAGGAAGGGGAAGAGGACC-3' and R-5'- GTAGGCACACTCGGTATGGG -3'), *VASH2* (F-5'- GTTCCACGTCAACAAGAGCG and R-5'- CGACAGCCTGTAGTTTGGGA -3'), *SVBP* (F-5'- CAGCAGAGTTGAGAAGGCCA -3' and R-5'- CCAGGAGGCTGCATCTGTTT -3'); Polymerase activation at 95 ˚C for 10 minutes and 40 cycles of denaturation at 95˚C for 15 seconds and annealing/extension at 60˚C for 1 minutes. Relative gene expression of *VASH1, VASH2* and *SVBP* was calculated using the delta Ct method (with a formula 2^ (-delta Ct)) normalized to *GAPDH*.

Microtubule fractionation assay

Isolated rat cardiomyocytes were pelleted by gravity, washed with warm microtubule stabilizing buffer containing 0.1 mol/L PIPES (pH 6.8), 2mmol/L EGTA, 0.1 mmol/L EDTA, 0.5 mmol/L $MgCl_2$, 20% glycerol, and centrifuged at 300 rpm for 2 minutes. The resulting pellet was resuspended in 150 µl microtubule-stabilizing buffer supplemented with 0.1% Triton X-100 and 1X protease and phosphatase Inhibitor cocktail (Cell Signaling #5872S) and incubated for 30 minutes at 37 °C. Next, cells were centrifuged at 300 rpm for 2 minutes and the supernatant was collected as the free tubulin fraction. The resulting pellet was resuspended in 150 µl RIPA buffer (Cayman #10010263) supplemented with extra 0.8% SDS, disrupted by pipetting every 15 minutes on ice for 1 hour, then boiled at 100 °C for 3 minutes. Finally, the fraction was

centrifuged at 12,000 g for 2 minutes and the supernatant was collected as the polymerized fraction.

Western blot

For whole cell protein extraction, isolated rat cardiomyocytes were lysed in RIPA buffer (Cayman #10010263) supplemented with protease and phosphatase Inhibitor cocktail (Cell Signaling #5872S) on ice for 1 hour. The supernatant was collected and combined with 4X loading dye (Li-COR #928-40004), supplemented with 10% 2-mercaptoethonol, and boiled for 8 minutes. The resulting lysate was resolved on SDS-PAGE gel and protein was blotted to nitrocellulose membrane (Li-COR #926-31902) with mini Trans-Blot Cell (Bio-Rad). Membranes were blocked for an hour in Odyssey Blocking Buffer (TBS) (LI-COR #927-50000) and probed with corresponding primary antibodies overnight at 4 °C. Membranes were rinsed with TBS containing 0.5% Tween 20 (TBST) three times and incubated with secondary antibodies TBS supplemented with extra 0.2% Tween 20 for 1 hour at room temperature. Membranes were washed again with TBST (0.5% Tween 20) and imaged on an Odyssey Imager. Image analysis was performed using Image Studio Lite software (LI-COR). All samples were run in duplicates and analyzed in reference to GAPDH.

Antibodies and labels

Detyrosinated tubulin; rabbit polyclonal (Abcam ab48389); western blot: 1: 1,000.

Alpha tubulin; mouse monoclonal, clone DM1A (Cell Signaling #3873); western blot: 1:1,000

TTL; rabbit polyclonal (Proteintech 13618-1-AP); western blot: 1:500.

GAPDH; mouse monoclonal (VWR GenScript A01622-40); western blot: 1:1,000.

IRDye 800CW Donkey anti-Mouse IgG (H + L) (LI-COR 925-32212); western blot: 1:10,000.

IRDye 680RD Donkey anti-Rabbit IgG (H + L) (LI-COR 925-68073); western blot: 1:10,000.

IRDye 680RD Donkey anti-Mouse IgG (H + L) (LI-COR 926-68072); western blot: 1:10,000.

IRDye 800CW Donkey anti-Rabbit IgG (H + L) (LI-COR 926-32213); western blot: 1:10,000.

VASH1; rabbit polyclonal (Abcam ab199732); western blot 1:5000–1:1000

A novel antibody for human and mouse VASH1 (named anti-VASH1 Gre) was produced in rabbits by using a peptide C-RIRGATDLPKIPIPSVPTFQPTTPV-NH2 (corresponding to exposed region of the protein, see Wang, Bosc and Choi et al.)[70] linked at the N-terminal to the keyhole limpet hemocyanin protein via the cysteine. Sera from rabbits were purified on the respective peptides. Validation of these antibodies was performed in HEK293T cells protein extracts (see **Appendix Figure 1**). HEK293T cultures and

transfections, as well as SDS-PAGE and immunoblots, were performed as in Aillaud et al.[48]

Co-immunoprecipitation (co-IP)

Isolated rat cardiomyocytes were lysed in IP buffer containing Tris 50mmol/L pH 8, NaCL 150mmol/L, NP40 1% and protease inhibitor cocktail (Cell Signaling #5872S) on ice for 30 minutes with pipetting every 10 minutes. Protein concentration was quantified using Braford dye reagent (Bio-Rad #5000205). Equal amount of protein (1.5 mg) from each sample was incubated with 6.5µg of anti-SVBP (Gre) and 10µl of Dynabeads protein G (Invitrogen 10004D, rinsed four times with ice-cold PBS before used), mixed on a tube revolver (Thermo Fisher #11-676-341F5). Negative controls for co-IP were run with Rabbit IgG (6.5µg) or without antibody. After overnight incubation at 4˚C, beads were rinsed with IP buffer for four times and eluted at room temperature using 30µl 1X Laemli buffer (Bio-Rad) supplemented with 2-mercaptoethonol. Elution supernatant was then transferred to fresh tubes and heated at 70˚C for 5 min. Fifteen µl of the elution from co-IP and whole cells lysates were used in western blot, performed as described above except the followings. Blots were stained with anti-VASH1 (Gre) at 1:1,000 at 4˚C overnight and a secondary antibody against native rabbit IgG at 1:1,000 (TrueBlot anti-rabbit IgG HRP from Rockland #18-8816-31) at room temperature for 1 hour. Blots were developed using a chemiluminescent substrate (West Pico Plus, Thermo Fisher #34577) and autoradiography film (Hyblot CL #E3012).

Nanoindentation

Mechanical properties at the microscopic scale were measured using nanoindentation[69] (Piuma Chiaro, Optics11, The Netherlands). Freshly isolated human myocytes were attached to glass bottom dishes coated with MyoTak[7] in normal Tyrode's solution containing 140 mmol/L NaCl, 0.5mmol/L $MgCl_2$, 0.33 mmol/L NaH_2PO_4, 5 mmol/L HEPES, 5.5 mmol/L glucose, 1 mmol/L CaCl2, 5 mmol/L KCl, pH to 7.4 at room temperature. A spherical nano-indentation probe with a radius of 3.05 μm and a stiffness of 0.026 N m^{-1} was used. Myocytes were indented to a depth of 1.5–3.5 μm with velocities of 0.1, 0.25, 0.5, 1.0, 2.0, 5.0, 10.0, 20.0, 50.0, 100.0, and 150.0 μm s^{-1}. The tip was held in this indentation depth for 1 s, and retracted over 2 s. The Young's moduli were calculated automatically by the software, by fitting the force versus indentation curve to the Hertz equation.

Statistics

Statistical analysis and graphing were performed using OrginPro software (OriginLabs). Values are presented as mean ± s.e.m. in line graphs and bar graphs (Figure 3D through F; Figure 4D), and when stated in the results. For box plots, box represents 25th to 75th percentiles, the whiskers 1 s.d. and mean line. Data was checked for normality via Kolmogorov Smirnov test within OriginPro. All experiments were replicated in multiple rat or human hearts (biologically independent samples/independent experiments) for each condition, indicated by

the N number in each figure and figure legend. The exact n values used to calculate statistics and the statistical tests for significance are stated in individual graphs or figure legends. Two-sided t-tests were used to determined statistical significance between experimental conditions vs. control (**Figure 4F**; **Figure 4G** VASH2 KD). One-way analysis of variance (ANOVA) (**Figure 4C and 4D**; **Figure 6B and 6C**) or two-way ANOVA (**Figure 7C**) with post-hoc Bonferroni test. Given that multiple comparisons were both repetitive and restricted and could increase the chance of type 1 error (testing multiple parameters derived from one experiment e.g. contractility), the Bonferroni correction was applied after two-sided *t*-tests to adjust the significance threshold by dividing it with the number of tests, as described in each figure legend where appropriate, and unadjusted P values are reported in the figures (**Figure 4B**; **Figure 7D** through **F**; **Figure 7B** through **7D**).

CHAPTER 4: DESMIN INTERMEDIATE FILAMENTS AND TUBULIN DETYROSINATION STABLIZE GROWING MICROTUBULES AT THE CARDIOMYOCYTE Z-DISC

Adapted from manuscript currently in review for publication in eLife: **Salomon A.K**., Okami N., Heffler, J., Lee JJ., Robison P., Bogush AI., Prosser BL. (2021). Desmin intermediate filaments and tubulin detyrosination stabilize growing microtubules in the cardiomyocyte.

Introduction

Microtubules are polymers of α- and β-tubulin that are characterized by cyclical transitions between polymerization and depolymerization, a behavior called dynamic instability[12]. Tuning this dynamic behavior confers unique functionality to specific sub-populations of microtubules[83]. Control of microtubule dynamics is cell type- and context-specific and can occur either by modulating polymer addition or subtraction at the ends, or through lateral interaction with the microtubule polymer[17]. The temporal and spatial control of dynamics can be tuned by post-translational modification of tubulin, which in turn affects the biophysical properties of the microtubule and interactions with microtubule associated proteins (MAPs)[84]. For example, detyrosination, the post translational removal of the C-terminal tyrosine residue on α-tubulin, has been shown to increase microtubule stability in mitotic cells by preventing their interaction with depolymerizing MAPs[55].

In the cardiomyocyte, microtubules fulfill both canonical roles in intracellular trafficking and organelle positioning[66], as well as non-canonical functions matched to the unique demands of working myocytes. In the interior of

the myocyte, microtubules form a predominantly longitudinal network that runs perpendicular to the transverse Z-discs that define the sarcomere, the basic contractile unit of muscle **(Figure 10A**). Sub-populations of microtubules form physical connections with the Z-disc that serve as lateral reinforcements along the length of the microtubule[32]. Upon stimulation and sarcomere shortening, these physically coupled microtubules buckle at short stereotypical wavelengths between sarcomeres to resist the change in myocyte length[32]. The physical ramifications of these reinforced microtubules for the myocyte are significant, as reinforced microtubules can resist 1000x more force than uncoupled microtubules[30,85]. This viscoelastic resistance becomes particularly problematic in heart failure, where proliferation of longitudinal, coupled microtubules stiffens the cardiomyocyte and impairs myocyte motion[46].

Physical coupling of the microtubule to the sarcomere is tuned by detyrosination. Genetic reduction of detyrosination by overexpression of tubulin tyrosine ligase (TTL), the enzyme responsible for ligating the terminal tyrosine residue on detyrosinated tubulin, reduces sarcomeric buckling and the viscoelastic resistance provided by microtubules, increasing myocyte contractility[46]. Tyrosination status also governs microtubule-dependent mechanotransduction in muscle that regulates downstream second messengers and is implicated in myopathic states [8]. Given its ability to lower stiffness and improve the function of myocardium from patients with heart failure[46], tyrosination is under pursuit as a novel therapeutic approach. Yet how detyrosination

promotes the interaction of microtubules with the sarcomere to mediate their mechanical impact remains poorly understood.

Several observations suggest this interaction may be mediated at least in part through desmin intermediate filaments that wrap around the Z-disk. Detyrosination promotes microtubule interaction with intermediate filaments[32,86], and in the absence of desmin, microtubules are disorganized and detyrosination no longer alters myocyte mechanics[32]. Additionally, a recent pre-print indicates that intermediate filaments can directly stabilize dynamic microtubules in vitro[56].

Despite this evidence, the effects of desmin or detyrosination on the dynamics of cardiomyocyte microtubules have not been investigated. We hypothesized that desmin may serve to stabilize growing microtubules at the Z-disk, which would represent an important intermediary in laterally reinforcing the network and coupling microtubules to the sarcomere. Here, using a combination of genetic manipulations, biochemical assays, and direct live-cell observation of dynamic microtubules, we directly interrogated the effect of tyrosination status and desmin depletion on microtubule dynamics. We find that desmin dictates the spatial organization of microtubule dynamics and that growing microtubules are stabilized at the Z-disc in a desmin-dependent fashion. Additionally, we find that tyrosinated microtubules are more dynamic, a characteristic that precludes their ability to efficiently grow between adjacent sarcomeres and form stabilizing interactions at the Z-disk. These findings provide insight into the organizing

principles of myocyte cytoarchitecture and into the mechanism of action for therapeutic strategies that target detyrosinated microtubules.

Results

Tyrosination alters the dynamics of the microtubule network

We first sought to determine the effect of detyrosination on the dynamics of the cardiomyocyte microtubule network. To reduce detyrosination, we utilized adenoviral delivery of TTL into isolated adult rat cardiomyocytes[32]. TTL binds and tyrosinates tubulin in a 1:1 complex, and so we also utilized adenoviral delivery of TTL-E331Q (E331Q), a verified catalytically dead mutant of TTL[14], to separate effects of tubulin tyrosination from tubulin sequestration. We have previously confirmed that TTL overexpression under identical conditions reduces detyrosination below 25% of initial levels, while TTL-E331Q does not significantly affect detyrosination levels with similar overexpression[42]. To specifically quantify the effects of reducing detyrosination on the dynamic microtubule population, we adapted a subcellular fractionation assay from Fasset et al., 2009[87] that allowed us to separate free tubulin from polymerized tubulin in the dynamic (i.e. cold-sensitive) microtubule pool (**Figure 10B)**.

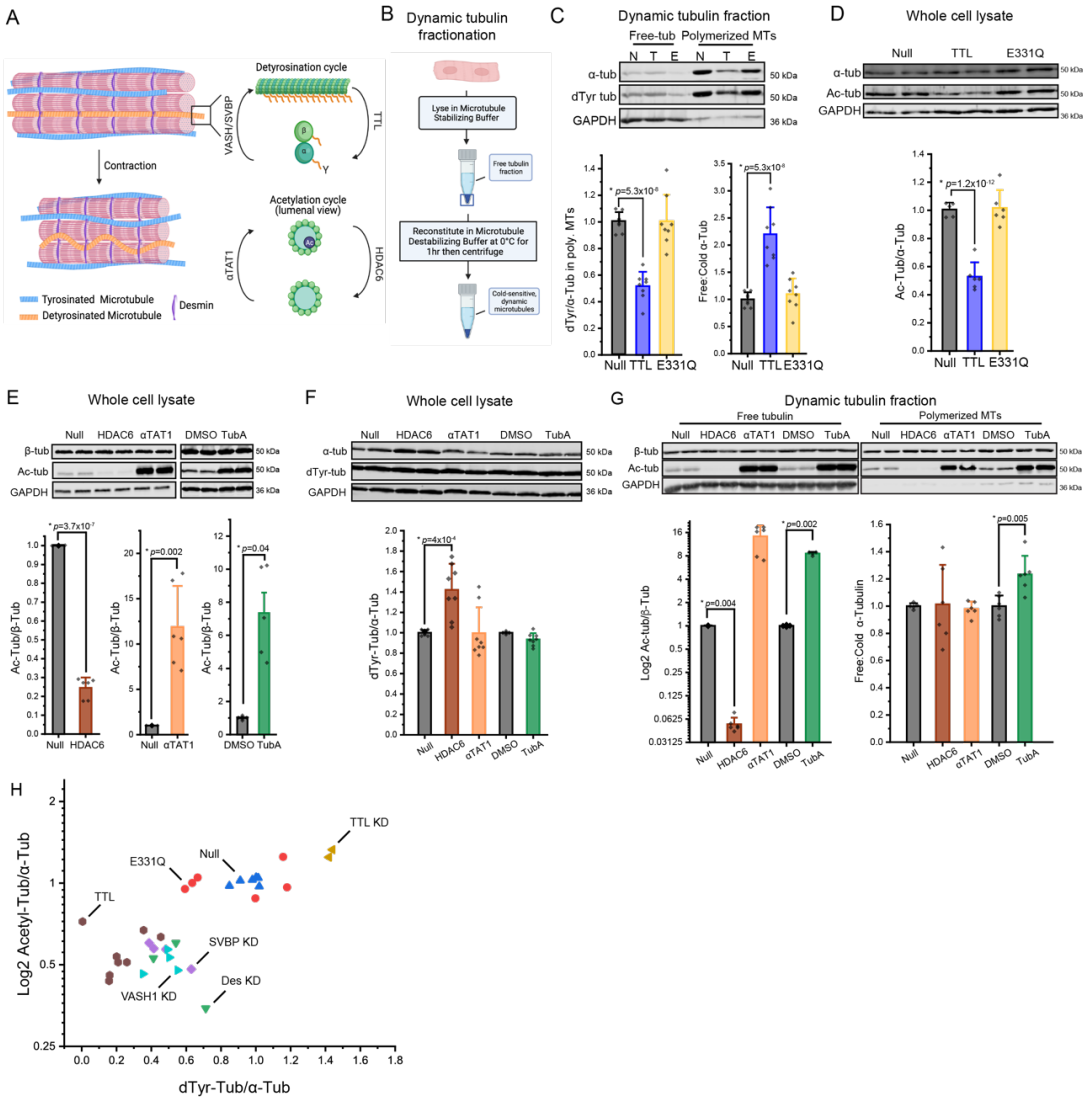

Figure 10. Tyrosination specifically alters microtubule stability. A Left, Schematic depicting detyrosinated microtubules (orange) buckling due to physical coupling with desmin at the Z-disc. Uncoupled tyrosinated microtubules (blue) do not buckle[32]. Right, Detyrosination and Acetylation cycles. **B** Overview of the cell fractionation assay adapted from Fasset et al. [87] that allows for separation of free tubulin and polymerized microtubules within the dynamic tubulin pool. **C** Representative western blot (**top)** and quantification (**bottom)** of α-tubulin, detyrosinated (dTyr) tubulin, and GAPDH in free and cold-sensitive microtubule fractions from adult rat cardiomyocytes infected with either null, TTL, or TTL-E331Q adenovirus. Detyrosinated tubulin values normalized to α-tubulin in cold-sensitive fraction. **D** Representative western blot (**top)** and quantification (**bottom)** of α-tubulin, acetylated tubulin, and GAPDH in whole-cell lysate from null, TTL, or E331Q expressing myocytes. **E** Validation of HDAC6 and αTAT1 constructs and Tubastatin a (TubA) treatment. Representative western blot (**top**) and quantification (**bottom**) of β-tubulin, acetylated tubulin, and GAPDH in whole-cell lysate from adult rat cardiomyocytes infected with HDAC6, αTAT1, or null adenovirus or treated with 1 μM TubA or DMSO overnight. **F** Representative western blot (**top**) and quantification **(bottom**) of α-tubulin, dTyr, and GAPDH in whole cell lysate from adult rat cardiomyocytes infected with HDAC6, αTAT1, or null adenovirus or treated with 1 μM TubA or DMSO overnight. **G** Representative western blot (**top)** and

quantification (**bottom**) of β-tubulin, acetylated tubulin, and GAPDH in free and polymerized dynamic fractions. Lysate from myocytes infected with HDAC6, αTAT1, or null adenovirus or treated with 1 μM TubA or DMSO overnight. **H** Relationship between detyrosinated tubulin levels and acetylated tubulin in lysate from cardiomyocytes infected with Null, TTL, E331Q, shTTL, shVASH1, shSVBP, or shDes adenovirus. Western blot data points represent technical replicates (2 from each biological replicate) normalized to their respective controls (N=4 in C+F; N=3 in D, E, G). Statistical significance determined via two-sample T test with alpha adjusted for multiple comparisons. Data are presented as mean±SEM unless otherwise specified.

Expression of TTL, but not E331Q, resulted in significantly less detyrosinated tubulin in the dynamic microtubule pool (**Figure 10C**). Further, only TTL expression shifted tubulin away from the polymerized fraction towards the free tubulin fraction, resulting in an increased ratio of free: polymerized tubulin (**Figure 10C, Figure 11A**). This suggests that tyrosination effects the cycling of tubulin within the dynamic microtubule pool. If indeed tyrosinated microtubules are more dynamic, then levels of acetylation, a canonical marker of long-lived microtubules[88], should also be decreased by TTL. Consistent with this, TTL, but not E331Q, led to a robust reduction in levels of microtubule acetylation, suggesting that tyrosination reduces microtubule lifetime in the cardiomyocyte (**Fig 10D)**.

As acetylation itself is linked to microtubule stability[53,89], the TTL-dependent change in the dynamic microtubule pool **(Fig 10C)** could be directly related to tyrosination or secondary to the associated reduction in acetylation **(Fig 10D)**. To discriminate between these two hypotheses, we directly modulated acetylation. To this end, we developed adenoviral constructs encoding histone deacetylase 6 (HDAC6) and α tubulin acetyltransferase 1 (αTAT1). HDAC6

expression reduced total microtubule acetylation to 25% of initial levels (**Fig 10E**) and αTAT1 expression increased acetylation 12-fold (**Fig 10E**). Because αTAT1 has been shown to modulate microtubule dynamics independent of enzymatic activity[90], we also used a pharmacological inhibitor of HDAC6, Tubastatin A (TubA) to increase acetylation through an orthogonal approach (**Fig 10E**). Having validated robust tools to modulate acetylation, we next determined the effect of acetylation on the dynamic microtubule pool utilizing the same fractionation assay. HDAC6 expression resulted in less acetylation in the cold-sensitive fraction while both αTAT1 expression and TubA treatment increased levels of acetylated tubulin. Neither genetic methods to increase or decrease acetylation altered the free:polymerized tubulin (**Fig 1G, S. Fig 1B**); however, TubA treatment modestly increased the free:polymerized tubulin ratio, suggesting that while microtubule dynamics are likely unaffected by changing levels of acetylation, the presence of HDAC6 protein may affect microtubule dynamics as observed previously[91]. Given that modulating tyrosination altered levels of acetylation (**Fig 1D**), we also asked whether this relationship was reciprocal. However, whole cell levels of detyrosination were largely unaffected by modulating acetylation (**Fig 1F**), except for a modest increase with HDAC6 expression that may be related to HDAC6 association with microtubules increasing their stability and availability for detyrosination[91].

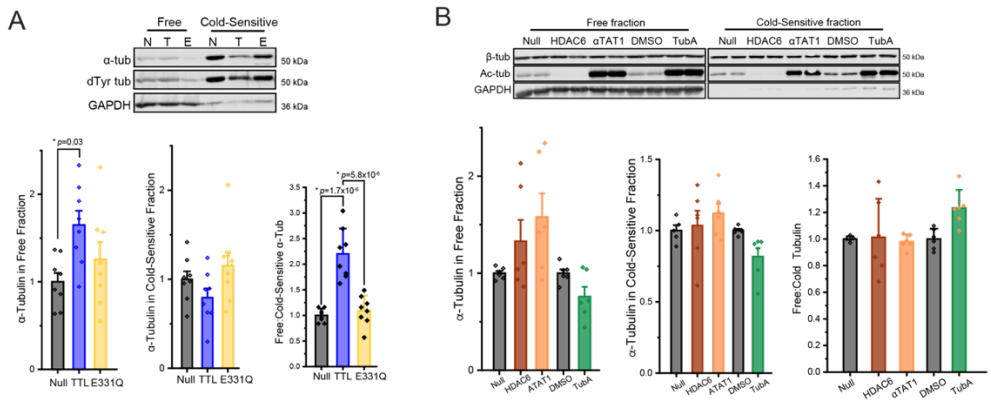

Figure 11. Quantification of free and polymerized tubulin fractions presented in figure 10. **A** Representative western blot (**top**) and quantification (**bottom**) for α-tubulin, dTyr tubulin, and GAPDH in free and cold-sensitive fractions from rat cardiomyocytes infected with null, TTL, or E331Q adenovirus. **B** Representative western blot (**top**) and quantification (**bottom**) for α-tubulin, dTyr tubulin, and GAPDH in free and cold-sensitive fractions from rat cardiomyocytes either infected with null, HDAC, or ATAT1 adenovirus or treated with DMSO or TubA. Statistical significance determined via ANOVA with post hoc Bonferroni test.

Tyrosination increases catastrophes of growing microtubules

I next wanted to more precisely quantify the effects of tyrosination on the dynamics of individual microtubules. Microtubule dynamics (**Figure 12A)** are characterized by their rates of growth (polymerization) and shrinkage (depolymerization) as well as the frequency of transitions between these two states. Events are categorized as catastrophes (transitions from growth to shrinkage), rescues (transitions from shrinkage to growth), and pauses (neither growth nor shrinkage). We directly observed the microtubule plus-ends by time-lapse imaging of a fluorescent end-binding protein 3 (EB3-GFP) construct expressed via adenovirus in isolated rat cardiomyocytes (**Movie 1** in Appendix**)**. By creating kymographs from these videos, we were able to quantify dynamic events (rescue, catastrophe, and pause) in addition to microtubule growth and

shrinkage kinetics (**Fig 12B)**. We harnessed off-target EB3-GFP Z-disc localization to characterize dynamic events as occurring on or off the Z-disc, as in Drum et al.[50] As we noted higher variability in measurements from one cell isolation to another than between cells from the same isolation, experimental data were normalized to control data that were acquired from the same animals.

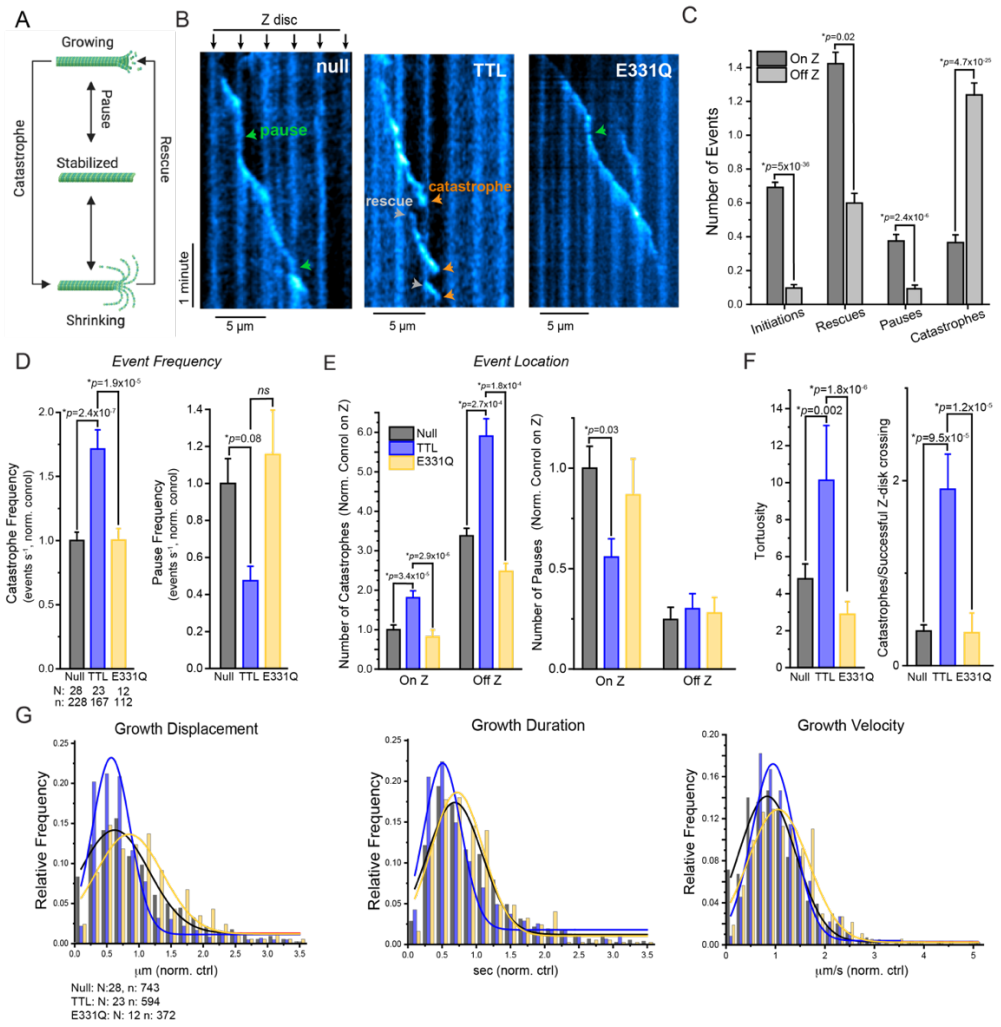

Figure 12. Tyrosinated microtubules are more dynamic. A Schematic of microtubule dynamic events. **B** Representative kymographs from cardiomyocytes infected with EB3-GFP plus null, TTL or E331Q adenovirus. Arrowheads denote Z-discs. **C** Number of initiations, rescues, pauses, and catastrophes that occur on and off the Z-disc in isolated cardiomyocytes infected with null adenovirus. **D** Cell-wide catastrophe (**left**) and pause (**right**) frequency in myocytes infected with null, TTL, or E331Q adenovirus. **E** Number of catastrophes (**left)** and pauses (**right)** that occur on

and off the Z-disc in myocytes infected with null (black), TTL (blue), or E331Q (yellow) adenovirus. **F** Gross measurements of microtubule dynamics. Tortuosity, the distance a microtubule grows divided by its displacement (**left**), and number of catastrophes in relation to number of successful Z-disk crossing (**right),** in myocytes infected with null, TTL, or E331Q adenovirus. **G** Frequency distribution of average microtubule growth displacement, duration, and velocity in myocytes infected with null, TTL, or E331Q adenovirus. Data are normalized to the average null value for the corresponding experiment. Statistical significance was determined with Kruskal-Wallis ANOVA with post-hoc test. Data are presented as mean±SEM unless otherwise specified.

We began with multiple control experiments. Although EB interaction is thought to be unaffected by microtubule detyrosination[92], we wanted to validate that EB3 labeling of microtubules did not systematically differ with TTL expression. EB3 fluorescence intensity along the length and at the tip of the microtubule was unchanged in control, TTL or E331Q expressing cells (**Figure 13A**), indicating that EB3 expression or labeling of microtubules was not altered by our experimental interventions.

As adult ventricular cardiomyocytes are normally paced in vivo but quiescent in vitro, we sought to determine whether electrical pacing and evoked contractions would overtly alter microtubule dynamics. To this end, we timed the imaging of EB3 puncta to occur during the diastolic rest interval between each contraction of cardiomyocytes that were electrically paced at 0.5Hz. Internally controlled, pre- and post-comparisons of microtubule dynamics before and during electrical stimulation showed no significant effect of stimulation on microtubule dynamic events or growth kinetics in rat cardiomyocytes **(Figure 13B**). As such, for the remainder of this study we interrogated quiescent cardiomyocytes to minimize movement artifacts.

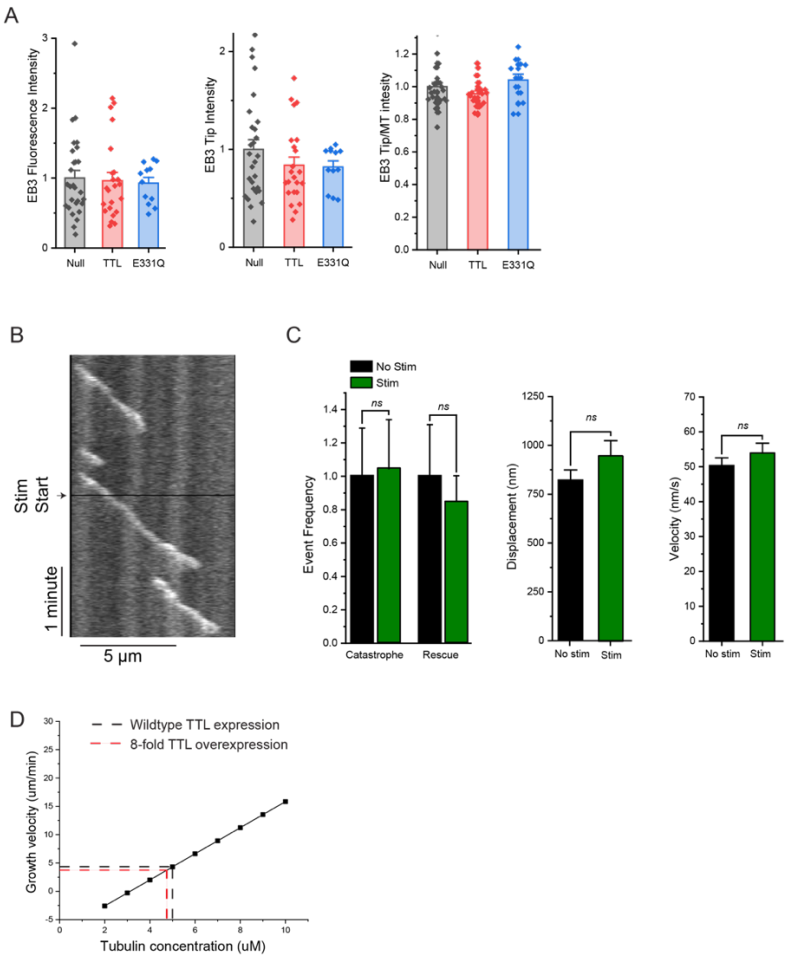

Figure 13. Supporting data for figure 12. A Background (**left)** EB3-GFP fluorescence intensity, EB3 tip fluorescence intensity (**center**) and the ratio of EB3 tip fluorescence intensity to microtubule EB3 intensity (**right)** in isolated rat cardiomyocytes co-infected with null, TTL, or E331Q adenovirus. Statistical significance determined via ANOVA with post hoc Bonferroni test. **B** Representative EB3-GFP kymograph from isolated rat cardiomyocyte before and after 0.5 Hz electrical stimulation. **C** Quantification of catastrophe frequency, rescue frequency, microtubule growth displacement and growth velocity before and after electrical stimulation. **D** To reduce levels of detyrosination in this study we relied on overexpression of TTL, which is known to associate with the free α/β tubulin heterodimer in a 1:1 complex with a K_d of 1 μM[44]. Due to the nature of this interaction, TTL overexpression can decrease the amount of "polymerization-competent" tubulin, leading to a decrease of *in vitro* microtubule polymerization[44]. The relationship between free tubulin concentration and microtubule polymerization is described as a simple 1D model below, where ν_g is the velocity of microtubule growth, *d* is the dimer length (assumed to be 8 nm), k_{on} is the tubulin dimer association constant per protofilament (assumed to be 4.8 $\mu M^{-1}s^{-1}$)[30], k_{off} is the tubulin dissociation rate constant per protofilament (assumed to be 15s^{-1})[30] , and [Tb] is the concentration of free tubulin[51].

$$\nu_g = d\left(k_{on}[Tb] - k_{off}\right).$$

Solving for the equation of the line at a physiologic tubulin concentration of 5μM provides a theoretical value of 4.32 μm s^{-1} for growth velocity. Using the K_d value for TTL-tubulin interaction at a tubulin concentration of 5μM suggests that an 8-fold overexpression of TTL [42]will produce 0.2 μM of TTL-tubulin complex. If we assume that tubulin bound to TTL cannot be polymerized, then only 4.8 μM of free tubulin is polymerization-competent at any time. This change in polymerization-competent tubulin would lead to ~10% decrease in growth velocity. We did not observe an effect of E331Q on microtubule growth kinetics or on event frequency suggesting that the local tubulin concentration at the microtubule plus-tip is unaffected by the sequestration activity of TTL. Statistical significance determined via 2-sided t test.

Under basal conditions, we observed a stark spatial bias in microtubule dynamic behavior, similar to that observed by Drum et al[50]. The initiation of microtubule growth, as well as pausing of growth, predominantly occurred on the Z-disc (**Figure 12C)**. Conversely, catastrophes predominantly occurred off the Z-disc, while rescue from catastrophe again occurred more frequently at the Z-disc. As exemplified in **Movies 1-2** (in the appendix), in control (AdV-null) expressing myocytes microtubules tend to grow iteratively from one Z-disk to another, often pausing at each Z-disk region. If a microtubule undergoes catastrophe before reaching a Z-disk, it tends to shrink to a previous Z-disk, where rescue is more likely to occur. These data suggest factors at the Z-disc region strongly bias microtubule behavior and support the initialization as well as stabilization of growing microtubules.

We next interrogated the role of tyrosination. As seen in **Movie 3** (in the appendix), microtubules in TTL treated cells also initiated growth at the Z-disk, but often had shorter runs and underwent catastrophe prior to reaching a subsequent Z-disk. Consistently, TTL overexpression significantly increased the frequency of catastrophes, while tending to reduce the frequency of pausing

(**Figure 12B** and **D**). E331Q expression did not alter event frequency **(Movie 4** in the appendix**)**, suggesting a tyrosination-specific effect on microtubule dynamics. Further examination of spatial dynamics revealed that TTL similarly increased the number of catastrophes both on and off the Z-disc while reducing the number of pauses specifically on the Z-disc (**Figure 12E**). As a readout of inefficient growth, TTL increased microtubule tortuosity, the ratio of growth distance to growth displacement (**Figure 12F**). Combined, the lack of stabilization at the Z-disc and more frequent catastrophes resulted in tyrosinated microtubules breaking down ~4 fold as often before successfully crossing a Z-disk when compared to either null or E331Q expressing cells (**Figure 12F**). Consistent with an increased frequency of catastrophe, growth events in TTL myocytes were shorter in duration and traveled less distance, despite similar growth velocity (**Figure 12G).** Of note, cells expressing E331Q showed comparable growth metrics and event frequencies to control infected myocytes, indicating that TTL's effect on microtubule dynamics is due to tyrosination and not tubulin binding. Substantial overexpression of TTL or E331Q could reduce growth velocity by limiting tubulin available for polymerization; we calculated the predicted effect of our level of overexpression on tubulin growth velocity and found a negligible effect on growth kinetics (**Figure 13D)**, consistent with our experimental observations (**Figure 12G)**.

I next sought to provide an underlying mechanism for the tyrosination-dependent increase in catastrophe rate. I hypothesized that knockdown of MCAK

in, a depolymerizing kinesin with preference for tyrosinated microtubules, in TTL expressing myocytes would prevent the observed increase in catastrophe frequency. To knockdown MCAK protein I purchased three short interfering RNAs (siRNAs) specific for Kif2c, the RNA transcript for MCAK. To validate the siRNAs I used the H9C2 rat cardiac myoblast cell line as these cells are proliferative and should express more MCAK protein than adult myocytes. I also used H9C2 cells to validate the commercially obtained antibody and qPCR primers to quantify Kif2c expression. siRNAs for Kif2c were transfected into H9C2s and allowed to express for 48 hours. Incubation of H9C2 lysate with the antibody for MCAK resulted in a very faint band at the predicted molecular weight (**Figure 14A** and **B)** suggesting quantification of MCAK protein knockdown with the current antibody is unreliable. I selected siRNA #1 (siKif2c-1) to be made into a short hairpin RNA (shRNA) and packaged into AAV. Expression of shRNA specific for Kif2c in adult rat cardiomyocytes resulted in knockdown when quantified by qPCR (**Figure 14C)**; however, copy numbers of Kif2c in control cells were high and close to the limit of detection suggesting expression of MCAK is very low in the adult myocyte. Further validation is required to ensure that MCAK is expressed in the adult rat cardiomyocyte and if MCAK knockdown is successful before the stated hypothesis can be answered.

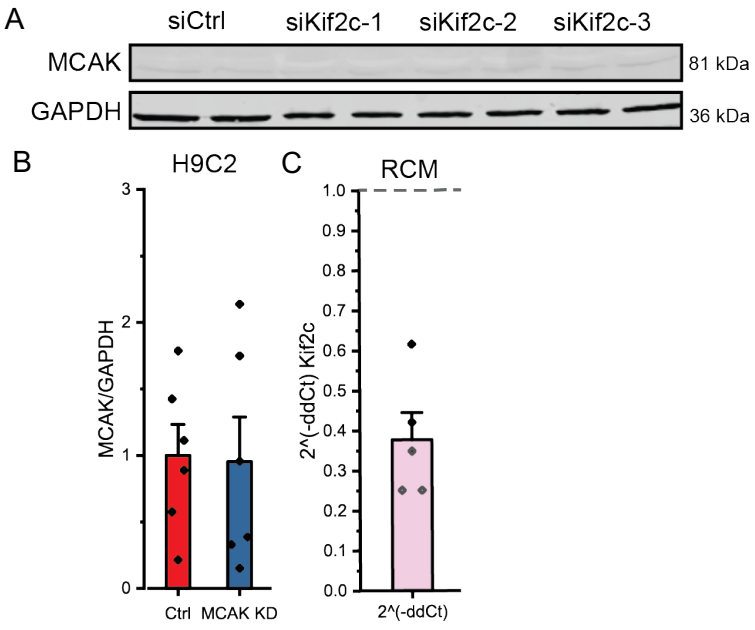

Figure 14. Partial validation of MCAK knockdown. A Lysate from H9C2 cells transfected with three siRNAs for Kif2c (MCAK transcript). Faint band at the predicted molecular weight was quantified. **B** Quantification of H9C2 cells transfected with siRNA Kif2c-1from **A**. **C** Quantification of Kif2c transcript by qPCR from adult rat cardiomyocytes transfected with shRNA for Kif2c. Transcript was quantified by delta ct method compared to gapdh expression. For **B** N=3 independent plates of cells and **C** N=3 rats.

Desmin structures the growing microtubule network

We hypothesized that desmin intermediate filaments could be the Z-disc stabilizing factor for growing microtubules, based in part on the gross microtubule misalignment observed in the absence of desmin[93], and from our observation that microtubules tend to traverse the Z-disc at desmin-enriched regions[46].

To determine if desmin regulates the dynamic population of microtubules, we utilized the previously described fractionation assay **(Figure 11B)** with lysate

from rat cardiomyocytes infected with adenoviruses encoding shRNA against desmin (Des KD) or a scramble control (scram).

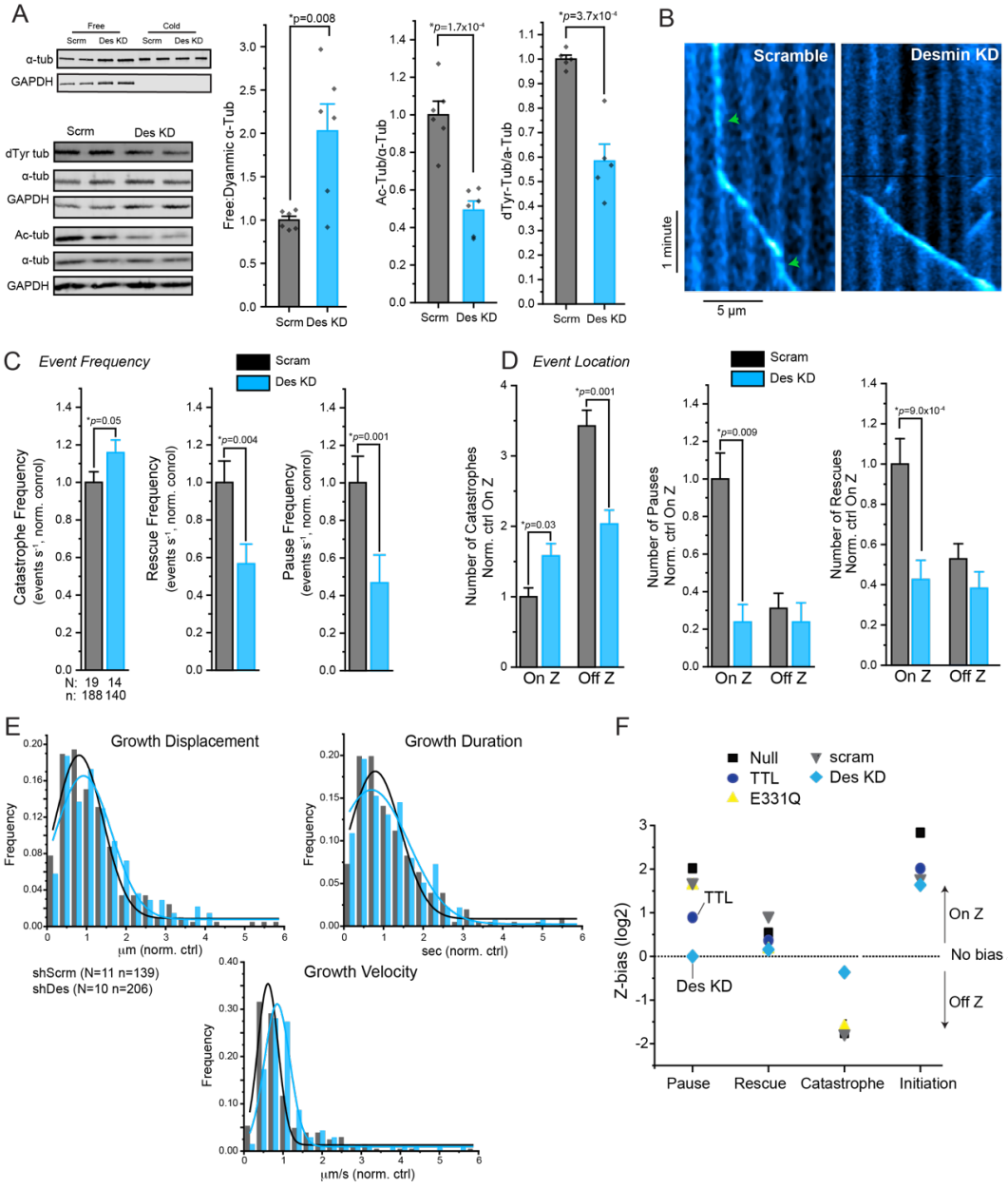

Figure 15. Desmin stabilizes the growing microtubule at the Z-disc. A Representative western blot (**left**) and quantification (**right**) of α-tubulin, dTyr, acetylated tubulin, and GAPDH in free, cold-sensitive, or whole-cell lysate from isolated rat cardiomyocytes expressing either scramble (scrm) or desmin specific shRNA (Des KD). **B** Representative EB3-GFP kymograph

from control or desmin KD myocytes. **C** Cell-wide catastrophe (**left)**, rescue (**middle**), and pause (**right)** frequency with or without desmin KD. **D** Number of catastrophes (**left)**, pauses (**middle)**, and rescues (**right)** that occur on or off the Z-disc with or without desmin KD. **E** Frequency distribution of average microtubule growth displacement, duration, and velocity with or without desmin KD. **F.** Z-disc bias score (log2 transform of the ratio of events that occurred on vs. off the Z-disk) for all experimental conditions. Data are normalized to the average control value for the corresponding experiment. Statistical significance determined with Two Sample Kolmogorov-Smirnov Test. Data are presented as mean±SEM unless otherwise specified.

This construct has been previously validated to reduce desmin protein levels ~70% under identical conditions[6]. Desmin depletion resulted in an increased free to polymerized ratio in the dynamic microtubule pool (**Figure 15A, Figure 16A)**, suggesting that desmin coordinates the stability of dynamic microtubules. We next quantified microtubule acetylation and detyrosination, markers of long-lived microtubules, and found that both were decreased in desmin depleted myocytes, without alterations in whole cell tubulin content (**Figure 15A**).

We next directly quantified plus-end microtubule dynamics by EB3-GFP upon desmin depletion. As seen in **Movies 5-6 (**in the appendix), upon desmin depletion microtubule growth still initiated at the Z-disk, but the iterative, longitudinal growth from one Z-disk to another seen in control cells was lost. Instead, microtubules often grew past Z-disk regions without pausing (**Figure 15B)**, and when breaking down they were less likely to be rescued at the previous Z-disk. Blind quantification of global event frequency revealed that desmin depletion modestly increased the frequency of catastrophes while more robustly reducing both the frequency of rescues and pauses (**Figure 15C**). Interrogation of where dynamic events occurred in relation to the Z-disk revealed

that desmin depletion specifically increased the number of catastrophes that occurred only on the Z-disk (**Figure 15D**), while reducing the number of catastrophes that occurred off the Z-disk. More strikingly, desmin depletion markedly reduced the number of pauses and rescues that occur specifically on the Z-disk, while not affecting pause or rescue behavior elsewhere (**Figure 15D**). Growth events tended to travel longer distance with higher velocities in Des KD cells (**Figure 15E).** Together, these results indicate that desmin is spatially coordinates microtubule dynamics and stabilizes both the growing and shrinking microtubule at the Z-disk.

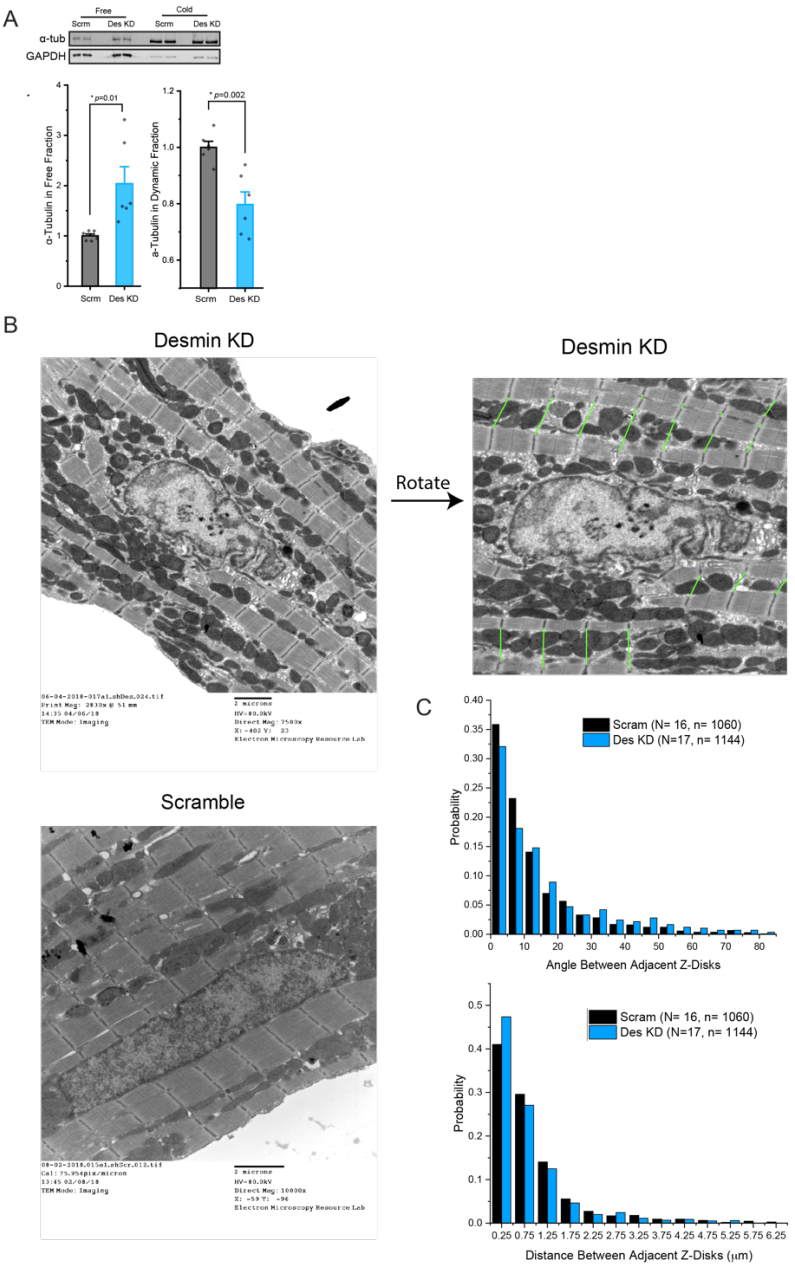

Figure 16. Supporting data for figure 15. A Representative western blot (**top**) and quantification (**bottom**) for α-tubulin and GAPDH in free and cold-sensitive fractions from rat cardiomyocytes infected with adenovirus containing scramble shRNA (scrm) or shRNA for desmin (Des KD). **B** Representative electron microscopy images of isolated rat cardiomyocytes with or without desmin knockdown. **C** Probability density plot of angle (**top)** and distance **(bottom)** between adjacent Z-discs with or without desmin knockdown.

As the Z-disk region coordinates microtubule dynamics, we sought to summarize how our different interventions (TTL, Desmin KD) affected the spatial organization of microtubule behavior. By taking the ratio of events that occurred on vs. off the Z-disk and performing a log2 transform, we calculated a Z-disk bias for each type of dynamic event (**Figure 14F**). Of note, this metric only reflects the spatial bias of events, not their frequencies. TTL reduced the preference for microtubule pausing at the Z-disk, but did not affect the spatial preference of rescues, catastrophes, or initiations (TTL increased catastrophe frequency in a spatially-agnostic fashion). Desmin depletion, on the other hand, virtually eliminated any spatial preference of pausing, rescue, or catastrophe behavior. Initiations had a strong Z-bias regardless of intervention, which likely reflects nucleating events from microtubule organizing centers at Golgi outposts proximal to the Z-disk that are not affected by these manipulations[49].

Cardiomyocytes from global, desmin germ-line knockout mice are characterized by misaligned and degenerated sarcomeres[94] with a disorganized microtubule network [32]. Gross restructuring of the myofilaments could affect microtubule dynamics due to a change in the physical environment that is permissive to microtubule growth, for example by increasing the spacing between Z-discs of adjacent myofilaments. To assess if our acute desmin depletion altered myofilament spacing or alignment, we performed quantitative measurements on electron micrographs from desmin depleted cardiomyocytes. Blind analysis indicated that acute desmin depletion did not change myofilament

spacing or alignment at this level of resolution (**Figure 15B**), consistent instead with a direct stabilizing effect of desmin intermediate filaments on the microtubule network.

We next wanted to visualize the effect of desmin depletion on whole-cell microtubule network organization. Airyscan imaging and blind image quantification indicated a reduction of the percent cell area occupied by both detyrosinated and tyrosinated microtubules (**Figure 17A-B**), consistent with reduced stability of microtubules upon desmin depletion. As a reduction in detyrosinated microtubules and their association with the Z-disc is associated with reduced cardiomyocyte viscoelasticity[32], we hypothesized that desmin-depleted myocytes would be less stiff. To test this, we performed transverse nanoindentation of cardiomyocytes and quantified Young's modulus of the myocyte over a range of indentation rates. Desmin depletion specifically reduced the rate-dependent (viscoelastic) stiffness of the myocyte (**Figure 17C)**, without significantly altering rate-independent (elastic) stiffness. Reduced viscoelasticity is consistent with reduced transient interactions between dynamic cytoskeletal filaments. To directly test if the reduction in desmin alters microtubule buckling between sarcomeres, we performed a semi-automated, blind analysis of microtubule buckling, as in our previous work[32]. In control cells, most microtubules buckle in a clear sinusoidal pattern with a wavelength corresponding to the distance of a contracted sarcomere (~1.5-1.9 μm) (**Figure 17D** and **G, Movie 7**). Upon desmin depletion, fewer polymerized microtubules

were observed in general, with more chaotic deformations and organization upon contraction **Movie 8**). For microtubules that did buckle, the amplitude of buckles was reduced (**Figure 17E**), as well as the proportion of microtubules that buckled at wavelengths corresponding to the distance between 1 or 2 sarcomeres (1.5-1.9 or 3.0-3.8 μm, respectively, **Figure 17F)**. Combined, these results are consistent with desmin coordinating the physical tethering and lateral reinforcement of detyrosinated microtubules at the cardiomyocyte Z-disk to regulate myocyte viscoelasticity.

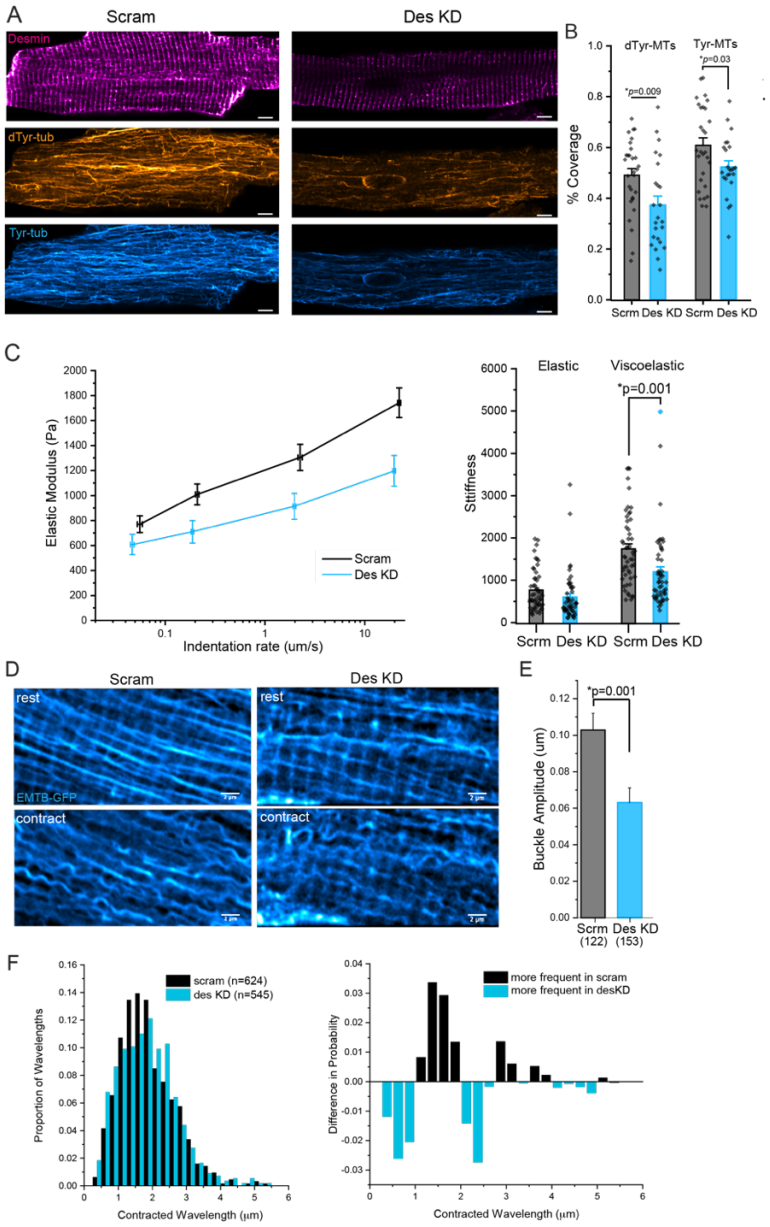

Figure 17. Desmin facilitates the microtubule contribution to viscoelastic resistance. A. Representative Airyscan images of desmin (magenta), detyrosinated tubulin (orange), and tyrosinated tubulin (cyan) in isolated adult rat cardiomyocytes with or without desmin KD. **B** Quantification of percent cell area coverage of detyrosinated microtubules and tyrosinated microtubules with or without desmin KD. **C** Nanoindentation measurement of cardiomyocyte viscoelasticity. Left, Stiffness (elastic modulus) as a function of probe indentation velocity with or without desmin KD. Right, quantification of rate-dependent (viscoelastic) and independent (elastic) stiffness. **D** Representative images of microtubules in a cardiomyocyte at rest (top) and at the peak of contraction (bottom) with or without desmin KD. **E** Quantification of microtubule buckle amplitude. **F** Left, histogram of wavelength distribution of individual microtubule buckles.

Right, distribution difference (scram – des KD from **G**). Statistical significance determined via 2-sided t test.

Discussion

In this paper we identify that 1) the dynamic, catastrophe-prone nature of tyrosinated microtubules precludes their ability to faithfully grow to subsequent Z-discs; and 2) desmin intermediate filaments structure and stabilize the growing microtubule network.

This study represents the first direct observation that tyrosination increases the dynamics of cardiac microtubules. Increased dynamicity seems unlikely to arise from the PTM itself, [39] as the C-terminal tyrosine is not believed to be critical involved in the formation of lateral contacts with other tubulin dimers in the microtubule lattice. Yet, removal of this large hydrophobic residue and subsequent exposure of acidic residues will alter hydrophobic and electrostatic interactions on the outer surface of the polymerized microtubule. Through such a mechanism, tyrosination can promote microtubule dynamics via increased interaction with destabilizing MAPs, or through decreased interaction with stabilizing MAPs [39,40].

For example, detyrosination reduces the affinity of the depolymerizing kinesin MCAK for the microtubule, increasing microtubule stability[55]. We hypothesized that increased MCAK affinity may contribute to the increased rate of catastrophe we observed in tyrosinated microtubules; yet due to its low

abundance in the cardiomyocyte, our attempts to detect and knock down MCAK levels were unreliable, precluding the immediate test of this hypothesis. The low abundance of MCAK, while not ruling out a physiological rule, also motivates interrogation into alternative stabilizing or destabilizing effector proteins.

We also identified that the intermediate filament desmin provides structure to the growing microtubule network by stabilizing microtubules at the Z-disc. What is the mechanism of desmin-dependent stabilization? A recent elegant *in vitro* study using reconstituted vimentin intermediate filaments and microtubules indicates that intermediate filaments are sufficient to stabilize growing microtubules through electrostatic and hydrophobic interactions[56]. The interaction with intermediate filaments reduces catastrophes and promotes rescues, in strong accordance with our *in cellulo* findings here. While MAPs may also be involved in modulating microtubule-intermediate filament interactions, this direct effect is sufficient to explain the primary phenotypes observed upon desmin depletion (i.e. increased catastrophes and reduced pausing in the absence of desmin at the Z-disk, and a loss of Z-disk rescues).

The intermediate filament stabilization of growing microtubules would then provide a longer-lived microtubule substrate to facilitate reinforcing, detyrosination-dependent interactions, such as those previously documented between desmin and the microtubule through intermediates such as Kinesin-1[58]

or members of the plakin family of scaffolding proteins[57]. Desmin-mediated interaction along the length of the microtubule may also lead to the loss of tubulin dimers at sites of contact; these lattice defects are replaced by GTP-tubulin, which upon microtubule catastrophe may function as a rescue sites[95]. Lateral interactions between microtubules and intermediate filaments govern microtubule mechanical behavior upon compressive loading of microtubules[85] allowing desmin to orchestrate microtubule buckling in the cardiomyocyte. [34]

Methods

Animals

Animal care and procedures were approved and performed in accordance with the standards set forth by the University of Pennsylvania Institutional Animal Care and Use Committee and the Guide for the Care and Use of Laboratory Animals published by the US National institutes of Health.

Rat cardiomyocyte isolation and culture

Primary adult ventricular myocytes were isolated from 6- to 8-week-old Sprague Dawley rats as previously described[7]. Briefly, rats were anesthetized under isoflurane while the heart was removed and retrograde perfused on a Lutgendorf apparatus with a collagenase solution. The digested heart was then minced and triturated using a glass pipette. The resulting supernatant was

separated and centrifuged at 300 revolutions per minute to isolate cardiomyocytes that were resuspended in rat cardiomyocyte media at a density that ensured adjacent cardiomyocytes did not touch. Cardiomyocytes were cultured at 37°C and 5% CO_2 with 25 µmol/L of cytochalasin D. The viability of rat cardiomyocytes upon isolation was typically on the order of 50-75% rod-shaped, electrically excitable cells, and the survivability for 48hrs of culture is >80% (See Heffler et al. [6]for our quantification of cardiomyocyte morphology in culture).

Rat cardiomyocyte media: medium 199 (Thermo Fisher 115090) supplemented with 1x Insulin-transferrin-selenium-X (Gibco 51500056), 1 µg $µl^{-1}$ primocin (Invivogen ant-pm-1), 20 mmol/L HEPES at pH 7.4 and 25 µmol/L cytochalasin D.

Fractionation assay of free tubulin and cold-sensitive microtubules

Free tubulin was separated from cold-labile microtubules using a protocol adapted from Tsutsui et al., 1993 and Ostlud et al., 1979. Isolated rat cardiomyocytes were washed once with PBS and homogenized with 250 ul of microtubule stabilizing buffer using a tissue homogenizer. The homogenate was centrifuged at 100,000 xg for 15 minutes at 25°C and the resulting supernatant was stored at -80°C as the free tubulin fraction. The pellet was resuspended in ice-cold microtubule destabilizing buffer and incubated at 0°C for 1 hour. After

centrifugation at 100,000 xg for 15 minutes at 4°C the supernatant containing the cold-labile microtubule fraction was stored at -80°C.

Microtubule stabilizing buffer: 0.5 mM $MgCl_2$, 0.5 mM EGTA, 10mM Na_3PO_4, 0.5 mM GTP, and 1X protease and phosphatase inhibitor cocktail (Cell Signaling #5872S) at pH 6.95

Microtubule destabilizing buffer: 0.25 M sucrose, 0.5 mM $MgCl_2$ 10 mM Na_3PO_4, 0.5 mM GTP, and 1X protease and phosphatase inhibitor cocktail (Cell Signaling #5872S) at pH 6.95

Western blot

For whole cell protein extraction, isolated rat cardiomyocytes were lysed in RIPA buffer (Cayman #10010263) supplemented with protease and phosphatase Inhibitor cocktail (Cell Signaling #5872S) on ice for 1 hour. The supernatant was collected and combined with 4X loading dye (Li-COR #928-40004), supplemented with 10% 2-mercaptoethonol, and boiled for 10 minutes. The resulting lysate was resolved on SDS-PAGE gel and protein was blotted to nitrocellulose membrane (Li-COR #926-31902) with mini Trans-Blot Cell (Bio-Rad). Membranes were blocked for an hour in Odyssey Blocking Buffer (TBS) (LI-COR #927-50000) and probed with corresponding primary antibodies overnight at 4 °C. Membranes were rinsed with TBS containing 0.5% Tween 20 (TBST) three times and incubated with secondary antibodies TBS supplemented with extra 0.2% Tween 20 for 1 hour at room temperature. Membranes were

washed again with TBST (0.5% Tween 20) and imaged on an Odyssey Imager. Image analysis was performed using Image Studio Lite software (LI-COR). All samples were run in duplicates and analyzed in reference to GAPDH.

Antibodies and labels

Acetylated tubulin; mouse monoclonal (Sigma T6793-100UL); western blot: 1: 1,000

Detyrosinated tubulin; rabbit polyclonal (Abcam ab48389); western blot: 1: 1,000

Alpha tubulin; mouse monoclonal, clone DM1A (Cell Signaling #3873); western blot: 1:1,000

Beta tubulin; rabbit polyclonal (Abcam ab6046); western blot: 1,000

Tyrosinated tubulin; mouse monoclonal (Sigma T9028-.2ML); Immunofluorescence: 1:1000

Desmin; rabbit polyclonal (ThermoFisher PA5-16705); western blot and immunofluorescence: 1: 1,000

GAPDH; mouse monoclonal (VWR GenScript A01622-40); western blot: 1:1,000

Goat anti-mouse AF 488 (1:1000 Life Technologies A11001)

Goat anti-rabbit AF 565 (1:1000 Life Technologies A11011)

IRDye 680RD Donkey anti-Mouse IgG (H + L) (LI-COR 926-68072); western blot: 1:10,000.

IRDye 800CW Donkey anti-Rabbit IgG (H + L) (LI-COR 926-32213); western blot: 1:10,000.

Microtubule Dynamics by EB3

Isolated rat cardiomyocytes were infected with an adenovirus containing an EB3-GFP construct. After 48 hours, cells were imaged on an LSM Zeiss 880 inverted confocal microscope using a 40X oil 1.4 numerical aperture objective. Cells expressing EB3-GFP only at the tip were imaged for four minutes at a rate of 1fps. Files were blinded, Gaussian blurred, and Z-compressed using Image J (National Institutes of Health) to generate kymographs. The number of catastrophes, rescues, and pauses were recorded per kymograph in addition to manual tracing of microtubule runs to quantify time, distance, and velocity of microtubule growth or shrinkage. We refer to the entire kymograph as the microtubule 'track' that is made up of individual growth and shrinkage events we call 'runs'. Catastrophe and rescue frequency were calculated per cell by dividing the number of catastrophes or rescues by total time spent in growth or shrinkage time, respectively. Catastrophes and rescues occurring specifically on or off the Z-disc were normalized by the total time of microtubule growth and shrinkage. Experimental values were normalized to their respective control cells (Null for TTL and E331Q, or shScrm for shDes) acquired from the same animals. A minimum of 3 separate cell isolations were performed for each group.

Immunofluorescence

Cells were fixed in pre-chilled 100% methanol for 8 minutes at -20°C. Cells were washed 4x then blocked with Sea Block Blocking Buffer (abcam #166951) for at least 1 hour followed by antibody incubation for 24-48 hours. Incubation was followed by washing 3x with Sea Block, then incubated with secondary antibody for 1 hour. Fixed cells were mounted using Prolong Diamond (Thermo #P36961)

We used ImageJ to calculate the percent area fraction of both desmin and microtubules. An ROI was drawn to include the entire cell boundary minus the nucleus. For each image we identified the percent fractional coverage of a fluorescence signal over a manually identified threshold as described previously[46].

Buckling analysis

Adult rat cardiomyocytes were isolated as previously described and infected with adenovirus carrying the microtubule-binding protein EMTB chimerically fused to 3 copies of GFP. The purpose of this construct was to label microtubules fluorescently for imaging. The cells were allowed 48 hours to express the construct. All cells chosen were those that contained sufficient brightness and contrast to observe microtubule elements and where the health of the myocyte was not compromised. To interrogate microtubule buckling amplitude and wavelength, cells were induced to contract at 1 Hz 25 V and

imaged during the contraction. For analysis, images were blinded, and a microtubule was located that could be followed during the contraction. The backbone was manually traced at rest and during its peak of contraction and the ROI was saved. The ROI was then analyzed using a macro that rotated so that the ROI had the peak of contraction 90 degrees to the axis of contraction to protect from aliasing errors. The program then calculated the distance between the axis of the ROI and its peak and calculated the peak (amplitude) and the width (half wavelength).

Electron Microscopy

Transmission electron microscopy images were collected as previously described [6]. Images at 7500x were rotated so the cells were parallel to the longitudinal axis. ROIs were generated between adjacent Z-discs to quantify sarcomere spacing and the angle relative to 90°.

Statistics

Statistical analysis was performed using OriginPro (Version 2018). Normality was determined by Shapiro-Wilk test. For normally distributed data, two sample t-test or one-way ANOVA was utilized as appropriate. For non-normally distributed data, two sample Kolmogrov-Smirnov test or Kruskal-Wallis ANOVA was utilized as appropriate. Specific statistical tests and information of biological and technical replicates can be found in the figure legends. Unless

otherwise noted, ‘N’ indicates the number of cells analyzed and ‘n’ indicates number of microtubule runs.

CHAPTER 5: DISCUSSION AND FUTURE DIRECTIONS

Adapted from:

Chen, C. Y*., **Salomon, A. K*.,** Caporizzo, M. A., Curry, S., Kelly, N. A., Bedi, K., … & Prosser, B. L. (2020). Depletion of vasohibin 1 speeds contraction and relaxation in failing human cardiomyocytes. *Circulation research*, 127(2), e14-e27.

Manuscript currently in review at eLife: **Salomon A.K**., Okami N., Heffler, J., Lee JJ., Robison P., Bogush AI., Prosser BL. (2021). Desmin intermediate filaments and tubulin detyrosination stabilize growing microtubules in the cardiomyocyte.

In this dissertation I define the mechanical role of the cardiac microtubule network and begin to shed light on how the network is formed. Specifically, I find that: 1) Depolymerization of the microtubule network improves contractility of cardiomyocytes isolated from failing human hearts; 2) The VASH-SVBP complex functions as a tubulin carboxypeptidase in cardiomyocytes and knockdown improves contractility of failing human cardiomyocytes; 3) The dynamic, catastrophe-prone nature of tyrosinated microtubules precludes their ability to faithfully grow between subsequent Z-discs; and 4) Desmin intermediate filaments provide structure to and stabilize dynamic microtubules.

Although the cardiomyocyte microtubule network is necessary for the function of the myocyte, its presence contributes viscoelastic resistance to myocyte motion. In the healthy myocyte, the resistive force provided by microtubules buckling at a short wavelength is thought to equal 5-40% of the total force generated by the myocyte.[32] While this resistance is negligible for the healthy myocyte as contraction is obviously not stalled, the densification of the

microtubule network that occurs in heart disease is sufficient to depress myocyte contractility. Why might the microtubule network increase in density during disease if its presence hinders contractility? In disease ventricular pressure can change, potentiating an increase in wall stress felt by the myocardium. Microtubules are known to be stabilized under tension and align with the direction of maximal tensile stress in plant cells[96]. Cardiomyocyte microtubules may function in a similar way. By sensing changes in the direction and magnitude of tensile stress, the microtubule network may reactively coordinate changes in myocyte geometry. For example, increased microtubule polymerization and stability in one axis may bias the localization of transcripts necessary for the formation of the sarcomere, allowing the cell to change shape so that it may compensate for the change in ventricular pressure. [9,97]

The viscoelastic resistance provided by the microtubule network is tuned by detyrosination. Expression of TTL or knockdown of VASH1-SVBP specifically resulted in increased myocyte relaxation velocity. Diastolic dysfunction, or slowed myocyte relaxation, is a hallmark of both hypertrophic cardiomyopathy (HCM) and heart failure with preserved ejection fraction (HFpEF).[4,62] Reducing cardiomyocyte stiffness and improving myocyte relaxation may reduce relaxation times, increase ventricular compliance, and reduce diastolic pressures, all of which may benefit patients with diastolic dysfunction. As there is no cure for HCM or HFpEF, current disease management is focused on preventing thrombotic events and sudden cardiac death either through pharmacological therapies or

surgical intervention (Solomon 2020). Therefore, pharmacological approaches to promote myocyte relaxation to treat HCM represent an unmet clinical need. Current pharmacological approaches in development including calcium desensitizers[98,99], genome editing with CRISPR[100], and most notably mavacamten, a myosin inhibitor in clinical trials.[101] It is unclear if the therapeutic benefit of such approaches arises from the faster relaxation, reduced systolic force production, or a net decrease in time under tension that may limit hypertrophic remodeling. Intriguingly, our results indicate an alternative, Ca^{2+}-independent mechanism to speed relaxation. Reducing viscoelasticity may speed cardiomyocyte relaxation without compromising systolic force production or increasing energetic demand, as would be the case for an increase in calcium cycling. How such a strategy would fit in the toolkit and compare to current approaches for treating different etiologies of diastolic or systolic dysfunction is of interest and will require extensive further study.

The differences between the enzymatic activity and expression of VASH1 and VASH2 in cardiomyocytes warrant further study. The catalytic activity of the vasohibins is contingent on interaction with SVBP, which maintains the structural integrity of the VASH active site.[70,71] Interestingly, SVBP transcript is more abundant in cardiac tissue than either isoform of VASH, suggesting regulation of the individual isoforms may reside in their individual transcription or post-translational modification. While VASH1 transcript is more abundant in cardiac tissue, VASH2 knockdown also resulted in reduced levels of microtubule

detyrosination. While we cannot determine the differences in enzyme kinetics between the two VASH isoforms from our data, it is possible that VASH2 may be expressed at a lower level but have an increased microtubule affinity compared to VASH1. Further, the effect of VASH2 knockdown on the contractility of cardiomyocytes from diseased hearts was not investigated. Future studies should characterize the expression of VASH2 in diseased cardiomyocytes and explore its role in mediating increased levels of detyrosination observed in disease.

This dissertation also represents the first direct observation that tyrosination increases the dynamics of cardiac microtubules. What is the mechanism underlying the effect of tyrosination on microtubule dynamics? As discussed previously, tyrosination likely alters the interaction of plus-end tip proteins (+Tips), such as CLIP-170 and p150 glued[92], which may tune microtubule dynamics through either direct or indirect effects. +Tip proteins also serve to couple the growing microtubule plus end with cellular effectors[29]. In the search and capture mechanism, dynamic microtubules 'search' for sites on the plasma membrane, chromosomes, and organelles to 'capture' via +Tip proteins.[102] The interaction of microtubules with cellular structures, such as chromosomes or the cell cortex, has been shown to promote rescue events through the formation of tension at the plus-end.[103]

Further study is required on the expression, activity, and regulation of +Tip proteins in both the healthy and diseased cardiomyocyte. Regulation of

microtubule dynamics is likely a critical intermediate in the formation of the dense microtubule network observed in disease. Much of what is known about the regulation of +Tip proteins comes from mitotic cells, were a milieu of microtubule associated proteins, regulatory proteins, and kinases is involved in maintaining proper spindle position and length to ensure proper cell division.[104] Preliminary investigation into the expression of MCAK, a key depolymerizing kinesin that preferentially interacts with tyrosinated microtubules, suggested that expression is very low to non-detectable in the cardiomyocyte. This is in agreement with other reports that suggest MCAK is expressed in proliferating skeletal myoblasts but downregulated to undetectable levels in differentiated mouse skeletal muscle.[105] Other depolymerizing kinesins such as Kif15 and Kif2a may act preferentially in the cardiomyocyte, and their expression and activity should be explored.[106] Further, dynamic microtubules are required for the differentiation of myoblasts.[107] An intriguing hypothesis then arises that any changes to microtubule dynamics in disease progression due to changes in the expression and regulation of +Tip proteins may be linked to the fetal reprogramming and dedifferentiation that occurs during heart disease.[108]

I found that microtubule acetylation does not impact microtubule dynamics; however, this result should be contextualized. Acetylation of the polymerized microtubule is known to occur rather slowly as αTAT1 has a slow catalytic rate (0.4 hr^{-1}).[109] Further, the lysine residue that serves as a substrate for αTAT1 is in the lumen of the microtubule, thus the enzyme must enter the

lumen though the microtubule ends or via lattice defects that accumulate through damage of the microtubule.[109] Although the expression of the αTAT1 construct in my experiments robustly increased acetylation, the pattern of acetylation likely differs from what would accumulate endogenously through cyclic strain of the microtubule. The accumulation of acetylation at points of high microtubule curvature may allow for increased resistance to catastrophe, allowing for self-repair of damaged microtubules with GTP tubulin.[95] The formation of these rescue sites (called GTP islands[110]) would likely have a subtle effect on the overall dynamics of the microtubule that would likely be missed by the cell-fractionation assay used to determine the effect of acetylation of microtubule dynamics. Further study on the effects of acetylation on microtubule dynamics is warranted and should include cyclic electrical stimulation to produce microtubule defects.

The intermediate filament desmin was also found to provide structure to the growing microtubule network by stabilizing microtubules at the Z-disc. What is the mechanism of desmin-dependent stabilization? A recent elegant *in vitro* study using reconstituted vimentin intermediate filaments and microtubules indicates that intermediate filaments are sufficient to stabilize growing microtubules through electrostatic and hydrophobic interaction[56]. The interaction with intermediate filaments reduces catastrophes and promotes rescues, in strong accordance with my *in cellulo* findings. While MAPs may also be involved in modulating microtubule-intermediate filament interactions, this direct effect is

sufficient to explain the primary phenotypes observed upon desmin depletion (i.e. increased catastrophes and reduced pausing in the absence of desmin at the Z-disk, and a loss of Z-disk rescues).

The intermediate filament stabilization of the growing microtubule would subsequently allow for more durable interactions between intermediate filaments and the microtubule, contributing to the long-range stability of the network. For example, microtubules are known to be cross-linked with intermediate filaments via Kinesin-1[58] or members of the plakin family of scaffolding proteins.[57] Through interaction with microtubules, intermediate filaments have been shown to inhibit microtubule dynamics, contributing to microtubule stability in motor neurons.[111] Additionally, the formation of extensive cross-links between desmin intermediate filaments and the microtubule network, likely increases the steric hinderance of tubulin associated with microtubules at the Z-disc. An interesting possibility arises that molecular crowding further reinforces microtubule stability observed by desmin intermediate filaments.

Combined with past and current work, I propose a unifying model for microtubule-intermediate filament interactions in the cardiomyocyte and how they contribute to myocardial mechanics (**Figure 17)** . Detyrosinated microtubules, with less frequent depolymerization, experience more chance interactions with intermediate filaments at the Z-disc. The altered surface chemistry of detyrosinated microtubules may also strengthen the electrostatic interactions with intermediate filaments and additional cross-linking proteins. The periodic, lateral

reinforcement of microtubules increases their stability, leading to longer-lived microtubules and providing a dynamic cross-link with the sarcomere, increasing the viscoelastic resistance to myocyte motion and the ability of microtubules to transduce mechanical stress. Increased microtubule lifetimes also promote microtubule acetylation, which itself increases the ability of microtubules to withstand mechanical stress[54] and increases myocyte viscoelasticity.[112] In the setting of heart disease, the increased abundance of both desmin intermediate filaments and detyrosinated microtubules thus promotes a feed-forward substrate for enhanced mechanotransduction and myocardial stiffening.

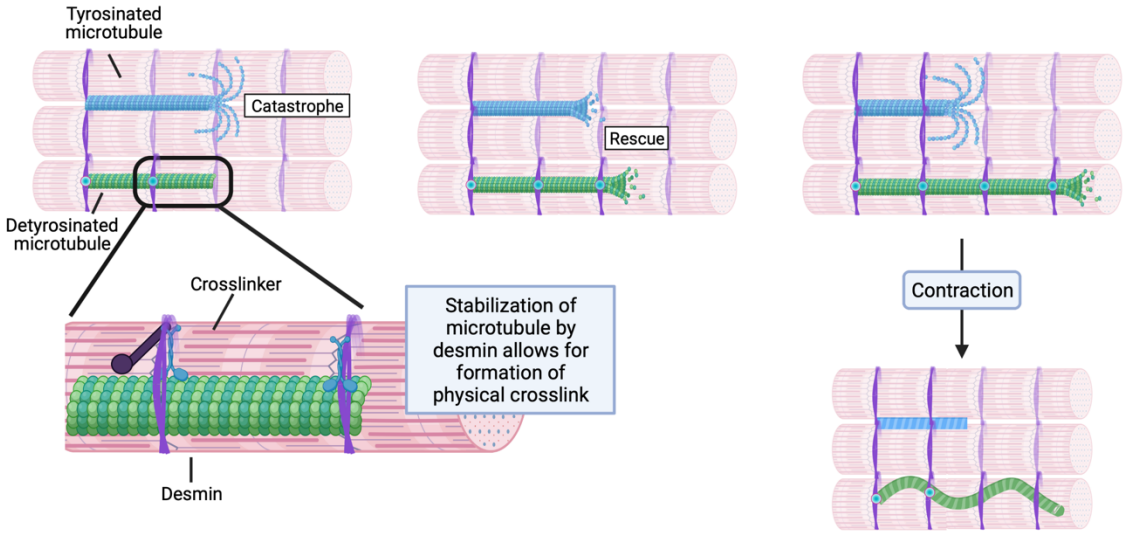

Figure 17. Current working model for how the microtubule network is shaped by tyrosination status and desmin intermediate filaments.

APPENDIX

Patient #	Etiology	Gender	Age (year)	Heart Weight (g)	LVMI	LVEF (%)	Experiments on cultured cells
1758	NF	Male	66	272	140.43	75	TTL/E331Q/Null contractility
1761	NF	Female	26	170	91.52	50	VASH1KD v Scram Contractility
1763	NF	Male	58	215	106.18	60	TTL/E331Q/Null contractility; VASH1 KD v Scram Contractility
1766	NF	Female	61	187	102.42	40	TTL/E331Q/Null contractility; VASH1 KD v Scram Contractility
1785	NF	Female	53	184	76.87	55	VASH1 KD v Scram Ca2+ and Contractility
1789	NF	Female	65	152	88.75	70	VASH1 KD v Scram Ca2+ and Contractility
1724	HFrEF	Female	56	283	132.06	15	TTL v Null Ca2+ and contractility
1725	HFrEF	Female	52	200	112.87	25	TTL v Null Ca2+ and contractility
1765	HFrEF	Male	30	217	115.19	15	TTL/E331Q/Null contractility
1768	HFrEF	Male	64	187	102.32	15	TTL/E331Q/Null contractility
1775	HFrEF	Female	65	277	138.61	15	TTL/E331Q/Null contractility, VASH1 KD v Scram Contractility
1777	HFrEF	Female	39	138	78.75	20	VASH1 KD v Scram Contractility
1780	HFrEF	Male	54	418	152.28	25	VASH1 KD v Scram Contractility
1787	HFrEF	Male	44	240	111.48	20	AFM
1788	HFrEF	Male	38	241	106.89	10	VASH1 KD v Scram Ca2+ and Contractility; SVBP KD v Scram Contractility
1791	HFrEF	Male	39	251	111.33	20	AFM; SVBP KD v Scram Contractility
1726	HFpEF	Female	46	285	160.69	65	TTL v Null contractility Ca2+ and contractility
1774	HFpEF	Female	34	291	187.51	75	VASH1 KD v Scram Contractility
1781	HFpEF	Male	62	265	130.81	60	VASH1 KD v Scram Contractility
1782	HFpEF	Female	69	184	128.38	70	VASH1 KD v Scram Contractility
1786	HFpEF	Male	48	357	171.88	75	AFM; VASH1 KD v Scram Ca2+ and Contractility
1790	HFpEF	male	54	267	122.26	60	AFM; VASH1 KD v Scram Ca2+ and Contractility; SVBP KD v Scram Contractility

Appendix Table 1. Descriptive statistics on human hearts in Chapter 3. A summary and detailed values for the human hearts used in this study, including etiology, gender, age, heart

weight, left ventricle mass index (LVMI) and left ventricular ejection fraction (LEVF) and experiments performed on isolated myocytes.

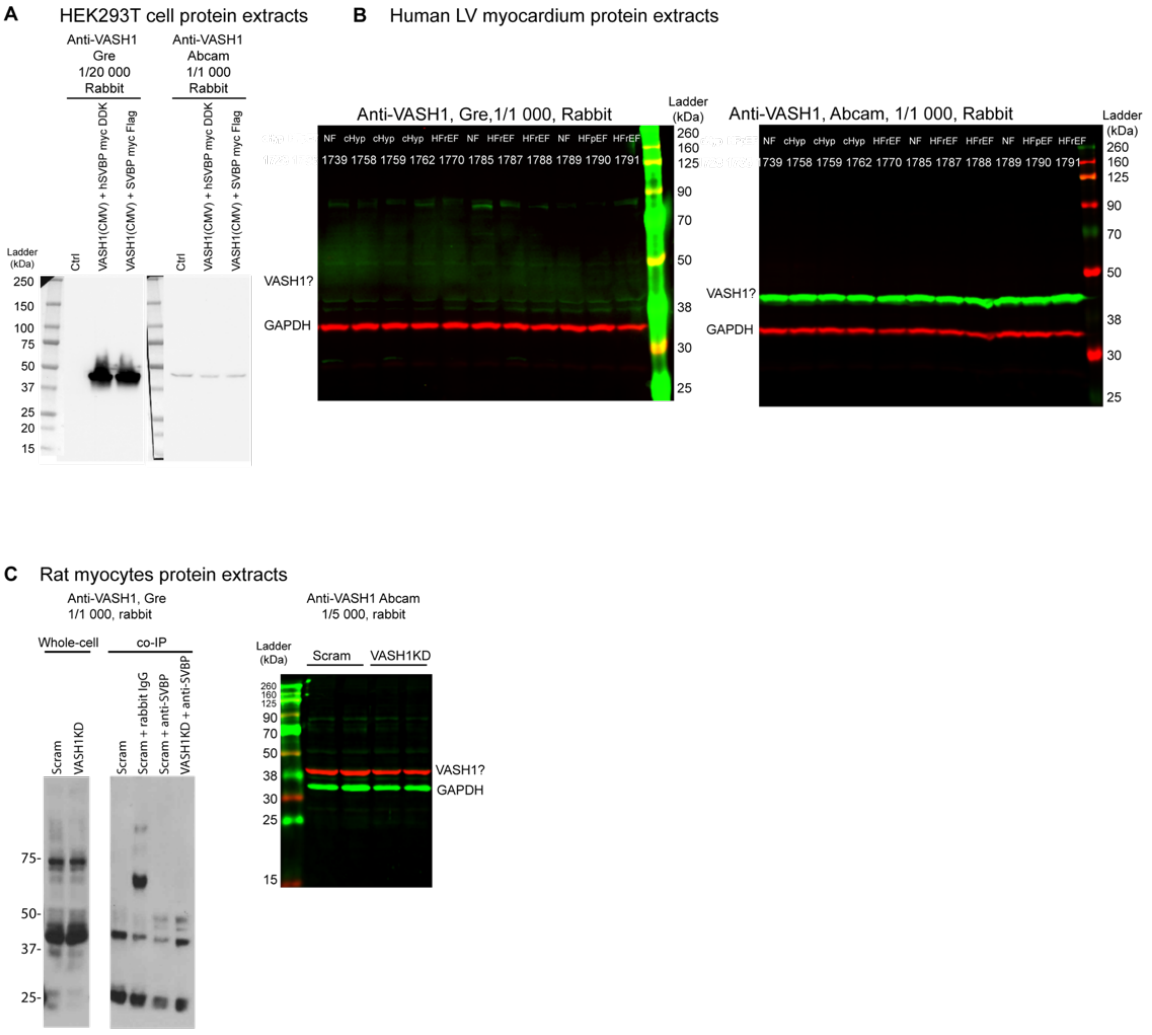

Appendix Figure 1. Validation of antibodies against VASH1. HEK293T cells were used to validate VASH1 antibodies as they do not endogenously express vasohibins. Immunoblots of protein extracts from (**A**) HEK293T cells co-transfected with plasmids encoding mouse VASH1 and mouse or human SVBP-myc-Flag (plasmids used in Aillaud et al Science 2017,[48] Wang et al 2019[70]). The VASH1 antibody made in Grenoble (Gre) detects a robust band with low antibody concentration (1/20,000) only in the VASH1 overexpressing cells, while the VASH1 antibody from Abcam detects a weaker signal at higher concentrations (1/1,000) in all conditions and is insensitive to overexpression, indicating non-specificity. **B**, human LV myocardium blotted with anti-VASH1 antibodies. Gre antibody detects multiple weak bands around the predicted molecular weight of VASH1, while Abcam antibody detects an extremely robust, albeit likely non-specific band (due to non-specificity shown in **A** and **C**). **C**, immunoblots of protein extracts from rat myocytes: **left**, whole cell extract and co-IP with anti-SVBP (Gre) blotted with anti-VASH1 (Gre); **right**, whole cell extract

blotted with anti-VASH1 (Abcam). The Gre antibody reveals multiple bands in whole cell lysate, and upon co-IP with anti-SVBP bands around the molecular weight of VASH1 are detected, but are present even in negative control lanes (scram and scram + rabbit IgG). In sum, we were unable to reliably quantify VASH1 in rat cardiomyocytes or human tissue. Validation was completed by Christina Chen.

Figure 1B TTL contractility	Etiology	N (patients)	Treatment	n (cells)	Resting SL (µm)	Peak ontraction velocity (µm/s)	Peak shortening (µm)	Fractional shortening (%)	Peak relaxation velocity (µm/s)
	HF	3	Null	65	1.69 ± 0.011	-0.61 ± 0.037	0.14 ± 0.009	8.42 ± 0.518	0.81 ± 0.081
	HF	3	TTL	70	1.73 ± 0.011	-0.91 ± 0.048	0.17 ± 0.008	9.68 ± 0.471	1.24 ± 0.088

Figure 1B TTL Calcium	Etiology	N (patients)	Treatment	n (cells)	Rise time 90% (s)	Decay time 90 (s)	Decay time 25% (s)	Decay time 50% (s)	F/F0
	HF	3	Null	46	0.05 ± 0.004	0.99 ± 0.029	0.69 ± 0.024	0.37 ± 0.012	3.03 ± 0.146
	HF	3	TTL	50	0.05 ± 0.003	1.03 ± 0.032	0.73 ± 0.028	0.36 ± 0.011	2.84 ± 0.112

Figure 3B-D VASH KD contractility	Etiology	N (patients)	Treatment	n (cells)	Resting SL (µm)	Peak ontraction velocity (µm/s)	Peak shortening (µm)	Fractional shortening (%)	Peak relaxation velocity (µm/s)
	NF	3	Scram	87	1.79 ± 0.008	-1.45 ± 0.067	0.21 ± 0.005	11.97 ± 0.273	1.51 ± 0.056
	NF	3	VASH KD	86	1.81 ± 0.006	-1.91 ± 0.081	0.23 ± 0.005	12.87 ± 0.3	1.79 ± 0.062
	HFrEF	3	Scram	71	1.8 ± 0.012	-0.54 ± 0.05	0.13 ± 0.008	7.21 ± 0.474	0.71 ± 0.083
	HFrEF	3	VASH KD	75	1.8 ± 0.01	-0.91 ± 0.075	0.17 ± 0.009	9.48 ± 0.512	1.12 ± 0.099
	HFpEF	3	Scram	72	1.78 ± 0.013	-0.53 ± 0.055	0.12 ± 0.009	6.83 ± 0.483	0.41 ± 0.041
	HFpEF	3	VASH KD	78	1.78 ± 0.012	-0.85 ± 0.064	0.17 ± 0.008	9.47 ± 0.419	0.81 ± 0.065

Figure 3C-D TTL/TTL-E331Q contractility	Etiology	N (patients)	Treatment	n (cells)	Resting SL (µm)	Peak ontraction velocity (µm/s)	Peak shortening (µm)	Fractional shortening (%)	Peak relaxation velocity (µm/s)
	NF	3	Null	70	1.84 ± 0.008	-1.06 ± 0.072	0.16 ± 0.007	8.83 ± 0.396	1.63 ± 0.125
	NF	3	TTL	71	1.85 ± 0.009	-1.49 ± 0.098	0.19 ± 0.008	10.22 ± 0.467	1.9 ± 0.115
	NF	3	TTL-E331Q	72	1.85 ± 0.007	-1.54 ± 0.107	0.19 ± 0.008	10.51 ± 0.473	2.03 ± 0.171
	HF	3	Null	60	1.82 ± 0.01	-0.59 ± 0.049	0.12 ± 0.007	6.41 ± 0.397	0.7 ± 0.079
	HF	3	TTL	60	1.84 ± 0.01	-0.81 ± 0.056	0.14 ± 0.008	7.58 ± 0.44	1.2 ± 0.127
	HF	3	TTL-E331Q	61	1.84 ± 0.012	-0.78 ± 0.064	0.13 ± 0.007	7.1 ± 0.404	0.78 ± 0.092

Figure 4B VASH KD calcium	Etiology	N (patients)	Treatment	n (cells)	F0	F/F0	Rise time 50% (s)	Rise time 90% (s)	Decay time 50% (s)
	NF	2	Scram	66	69.22 ± 3.67	3.24 ± 0.19	0.025 ± 0.001	0.071 ± 0.003	0.611 ± 0.023
	NF	2	VASH KD	67	53 ± 3.7	3.99 ± 0.33	0.027 ± 0.002	0.072 ± 0.005	0.604 ± 0.023
	HF	3	Scram	67	82.72 ± 5.82	2.97 ± 0.23	0.034 ± 0.003	0.081 ± 0.005	0.603 ± 0.022
	HF	3	VASH KD	75	61.29 ± 3.19	3.09 ± 0.15	0.036 ± 0.003	0.089 ± 0.006	0.561 ± 0.018

Figure 4C VASH KD contractility	Etiology	N (patients)	Treatment	n (cells)	Resting SL (µm)	Peak ontraction velocity (µm/s)	Peak shortening (µm)	Fractional shortening (%)	Peak relaxation velocity (µm/s)
	NF	2	Scram	66	1.66 ± 0.013	-0.44 ± 0.025	0.12 ± 0.006	7.19 ± 0.381	0.47 ± 0.039
	NF	2	VASH KD	67	1.71 ± 0.013	-0.64 ± 0.037	0.15 ± 0.007	9.03 ± 0.426	0.76 ± 0.053
	HF	3	Scram	67	1.7 ± 0.013	-0.36 ± 0.035	0.11 ± 0.008	6.27 ± 0.484	0.33 ± 0.039
	HF	3	VASH KD	75	1.7 ± 0.013	-0.5 ± 0.038	0.13 ± 0.008	7.97 ± 0.482	0.58 ± 0.06

Online Figure 2 SVBP KD contractility	Etiology	N (patients)	Treatment	n (cells)	Resting SL (µm)	Peak ontraction velocity (µm/s)	Peak shortening (µm)	Fractional shortening (%)	Peak relaxation velocity (µm/s)
	HF	3	Scram	79	1.75 ± 0.01	-0.6 ± 0.055	0.16 ± 0.009	8.93 ± 0.497	0.7 ± 0.08
	HF	3	SVBP KD	81	1.71 ± 0.012	-0.83 ± 0.073	0.17 ± 0.01	10.11 ± 0.59	1 ± 0.116

Figure 1B TTL Contractility	Time to peak 50% (s)	Time to peak 90% (s)	Time to relax 50% (s)	Time to relax 90% (s)	Relaxation exponential fit (tau)
	0.18 ± 0.007	0.48 ± 0.033	0.38 ± 0.019	0.59 ± 0.024	0.44 ± 0.014
	0.13 ± 0.004	0.24 ± 0.011	0.24 ± 0.008	0.46 ± 0.023	0.33 ± 0.01
Figure 3B-D VASH KD Contractility	Time to peak 50% (s)	Time to peak 90% (s)	Time to relax 50% (s)	Time to relax 90% (s)	Relaxation exponential fit (tau)
	0.11 ± 0.003	0.3 ± 0.006	0.18 ± 0.006	0.34 ± 0.018	0.17 ± 0.008
	0.1 ± 0.002	0.26 ± 0.005	0.16 ± 0.006	0.31 ± 0.017	0.15 ± 0.009
	0.18 ± 0.008	0.42 ± 0.012	0.31 ± 0.013	0.55 ± 0.027	0.39 ± 0.032
	0.15 ± 0.007	0.37 ± 0.012	0.23 ± 0.009	0.44 ± 0.024	0.24 ± 0.017
	0.23 ± 0.014	0.51 ± 0.022	0.48 ± 0.019	0.72 ± 0.022	0.66 ± 0.034
	0.18 ± 0.01	0.42 ± 0.016	0.34 ± 0.019	0.58 ± 0.027	0.43 ± 0.034
Figure 3C-D TTL/TTL-E331Q Contractility	Time to peak 50% (s)	Time to peak 90% (s)	Time to relax 50% (s)	Time to relax 90% (s)	Relaxation exponential fit (tau)
	0.13 ± 0.005	0.31 ± 0.009	0.2 ± 0.009	0.37 ± 0.022	0.2 ± 0.016
	0.11 ± 0.004	0.27 ± 0.009	0.16 ± 0.006	0.3 ± 0.016	0.14 ± 0.007
	0.11 ± 0.004	0.27 ± 0.007	0.18 ± 0.009	0.36 ± 0.022	0.19 ± 0.012
	0.19 ± 0.01	0.39 ± 0.016	0.29 ± 0.017	0.61 ± 0.029	0.34 ± 0.03
	0.15 ± 0.008	0.33 ± 0.011	0.21 ± 0.01	0.44 ± 0.028	0.23 ± 0.017
	0.17 ± 0.008	0.35 ± 0.013	0.23 ± 0.01	0.57 ± 0.031	0.26 ± 0.015
Figure 4B VASH KD Calcium	Decay time 90% (s)	Decay exponential fit (tau)			
	1.197 ± 0.029	0.94 ± 0.05			
	1.179 ± 0.032	0.89 ± 0.05			
	1.2 ± 0.034	0.94 ± 0.05			
	1.126 ± 0.031	0.8 ± 0.04			
Figure 4C VASH KD Calcium	Time to peak 50% (s)	Time to peak 90% (s)	Time to relax 50% (s)	Time to relax 90% (s)	Relaxation exponential fit (tau)
	0.2 ± 0.007	0.48 ± 0.014	0.37 ± 0.012	0.6 ± 0.019	0.48 ± 0.028
	0.17 ± 0.004	0.46 ± 0.011	0.31 ± 0.011	0.5 ± 0.02	0.37 ± 0.023
	0.25 ± 0.012	0.55 ± 0.016	0.5 ± 0.015	0.79 ± 0.025	0.7 ± 0.029
	0.2 ± 0.007	0.48 ± 0.012	0.38 ± 0.015	0.64 ± 0.023	0.52 ± 0.03
Online Figure 2 SVBP KD Contractility	Time to peak 50% (s)	Time to peak 90% (s)	Time to relax 50% (s)	Time to relax 90% (s)	Relaxation exponential fit (tau)
	0.19 ± 0.007	0.47 ± 0.014	0.41 ± 0.015	0.63 ± 0.022	0.58 ± 0.03
	0.17 ± 0.005	0.42 ± 0.01	0.34 ± 0.013	0.56 ± 0.02	0.44 ± 0.027

Appendix Table 2. Statistical parameters of contractility and calcium transients of those presented in Chapter 3. Contractility and calcium transient measurements are shown as mean ± SEM, with number of myocytes and hearts studied in each group.

VASH1KD contraction time (90%) two way ANOVA

Overall ANOVA

	DF	Sum of Squares	Mean Square	F Value	P Value
Etiology	2	2.75809	1.37904	109.85259	0
Treatment	1	0.44096	0.44096	35.12647	6.04E-09
Interaction	2	0.0733	0.03665	2.91943	0.05496
Model	5	3.20211	0.64042	51.01505	0
Error	463	5.81231	0.01255	--	--
Corrected Total	468	9.01442	--	--	--

Mean comparison

Etiology	Prob	Alpha	Sig
HFrEF NF	1.57E-16	0.05	1
HFpEF NF	5.03E-39	0.05	1
HFpEF HFrEF	2.09E-07	0.05	1

Treatment	Prob	Alpha	Sig
shVASH scram	4.93E-08	0.05	1

Interaction

Etiology	Treatment	Etiology	Treatment	Prob	Alpha
NF	shVASH	NF	scram	0.4535	0.05
HFrEF	scram	NF	scram	1.93E-09	0.05
HFrEF	scram	NF	shVASH	1.57E-15	0.05
HFrEF	shVASH	NF	scram	0.00301	0.05
HFrEF	shVASH	NF	shVASH	1.56E-07	0.05
HFrEF	shVASH	HFrEF	scram	0.08284	0.05
HFpEF	scram	NF	scram	1.60E-27	0.05
HFpEF	scram	NF	shVASH	5.71E-36	0.05
HFpEF	scram	HFrEF	scram	9.52E-06	0.05
HFpEF	scram	HFrEF	shVASH	2.71E-13	0.05
HFpEF	shVASH	NF	scram	1.02E-09	0.05
HFpEF	shVASH	NF	shVASH	4.90E-16	0.05
HFpEF	shVASH	HFrEF	scram	1	0.05
HFpEF	shVASH	HFrEF	shVASH	0.08226	0.05
HFpEF	shVASH	HFpEF	scram	3.81E-06	0.05

TTL/E331Q contraction time (90%) two way ANOVA

Overall ANOVA

	DF	Sum of Squares	Mean Square	F Value	P Value
Etiology	1	0.53821	0.53821	69.45514	1.37E-15
Treatment	2	0.1782	0.0891	11.49798	1.41E-05
Interaction	2	0.00749	0.00374	0.48311	0.61723
Model	5	0.72188	0.14438	18.63151	1.34E-16
Error	388	3.00664	0.00775	--	--
Corrected Total	393	3.72852	--	--	--

Mean comparison

Etiology	Prob	Alpha	Sig
HF NF	1.23E-15	0.05	1

Treatment	Prob	Alpha	Sig
Null E331Q	0.00341	0.05	1
TTL E331Q	0.50226	0.05	0
TTL Null	1.42E-05	0.05	1

Interaction

Etiology	Treatment	Etiology	Treatment	Prob	Alpha
NF	Null	NF	E331Q	0.38027	0.05
NF	TTL	NF	E331Q	1	0.05
NF	TTL	NF	Null	0.09131	0.05
HF	E331Q	NF	E331Q	8.80E-06	0.05
HF	E331Q	NF	Null	0.05985	0.05
HF	E331Q	NF	TTL	7.27E-07	0.05
HF	Null	NF	E331Q	5.63E-12	0.05
HF	Null	NF	Null	2.46E-06	0.05
HF	Null	NF	TTL	2.18E-13	0.05
HF	Null	HF	E331Q	0.27378	0.05
HF	TTL	NF	E331Q	0.00692	0.05
HF	TTL	NF	Null	1	0.05
HF	TTL	NF	TTL	1.04E-03	0.05
HF	TTL	HF	E331Q	1	0.05
HF	TTL	HF	Null	0.00232	0.05

VASH1KD relaxation time (50%) two way ANOVA

Overall ANOVA

	DF	Sum of Squares	Mean Square	F Value	P Value
Etiology	2	4.75231	2.37616	180.3949	0
Treatment	1	0.76623	0.76623	58.171	1.38E-13
Interaction	2	0.30826	0.15413	11.70122	1.10E-05
Model	5	5.6686	1.13372	86.07057	0
Error	462	6.08545	0.01317	--	--
Corrected Total	467	11.75405	--	--	--

Mean comparison

Etiology	Prob	Alpha	Sig
HFrEF NF	1.19E-13	0.05	1
HFpEF NF	2.76E-58	0.05	1
HFpEF HFrEF	1.15E-22	0.05	1

Treatment	Prob	Alpha	Sig
shVASH scram	6.14E-12	0.05	1

Interaction

etiology	treatment	etiology	treatment	Prob	Alpha
NF	shVASH	NF	scram	1	0.05
HFrEF	scram	NF	scram	2.76E-11	0.05
HFrEF	scram	NF	shVASH	2.12E-14	0.05
HFrEF	shVASH	NF	scram	6.89E-02	0.05
HFrEF	shVASH	NF	shVASH	1.71E-03	0.05
HFrEF	shVASH	HFrEF	scram	3.17E-04	0.05
HFpEF	scram	NF	scram	6.14E-48	0.05
HFpEF	scram	NF	shVASH	1.18E-52	0.05
HFpEF	scram	HFrEF	scram	1.20E-16	0.05
HFpEF	scram	HFrEF	shVASH	1.26E-33	0.05
HFpEF	shVASH	NF	scram	6.03E-17	0.05
HFpEF	shVASH	NF	shVASH	1.21E-20	0.05
HFpEF	shVASH	HFrEF	scram	1.00E+00	0.05
HFpEF	shVASH	HFrEF	shVASH	7.23E-08	0.05
HFpEF	shVASH	HFpEF	scram	2.19E-12	0.05

TTL/E331Q relaxation time (90%) two way ANOVA

Overall ANOVA

	DF	Sum of Squares	Mean Square	F Value	P Value
Etiology	1	3.7062	3.7062	95.7975	2.66E-20
Treatment	2	1.0229	0.51145	13.21994	2.83E-06
Interaction	2	0.15695	0.07848	2.02848	0.13297
Model	5	4.90675	0.98135	25.36584	4.71E-22
Error	376	14.54663	0.03869	--	--
Corrected Total	381	19.45338	--	--	--

Mean comparison

Etiology	Prob	Alpha	Sig
HF NF	1.28E-20	0.05	1

Treatment	Prob	Alpha	Sig
Null E331Q	0.74587	0.05	0
TTL E331Q	4.31E-04	0.05	1
TTL Null	3.33E-06	0.05	1

Interaction

Etiology	Treatment	Etiology	Treatment	Prob	Alpha
NF	Null	NF	E331Q	1	0.05
NF	TTL	NF	E331Q	0.97709	0.05
NF	TTL	NF	Null	0.51414	0.05
HF	E331Q	NF	E331Q	6.26E-08	0.05
HF	E331Q	NF	Null	5.01E-07	0.05
HF	E331Q	NF	TTL	8.59E-13	0.05
HF	Null	NF	E331Q	3.69E-11	0.05
HF	Null	NF	Null	4.49E-10	0.05
HF	Null	NF	TTL	1.37E-16	0.05
HF	Null	HF	E331Q	1	0.05
HF	TTL	NF	E331Q	0.31838	0.05
HF	TTL	NF	Null	0.7061	0.05
HF	TTL	NF	TTL	8.20E-04	0.05
HF	TTL	HF	E331Q	0.00725	0.05
HF	TTL	HF	Null	5.30E-05	0.05

Appendix Table 3. Detailed two-way ANOVA report of human cardiomyocyte contractility kinetic data shown Chapter 3. Overall ANOVA and mean comparisons including interactions from two-way ANOVA of contraction time and relaxation time in VASH1KD and TTL/E331Q overexpression experiments are listed.

REFERENCES

1. Eisner, D. A., Caldwell, J. L., Kistamás, K. & Trafford, A. W. Calcium and Excitation-Contraction Coupling in the Heart. *Circ Res* **121**, 181–195 (2017).

2. Fukuta, H. & Little, W. C. The Cardiac Cycle and the Physiologic Basis of Left Ventricular Contraction, Ejection, Relaxation, and Filling. *Heart Fail Clin* **4**, 1–11 (2008).

3. Gaasch, W. H. & Zile, M. R. Left Ventricular Diastolic Dysfunction and Diastolic Heart Failure. *Annu Rev Med* **55**, 373–394 (2004).

4. Borlaug, B. A. & Paulus, W. J. Heart failure with preserved ejection fraction: pathophysiology, diagnosis, and treatment. *Eur Heart J* **32**, 670–679 (2011).

5. Periasamy, M. & Janssen, P. M. L. Molecular Basis of Diastolic Dysfunction. *Heart Fail Clin* **4**, 13–21 (2008).

6. Heffler, J. *et al.* A Balance Between Intermediate Filaments and Microtubules Maintains Nuclear Architecture in the Cardiomyocyte. *Circ Res* **126**, e10–e26 (2020).

7. Prosser, B. L., Ward, C. W. & Lederer, W. J. X-ROS Signaling: Rapid Mechano-Chemo Transduction in Heart. *Science* **333**, 1440–1445 (2011).

8. Kerr, J. P. *et al.* Detyrosinated microtubules modulate mechanotransduction in heart and skeletal muscle. *Nat Commun* **6**, 8526 (2015).

9. Scarborough, E. A. *et al.* Microtubules orchestrate local translation to enable cardiac growth. *Nat Commun* **12**, 1547 (2021).

10. Sui, H. & Downing, K. H. Structural Basis of Interprotofilament Interaction and Lateral Deformation of Microtubules. *Structure* **18**, 1022–1031 (2010).

11. Walker, R. A. *et al.* Dynamic instability of individual microtubules analyzed by video light microscopy: rate constants and transition frequencies. *J Cell Biology* **107**, 1437–1448 (1988).

12. Mitchison, T. & Kirschner, M. Dynamic instability of microtubule growth. *Nature* **312**, 237–242 (1984).

13. Holy, T. E. & Leibler, S. Dynamic instability of microtubules as an efficient way to search in space. *Proc National Acad Sci* **91**, 5682–5685 (1994).

14. Horio, T. & Murata, T. The role of dynamic instability in microtubule organization. *Front Plant Sci* **5**, 511 (2014).

15. Müller-Reichert, T., Chrétien, D., Severin, F. & Hyman, A. A. Structural changes at microtubule ends accompanying GTP hydrolysis: Information from a slowly hydrolyzable analogue of GTP, guanylyl (α,β)methylenediphosphonate. *Proc National Acad Sci* **95**, 3661–3666 (1998).

16. Roostalu, J. *et al.* The speed of GTP hydrolysis determines GTP cap size and controls microtubule stability. *Elife* **9**, e51992 (2020).

17. Akhmanova, A. & Steinmetz, M. O. Control of microtubule organization and dynamics: two ends in the limelight. *Nat Rev Mol Cell Bio* **16**, 711–726 (2015).

18. Roll-Mecak, A. The Tubulin Code in Microtubule Dynamics and Information Encoding. *Dev Cell* **54**, 7–20 (2020).

19. Hallak, M. E., Rodriguez, J. A., Barra, H. S. & Caputto, R. Release of tyrosine from tyrosinated tubulin. Some common factors that affect this process and the assembly of tubulin. *Febs Lett* **73**, 147–150 (1977).

20. Edde, B. *et al.* Posttranslational glutamylation of alpha-tubulin. *Science* **247**, 83–85 (1990).

21. Redeker, V. *et al.* Polyglycylation of tubulin: a posttranslational modification in axonemal microtubules. *Science* **266**, 1688–1691 (1994).

22. Chalfie, M. & Au, M. Genetic control of differentiation of the Caenorhabditis elegans touch receptor neurons. *Science* **243**, 1027–1033 (1989).

23. Fourest-Lieuvin, A. *et al.* Microtubule Regulation in Mitosis: Tubulin Phosphorylation by the Cyclin-dependent Kinase Cdk1. *Mol Biol Cell* **17**, 1041–1050 (2006).

24. Nogales, E. STRUCTURAL INSIGHTS INTO MICROTUBULE FUNCTION. *Annu Rev Biochem* **69**, 277–302 (2000).

25. Gittes, F., Mickey, B., Nettleton, J. & Howard, J. Flexural rigidity of microtubules and actin filaments measured from thermal fluctuations in shape. *J Cell Biology* **120**, 923–934 (1993).

26. Wang, N. *et al.* Mechanical behavior in living cells consistent with the tensegrity model. *Proc National Acad Sci* **98**, 7765–7770 (2001).

27. Mehrbod, M. & Mofrad, M. R. K. On the Significance of Microtubule Flexural Behavior in Cytoskeletal Mechanics. *Plos One* **6**, e25627 (2011).

28. Ingber, D. E. Tensegrity I. Cell structure and hierarchical systems biology. *J Cell Sci* **116**, 1157–1173 (2003).

29. Jiang, H. & Zhang, J. Mechanics of Microtubule Buckling Supported by Cytoplasm. *J Appl Mech* **75**, 061019 (2008).

30. Brangwynne, C. P. *et al.* Microtubules can bear enhanced compressive loads in living cells because of lateral reinforcement. *J Cell Biology* **173**, 733–741 (2006).

31. Capetanaki, Y., Milner, D. J. & Weitzer, G. Desmin in Muscle Formation and Maintenance: Knockouts and Consequences. *Cell Struct Funct* **22**, 103–116 (1997).

32. Robison, P. *et al.* Detyrosinated microtubules buckle and bear load in contracting cardiomyocytes. *Science* **352**, aaf0659 (2016).

33. Prezhdo, O. V. & Pereverzev, Y. V. Theoretical Aspects of the Biological Catch Bond. *Accounts Chem Res* **42**, 693–703 (2009).

34. Tsutsui, H., Ishihara, K. & Cooper, G. Cytoskeletal role in the contractile dysfunction of hypertrophied myocardium. *Science* **260**, 682–687 (1993).

35. Koide, M. *et al.* Microtubule Depolymerization Normalizes In Vivo Myocardial Contractile Function in Dogs With Pressure-Overload Left Ventricular Hypertrophy. *Circulation* **102**, 1045–1052 (2000).

36. Collins, J. F. *et al.* The Role of the Cytoskeleton in Left Ventricular Pressure Overload Hypertrophy and Failure. *J Mol Cell Cardiol* **28**, 1435–1443 (1996).

37. Bailey, B. A., Dipla, K., Li, S. & Houser, S. R. Cellular Basis of Contractile Derangements of Hypertrophied Feline Ventricular Myocytes. *J Mol Cell Cardiol* **29**, 1823–1835 (1997).

38. Webster, D. R., Gundersen, G. G., Bulinski, J. C. & Borisy, G. G. Differential turnover of tyrosinated and detyrosinated microtubules. *Proc National Acad Sci* **84**, 9040–9044 (1987).

39. Webster, D. R., Wehland, J., Weber, K. & Borisy, G. G. Detyrosination of alpha tubulin does not stabilize microtubules in vivo. *J Cell Biology* **111**, 113–122 (1990).

40. Khawaja, S., Gundersen, G. G. & Bulinski, J. C. Enhanced stability of microtubules enriched in detyrosinated tubulin is not a direct function of detyrosination level. *J Cell Biology* **106**, 141–149 (1988).

41. Chen, J. *et al.* α-tubulin tail modifications regulate microtubule stability through selective effector recruitment, not changes in intrinsic polymer dynamics. *Dev Cell* (2021) doi:10.1016/j.devcel.2021.05.005.

42. Chen, C. Y. *et al.* Depletion of Vasohibin 1 Speeds Contraction and Relaxation in Failing Human Cardiomyocytes. *Circ Res* **127**, e14–e27 (2020).

43. Hotta, T. *et al.* Parthenolide Destabilizes Microtubules by Covalently Modifying Tubulin. *Curr Biol* **31**, 900-907.e6 (2021).

44. Szyk, A., Deaconescu, A. M., Piszczek, G. & Roll-Mecak, A. Tubulin tyrosine ligase structure reveals adaptation of an ancient fold to bind and modify tubulin. *Nat Struct Mol Biol* **18**, 1250–1258 (2011).

45. Ersfeld, K. *et al.* Characterization of the tubulin-tyrosine ligase. *J Cell Biology* **120**, 725–732 (1993).

46. Chen, C. Y. *et al.* Suppression of detyrosinated microtubules improves cardiomyocyte function in human heart failure. *Nat Med* **24**, 1225–1233 (2018).

47. Nieuwenhuis, J. *et al.* Vasohibins encode tubulin detyrosinating activity. *Science* **358**, 1453–1456 (2017).

48. Aillaud, C. *et al.* Vasohibins/SVBP are tubulin carboxypeptidases (TCPs) that regulate neuron differentiation. *Science* **358**, 1448–1453 (2017).

49. Oddoux, S. *et al.* Microtubules that form the stationary lattice of muscle fibers are dynamic and nucleated at Golgi elementsSkeletal muscle microtubule dynamics. *J Cell Biology* **203**, 205–213 (2013).

50. Drum, B. M. L. *et al.* Oxidative stress decreases microtubule growth and stability in ventricular myocytes. *J Mol Cell Cardiol* **93**, 32–43 (2016).

51. Bowne-Anderson, H., Hibbel, A. & Howard, J. Regulation of Microtubule Growth and Catastrophe: Unifying Theory and Experiment. *Trends Cell Biol* **25**, 769–779 (2015).

52. Wloga, D., Joachimiak, E. & Fabczak, H. Tubulin Post-Translational Modifications and Microtubule Dynamics. *Int J Mol Sci* **18**, 2207 (2017).

53. Eshun-Wilson, L. *et al.* Effects of α-tubulin acetylation on microtubule structure and stability. *Proc National Acad Sci* **116**, 201900441 (2019).

54. Portran, D., Schaedel, L., Xu, Z., Théry, M. & Nachury, M. V. Tubulin acetylation protects long-lived microtubules against mechanical ageing. *Nat Cell Biol* **19**, 391–398 (2017).

55. Peris, L. *et al.* Motor-dependent microtubule disassembly driven by tubulin tyrosination. *J Cell Biology* **185**, 1159–1166 (2009).

56. Schaedel, L., Lorenz, C., Schepers, A. V., Klumpp, S. & Köster, S. Vimentin Intermediate Filaments Stabilize Dynamic Microtubules by Direct Interactions. *Biorxiv* 2020.05.20.106179 (2021) doi:10.1101/2020.05.20.106179.

57. Favre, B. *et al.* Plectin interacts with the rod domain of type III intermediate filament proteins desmin and vimentin. *Eur J Cell Biol* **90**, 390–400 (2011).

58. Liao, G. & Gundersen, G. G. Kinesin Is a Candidate for Cross-bridging Microtubules and Intermediate Filaments SELECTIVE BINDING OF KINESIN TO DETYROSINATED TUBULIN AND VIMENTIN*. *J Biol Chem* **273**, 9797–9803 (1998).

59. Tsutsui, H. *et al.* Role of microtubules in contractile dysfunction of hypertrophied cardiocytes. *Circulation* **90**, 533–555 (2003).

60. Yamamoto, S. *et al.* Role of Microtubules in the Viscoelastic Properties of Isolated Cardiac Muscle. *J Mol Cell Cardiol* **30**, 1841–1853 (1998).

61. Granzier, H. L. & Irving, T. C. Passive tension in cardiac muscle: contribution of collagen, titin, microtubules, and intermediate filaments. *Biophys J* **68**, 1027–1044 (1995).

62. Rakowski, H. & Carasso, S. Quantifying Diastolic Function in Hypertrophic Cardiomyopathy: The Ongoing Search for the Holy Grail. *Circulation* **116**, 2662–2665 (2007).

63. Caporizzo, M. A. *et al.* Microtubules provide a viscoelastic resistance to myocyte motion. *Biorxiv* 361824 (2018) doi:10.1101/361824.

64. Zile, M. R. *et al.* Cardiocyte cytoskeleton in patients with left ventricular pressure overload hypertrophy. *J Am Coll Cardiol* **37**, 1080–1084 (2001).

65. Dorsch, L. M. *et al.* Protein Quality Control Activation and Microtubule Remodeling in Hypertrophic Cardiomyopathy. *Cells* **8**, 741 (2019).

66. Caporizzo, M. A., Chen, C. Y. & Prosser, B. L. Cardiac microtubules in health and heart disease. *Exp Biol Med* **244**, 1255–1272 (2019).

67. Nieuwenhuis, J. & Brummelkamp, T. R. The Tubulin Detyrosination Cycle: Function and Enzymes. *Trends Cell Biol* **29**, 80–92 (2018).

68. Wen, J., You, K.-R., Lee, S.-Y., Song, C.-H. & Kim, D.-G. Oxidative Stress-mediated Apoptosis THE ANTICANCER EFFECT OF THE SESQUITERPENE LACTONE PARTHENOLIDE*. *J Biol Chem* **277**, 38954–38964 (2002).

69. Caporizzo, M. A., Chen, C. Y., Salomon, A. K., Margulies, K. B. & Prosser, B. L. Microtubules Provide a Viscoelastic Resistance to Myocyte Motion. *Biophys J* **115**, 1796–1807 (2018).

70. Wang, N. *et al.* Structural basis of tubulin detyrosination by the vasohibin–SVBP enzyme complex. *Nat Struct Mol Biol* **26**, 571–582 (2019).

71. Li, F., Hu, Y., Qi, S., Luo, X. & Yu, H. Structural basis of tubulin detyrosination by vasohibins. *Nat Struct Mol Biol* **26**, 583–591 (2019).

72. Liao, S. *et al.* Molecular basis of vasohibins-mediated detyrosination and its impact on spindle function and mitosis. *Cell Res* **29**, 533–547 (2019).

73. Laan, S. van der *et al.* Evolutionary Divergence of Enzymatic Mechanisms for Tubulin Detyrosination. *Cell Reports* **29**, 4159-4171.e6 (2019).

74. ANNIE, A. *et al.* METHODS AND PHARMACEUTICAL COMPOSITIONS FOR TREATING TUBULIN CARBOXYPEPTIDASES ASSOCIATED DISEASES. (2010).

75. Ghantous, A., Sinjab, A., Herceg, Z. & Darwiche, N. Parthenolide: from plant shoots to cancer roots. *Drug Discov Today* **18**, 894–905 (2013).

76. Shaw, R. M. *et al.* Microtubule Plus-End-Tracking Proteins Target Gap Junctions Directly from the Cell Interior to Adherens Junctions. *Cell* **133**, 376 (2008).

77. Kimura, H. *et al.* Distinctive localization and opposed roles of vasohibin-1 and vasohibin-2 in the regulation of angiogenesis. *Blood* **113**, 4810–8 (2009).

78. Mohan, N., Sorokina, E. M., Verdeny, I. V., Alvarez, A. S. & Lakadamyali, M. Detyrosinated microtubules spatially constrain lysosomes facilitating lysosome–autophagosome fusion. *J Cell Biol* **218**, 632–643 (2019).

79. Sirajuddin, M., Rice, L. M. & Vale, R. D. Regulation of microtubule motors by tubulin isotypes and post-translational modifications. *Nat Cell Biol* **16**, 335–344 (2014).

80. Barisic, M. *et al.* Microtubule detyrosination guides chromosomes during mitosis. *Science* **348**, 799–803 (2015).

81. Hammond, J. W. *et al.* Posttranslational Modifications of Tubulin and the Polarized Transport of Kinesin-1 in Neurons. *Mol Biol Cell* **21**, 572–583 (2010).

82. Singh, S. R. *et al.* Activation of Autophagy Ameliorates Cardiomyopathy in Mybpc3-Targeted Knockin Mice. *Circulation Hear Fail* **10**, e004140 (2018).

83. Forges, H. de, Bouissou, A. & Perez, F. Interplay between microtubule dynamics and intracellular organization. *Int J Biochem Cell Biology* **44**, 266–274 (2012).

84. Roll-Mecak, A. How cells exploit tubulin diversity to build functional cellular microtubule mosaics. *Curr Opin Cell Biol* **56**, 102–108 (2019).

85. Soheilypour, M., Peyro, M., Peter, S. J. & Mofrad, M. R. K. Buckling Behavior of Individual and Bundled Microtubules. *Biophys J* **108**, 1718–1726 (2015).

86. Gurland, G. & Gundersen, G. G. Stable, detyrosinated microtubules function to localize vimentin intermediate filaments in fibroblasts. *J Cell Biology* **131**, 1275–1290 (1995).

87. Fassett, J. T. *et al.* Adenosine regulation of microtubule dynamics in cardiac hypertrophy. *Am J Physiol-heart C* **297**, H523–H532 (2009).

88. Webster, D. R. & Borisy, G. G. Microtubules are acetylated in domains that turn over slowly. *J Cell Sci* **92 (Pt 1)**, 57–65 (1989).

89. Xu, Z. *et al.* Microtubules acquire resistance from mechanical breakage through intralumenal acetylation. *Science* **356**, 328–332 (2017).

90. Kalebic, N. *et al.* Tubulin Acetyltransferase αTAT1 Destabilizes Microtubules Independently of Its Acetylation Activity. *Mol Cell Biol* **33**, 1114–1123 (2013).

91. Asthana, J., Kapoor, S., Mohan, R. & Panda, D. Inhibition of HDAC6 Deacetylase Activity Increases Its Binding with Microtubules and Suppresses Microtubule Dynamic Instability in MCF-7 Cells*. *J Biol Chem* **288**, 22516–22526 (2013).

92. Peris, L. *et al.* Tubulin tyrosination is a major factor affecting the recruitment of CAP-Gly proteins at microtubule plus ends. *J Cell Biology* **174**, 839–849 (2006).

93. Watkins, S. C., Samuel, J. L., Marotte, F., Bertier-Savalle, B. & Rappaport, L. Microtubules and desmin filaments during onset of heart hypertrophy in rat: a double immunoelectron microscope study. *Circ Res* **60**, 327–336 (2018).

94. Brodehl, A., Gaertner-Rommel, A. & Milting, H. Molecular insights into cardiomyopathies associated with desmin (DES) mutations. *Biophysical Rev* **10**, 983–1006 (2018).

95. Aumeier, C. *et al.* Self-repair promotes microtubule rescue. *Nat Cell Biol* **18**, 1054–1064 (2016).

96. Hamant, O., Inoue, D., Bouchez, D., Dumais, J. & Mjolsness, E. Are microtubules tension sensors? *Nat Commun* **10**, 2360 (2019).

97. Göktepe, S., Abilez, O. J., Parker, K. K. & Kuhl, E. A multiscale model for eccentric and concentric cardiac growth through sarcomerogenesis. *J Theor Biol* **265**, 433–442 (2010).

98. Tadano, N. *et al.* Biological actions of green tea catechins on cardiac troponin C. *Brit J Pharmacol* **161**, 1034–1043 (2010).

99. Adhikari, B. B. & Wang, K. Interplay of Troponin- and Myosin-Based Pathways of Calcium Activation in Skeletal and Cardiac Muscle: The Use of W7 as an Inhibitor of Thin Filament Activation. *Biophys J* **86**, 359–370 (2004).

100. Nishiga, M., Qi, L. S. & Wu, J. C. Therapeutic genome editing in cardiovascular diseases. *Adv Drug Deliver Rev* **168**, 147–157 (2021).

101. Green, E. M. *et al.* A small-molecule inhibitor of sarcomere contractility suppresses hypertrophic cardiomyopathy in mice. *Science* **351**, 617–621 (2016).

102. Mimori-Kiyosue, Y. & Tsukita, S. “Search-and-Capture” of Microtubules through Plus-End-Binding Proteins (+TIPs). *J Biochem* **134**, 321–326 (2003).

103. Gardner, M. K., Zanic, M. & Howard, J. Microtubule catastrophe and rescue. *Curr Opin Cell Biol* **25**, 14–22 (2013).

104. Pearson, C. G. & Bloom, K. Dynamic Microtubules Lead the Way for Spindle Positioning. *Nat Rev Mol Cell Bio* **5**, 481–492 (2004).

105. Ginkel, L. M. & Wordeman, L. Expression and Partial Characterization of Kinesin- related Proteins in Differentiating and Adult Skeletal Muscle.pdf. *Mol Biol Cell* **11**, 4143–4158 (2000).

106. Walczak, C. E., Gayek, S. & Ohi, R. Microtubule-Depolymerizing Kinesins. *Cell Dev Biology* **29**, 417–441 (2012).

107. Straube, A. & Merdes, A. EB3 Regulates Microtubule Dynamics at the Cell Cortex and Is Required for Myoblast Elongation and Fusion. *Curr Biol* **17**, 1318–1325 (2007).

108. Nandi, S. S. & Mishra, P. K. Harnessing fetal and adult genetic reprograming for therapy of heart disease. *J Nat Sci* **1**, (2015).

109. Szyk, A. *et al.* Molecular Basis for Age-Dependent Microtubule Acetylation by Tubulin Acetyltransferase. *Cell* **157**, 1405–1415 (2014).

110. Théry, M. & Blanchoin, L. Microtubule self-repair. *Curr Opin Cell Biol* **68**, 144–154 (2021).

111. Kurup, N., Li, Y., Goncharov, A. & Jin, Y. Intermediate filament accumulation can stabilize microtubules in Caenorhabditis elegans motor neurons. *Proc National Acad Sci* **115**, 201721930 (2018).

112. Coleman, A. K., Joca, H. C., Shi, G., Lederer, W. J. & Ward, C. W. Tubulin acetylation increases cytoskeletal stiffness to regulate mechanotransduction in striated muscle. *J Gen Physiol* **153**, e202012743 (2021).